QUANTITATIVE MICROCHIP CAPILLARY ELECTROPHORESIS FOR INORGANIC ION ANALYSIS AT THE POINT OF CARE

Elwin Vrouwe

Promotiecommissie

Voorzitter:	Prof.dr.ir. A.J. Mouthaan	Universiteit Twente
Promotor:	Prof.dr.ir. A. van den Berg	Universiteit Twente
Assistent promotor:	Dr. R. Luttge	Universiteit Twente
Leden:	Prof.dr. T. Hankemeier	Universiteit Leiden
	Prof. U. Karst	Universiteit Twente
	Prof. Th. Laurell	Lund University
	Dr. H.A.G. Niederländer	Rijksuniversiteit Groningen
	Dr. W. Olthuis	Universiteit Twente
	Prof.dr. I. Vermes	Universiteit Twente

The research in this work was supported by the Technology Foundation STW, applied science division of NWO and the technology program of the Ministry of Economic Affairs

Print: Febodruk BV, Enschede

© E.X. Vrouwe, Enschede, 2005

No part of this work may be reproduced by print, photocopy or any other means without the permission in writing from the author.

ISBN 90-9019293-X

QUANTITATIVE MICROCHIP CAPILLARY ELECTROPHORESIS FOR INORGANIC ION ANALYSIS AT THE POINT OF CARE

PROEFSCHRIFT

ter verkrijging van
de graad van doctor aan de Universiteit Twente,
op gezag van rector magnificus,
prof.dr. W.H.M. Zijm,
volgens beluit van het College voor Promoties
in het openbaar te verdedigen
op vrijdag 15 april 2005 om 13.15 uur

door
Elwin Xander Vrouwe
geboren op 2 december 1974
te Alphen aan den Rijn

Dit proefschrift is goedgekeurd door:

Promotor:	Prof.dr.ir. A. van den Berg
Assistent promotor:	Dr. R. Luttge

Contents

Chapter 1

Scope and outline

This chapter presents the objectives of the project as well as background information on microchip analysis of inorganic ions. Microchip capillary electrophoresis is an exciting approach for a rapidly increasing number of analytical problems in life sciences and environmental applications. Here an overview is given about manic depression and its treatment with lithium. Although this work specifically addresses the method for point-of-care measurement of lithium in blood, it also opens up interesting possibilities for environmental on-site analyses, e.g. drinking water monitoring. To conclude this introducing chapter an outline of the thesis is given.

1.1 Introduction

The first papers on microchip capillary electrophoresis (CE) were published in 1992 and demonstrated that a significant improvement in speed is obtained by miniaturizing conventional separation methods [1,2]. In the broader concept of micro total analysis systems (μTAS), CE separations form an integral part enabling the analysis of complex samples [3-7]. The steadily growing number of publications on microchip CE each year shows the sustained interest and continuing development (Fig. 1.1). A significant amount of research is invested in the development of different functional components that form the building blocks of microchip systems. However, due to the complexity, the integration that is required for a practical application is seldom reached. In this thesis a microchip capillary electrophoresis system is presented for measuring inorganic ions. The main goal is to develop a system for point-of-care analysis of lithium in whole blood. Speed, accuracy, robustness and user-friendliness are the criteria which the system has to fulfill. Furthermore, the application of the system for monitoring drinking water quality is investigated. The following sections place the analysis of inorganic ions and in particular that of lithium in perspective.

1.2 Microchip capillary electrophoresis of inorganic ions for point-of-care analysis

1.2.1 Inorganic ion analysis

Inorganic ions are an essential requirement for life and are found in large amounts in drinking water, blood and every cell of an organism. In clinical laboratories inorganic

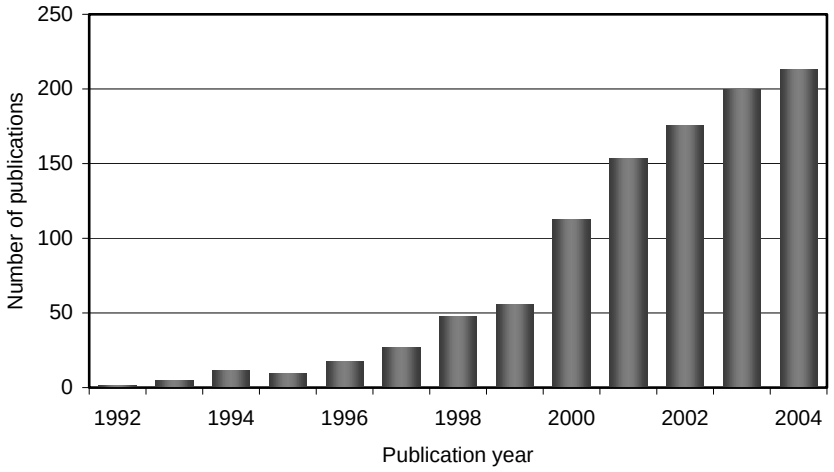

Figure 1.1: *Number of publications in scientific journals containing the keywords capillary electrophoresis and (micro)chip in the title or abstract. (Science Citation Index Expanded database)*

species are determined on a routine basis. For example, Table 1.1 shows the abundance of the main species found in blood plasma. Contemporary methods for metal ion analysis include atomic absorption and emission spectrometry, mass spectrometry, electrochemical methods (potentiometry, voltammetry), colorimetry and ion chromatography. For anionic species ion chromatography, colorimetry and potentiometry are key analytical methods [8]. Most equipment is operated by qualified personnel only and is not suitable for portable use. Samples are collected and transported to a central laboratory, which substantially adds to the overall cost of the analysis. Miniaturization using microchip technology offers the opportunity for on-site analysis with equipment that is simple to operate.

1.2.2 Microchip CE analysis of inorganic ions

Following the trend of miniaturization, microchips have been developed to measure inorganic ions in aqueous samples based on methods developed initially for conventional CE [9]. The potential of microchip CE has also encouraged manufacturers of laboratory instrumentation to develop complete systems. For instance, Agilent developed the 2100 Bioanalyzer (DNA, RNA, proteins and cells), Shimadzu the MCE-2010 (DNA), Bio-Rad the Experion (proteins, RNA) and Hitachi the SV1100 and SV1210 (DNA, RNA). Some systems run automatically and are capable of analyzing a large number of samples while others still require manual sample handling steps and are suitable mainly for rapid analysis of a small number of samples. All these systems have in common the use of optical detection methods, which make them less suitable for inorganic ion analysis. They are also not intended for point-of-care use as only trained personnel is able to operate the instruments since manual handling steps such as filling of the chip and sample cleanup are still required.

For the quantitative analysis of species in a complex matrix such as blood, the limitations

Table 1.1: Abundance of inorganic ions in blood plasma. Source: Medisch Spectrum Twente, Hospital group, Enschede, The Netherlands.

	Typical value in plasma (mmol/L)
Ammonia	0.015 - 0.045
Bicarbonate	21 - 27
Calcium	2.20 - 2.65
Chloride	97 - 107
Copper	0.011 - 0.020
Iron	0.015 - 0.030
Magnesium	0.6 – 1.1
Phosphate	0.9 - 1.5
Potassium	3.5 - 5.0
Sodium	135 - 145
Zink	0.011 - 0.017

that are encountered by conventional instruments are also not fully solved by the existing microchip CE methods. For example, the presence of blood cells and the high ionic strength of blood are critical issues, which are therefore thoroughly investigated in chapters 3 to 5. The combination of sample handling and separation on a single microchip offers new perspectives for analyzing samples that traditionally require separate sample pretreatment steps.

1.2.3 Point-of care analysis

One of the criteria for a point-of-care test is that its use has to be straightforward in order that a physician or patient can perform the test. For blood analysis this means that a drop of capillary blood obtained from a finger stick should suffice, requiring no manual sample handling. Tests of this type are for example available for the glucose concentration and blood coagulation time [10]. An example of a handheld instrument used in a clinical environment is the i-STAT analyzer [11]. The disposable cartridges employ a fluidic network to separate the plasma from the cells. Subsequently, various sensing principles are available to measure a range of blood parameters. Potassium, sodium and chloride for example are measured using ion-selective electrodes, while glucose is measured amperometrically and hematocrit conductometrically. Yet, using these principles a separate sensor is required for each blood constituent. In order to obtain a complete blood image, the use of a separation technique in combination with a non-selective sensor is a valuable addition to existing methods in clinical practice. Microchip CE combined with integrated sample handling can fulfil the conditions required for point-of-care testing.

Another important aspect of patient treatment is drug delivery. It has become possible to automatically administer drugs using, for example implantable insulin pumps, or via the skin using iontophoresis [12]. The latter method employs electrical fields to transport drugs through the skin by means of electromigration and electroosmosis. The same principles are used for performing electrophoretic separations. The combination of an automatic drug dosing system with a sensing device would be ideal to maintain a constant optimum concentration of a therapeutic drug. Advances in micromachining and microfluidics have already resulted in the development of painless microneedles for drug delivery and sampling [13]. Initial results on merging microsampling techniques with microchip capillary electrophoresis are discussed in chapter 6.

1.3 Lithium therapy for manic depression

1.3.1 Manic depression

Manic depression or bipolar mood disorder is an illness causing patients to experience large fluctuations in mood, energy and ability to function. The range of moods can vary from severe depression via mild depression, normal feeling, hypomania to severe mania. Some of the symptoms that are typical for depression and mania are summarized in tables

1.2 and 1.3, respectively. Approximately one percent of the population of age 18 and older suffers from this condition, although it is not always recognized as such. Over the course of the illness nearly one out of five persons commits suicide which makes it one of the most lethal psychiatric illnesses [14]. While the exact cause of the illness is not known, it does involve changes in brain chemistry and can be inherited.

A further distinction can be made between bipolar I disorder, characterized by recurrent episodes of mania and depression, and bipolar II disorder in which the depression is alternated by milder hypomanic episodes. Between the episodes most people are free from symptoms. Although depression and mania are unwanted conditions the hypomanic phase can be a desired condition where people feel extremely well and can become very productive.

Table 1.2: Signs and symptoms of mania. Reproduced from ref. 15.

Extreme irritability and distractibility
Excessive "high" or euphoric feelings
Increased energy, activity, restlessness, racing thoughts, and rapid talking
Decreased need for sleep
Unrealistic beliefs in one's abilities and powers
Uncharacteristically poor judgment
Increased sexual drive
Abuse of drugs, particularly cocaine, alcohol, and sleeping medications
Obnoxious, provocative, or intrusive behavior
Denial that anything is wrong

Table 1.3: Signs and symptoms of depression. Reproduced from ref. 15.

Persistent sad, anxious, or empty mood
Feelings of hopelessness or pessimism
Feelings of guilt, worthlessness, or helplessness
Loss of interest or pleasure in ordinary activities, including sex
Decreased energy, a feeling of fatigue or of being "slowed down"
Difficulty concentrating, remembering, making decisions
Restlessness or irritability
Sleep disturbances
Loss of appetite and weight, or weight gain
Chronic pain or other persistent bodily symptoms that are not caused by physical disease
Thoughts of death or suicide; suicide attempts

1.3.2 Lithium treatment

Lithium and Divalproex are the two most prescibed moodstabilizers for manic depression. Lithium is very effective, although the exact mechanism of its action is still largely unknown. Since lithium has a low therapeutic index, i.e. the ratio between the toxic concentration and the therapeutic concentration, monitoring is required. Generally the lithium concentration is determined in blood plasma or serum. The intracellular concentration of lithium in red blood cells is not routinely determined, but can provide information on how faithfully the patient follows the prescription [16]. The intracellular lithium concentration follows a delayed response compared to the plasma concentration. A normal extracellular and low intracellular lithium concentration therefore indicates that the patient does not comply to the prescription. A high extracellular concentration indicates an acute overdose and a high intracellular concentration indicates a chronic lithium overdose.

Typically, lithium is determined in serum derived from venous blood and the analysis can only be performed in a clinical laboratory. If a self-test for lithium is available, patients can monitor their own lithium level, and adjust the daily dosage accordingly. This can lead to a more constant lithium level, improved personal medical management and minimizes the side-effects associated with too high lithium concentrations.

1.4 Drinking water monitoring

Another example of a field in which inorganic ion analysis plays an important role is in water quality monitoring and environmental analysis. Water companies need to be sure that the drinking water they provide is suitable for consumption. Strict regulations are imposed on the maximum allowed concentration of many potential contaminants like heavy metals. Also species that are not critical for human health, e.g. calcium and magnesium are significant because these contribute to water hardness. Microchip electrophoresis provides the throughput needed for semi-continuous analysis of drinking water for use in water softening installations. At the same time a complete image of the water composition is obtained. In chapter 7 the analysis of inorganic anionic and cationic species in drinking water is presented for monitoring water quality.

1.5 Outline of this thesis

The information in each chapter is self-contained such that each chapter can be read separately from the others. As a consequence there is some duplication of information throughout the chapters.

In chapter 2 the factors affecting the performance of CE microchips are discussed. Based on these considerations a microchip with conductivity detection is designed. This chip is subsequently used for the experiments in the remaining chapters.

In chapter 3 the fabrication and performance of glass microchips for metal ion analysis are discussed. Without an optimization of the separating conditions the interaction of metal ions with the glass surface interferes with the separation. The use of background electrolyte additives or surface coatings provides the conditions needed to separate potassium, sodium and lithium.

In chapter 4 a method is presented to measure lithium directly in whole blood. Optimized experimental conditions are used to filter out the blood cells on the CE microchip by electrophoretic means. This allows direct analysis of blood from a finger stick on a CE microchip without any complex microfluidic structures. This chapter is adapted from a paper published in Electrophoresis.

In chapter 5 the sample loading conditions on the microchip are studied for the quantitation of lithium in blood. The combination of moving boundary electrophoresis and zone electrophoresis is used to measure analytes in a high ionic strength matrix without off-chip sample treatment. This chapter has been accepted for publication in Electrophoresis.

In chapter 6 disposable sample cups are introduced to measure whole blood directly from a finger stick and are intended for point-of-care testing. Serum samples from patients on lithium therapy are used and the results are compared to analyses performed in the hospital. The good agreement between the results confirms the validity of the method. This chapter is intended for publication.

Chapter 7 describes the application of the microchip for drinking water analysis. Complexing agents and electroosmotic flow modifiers are used to enable the analysis of inorganic anionic and cationic species in tap water. This chapter has been submitted for publication in Journal of Chromatography A.

In chapter 8 the results from the previous chapters are summarized and an outlook for further research and development is presented.

1.6 References

1. DJ Harrison, A Manz, Z Fan, H Lüdi and HM Widmer "*Capillary Electrophoresis and Sample Injection Systems Integrated on a Planar Glass Chip"*, Anal. Chem. 1992, **64**, 1926-1932.

2. A Manz, DJ Harrison, EMJ Verpoorte, JC Fettinger, A Paulus, H Lüdi and HM Widmer "*Planar chips technology for miniaturization and integration of separation techniques into monitoring systems: Capillary electrophoresis on a chip"*, J. Chromatogr. 1992, **593**, 253-258.
3. SC Jakeway, AJ De Mello and EL Russell "*Miniaturized total analysis systems for biological analysis"*, Fresenius J. Anal. Chem. 2000, **366**, 525-539.
4. AJ Tüdõs, GAJ Besselink and RBM Schasfoort "*Trends in miniaturized total analysis systems for point-of-care testing in clinical chemistry"*, Lab on a Chip 2001, **1**, 83-85.
5. A van den Berg and TSJ Lammerink "*Micro Total Analysis Systems; Microfluidic Aspects, Integration Concept and Applications"*, Topics in Current Chemistry 1998, **194**, 21-49.
6. S Verpoorte "*Micro Total Chemical Analysis Systems (μTAS)"*, Biocybernetics and Biomedical Engineering 1999, **19**, 143-153.
7. SJ Lee and SY Lee "*Micro total analysis system (μ-TAS) in biotechnology"*, Appl. Microbiol. Biotechnol. 2004, **64**, 289-299.
8. JA Dean. "*Analytical chemistry handbook"*, 1st edition, 1995, New York, McGraw-Hill
9. CJ Evenhuis, RM Guijt, M Macka and PR Haddad "*Determination of inorganic ions using microfluidic devices"*, Electrophoresis 2004, **25**, 3602-3624.
10. JM Hasenkam, HH Kimose, L Knudsen, H Grønnesby, J Halborg, TD Christensen, J Attermann and HK Pilegaard "*Self management of oral anticoagulant therapy after heart valve replacement"*, European Journal of Cardio-thoracic Surgery 1997, **11**, 935-942.
11. KA Erickson and P Wilding "*Evaluation of a Novel Point-of-Care System, the i-STAT Portable Clinical Analyzer"*, Clin. Chem. 1993, **39**, 283-287.
12. YN Kalia, A Naik, J Garrison and RH Guy "*Iontophoretic drug delivery"*, Adv. Drug Deliv. Rev. 2004, **56**, 619-658.
13. ML Reed and W-K Lye "*Microsystems for Drug and Gene Delivery"*, Proceedings of the IEEE 2004, **92**, 56-75.
14. GS Sachs, DJ Printz, DA Kahn, D Carpenter and JP Docherty. "*Medical treatment of bipolar disorders 2000. The expert consensus guideline series"*, 2000, McGraw-Hill Healthcare Information Programs
15. "*Diagnostic and statistical manual of mental disorders, 4th edition, text revision"*, 2000, Washington, American Psychiatric Association
16. M Camus, G Henneré, G Baron, G Peytavin, L Massias, F Mentré and R Farinotti "*Comparison of lithium concentrations in red blood cells and plasma in samples collected for TDM, acute toxicity, or acute-on-chronic toxicity"*, Eur. J. Clin. Pharmacol. 2003, **59**, 583-587.

Chapter 2

Microchip capillary electrophoresis

The capillary electrophoresis microchip forms the heart of the system for measuring inorganic ions. The design of the microchip and the optimization of the separation conditions are critical to reach the goal of analyzing complex samples. In this chapter the fundamentals of capillary electrophoretic separations are discussed followed by an overview of the microchip design parameters and their influence on the separation performance. In the second part of this chapter the aspects of on-chip conductivity detection are treated. Different electrode layouts are compared to optimize the sensitivity and dynamic range. The discussions in this chapter form the basis of the microchip design used in the subsequent chapters.

2.1 Introduction

In the early eighties capillary zone electrophoresis (CZE) was used for the first time as a high performance separation method [1]. Before that time electrophoresis was mainly used to separate proteins, DNA and RNA in slab gels as a non- or semi-quantitative method. The introduction of dedicated instruments established capillary electrophoresis (CE) as an analytical technique alongside ion chromatography (IC) and high performance liquid chromatography (HPLC) [2]. Traditionally, CE is used to separate charged biomolecules, IC is predominantly used for small ions while HPLC is also used for uncharged substances. For a review of the developments in capillary electrophoresis we refer to the papers by Kuhr [3,4]. Capillary electrophoresis is especially suitable when it comes to miniaturization as will become clear in this chapter. In order to design and optimize a microchip for separating inorganic ions in complex samples, the parameters that affect microchip CE performance are discussed in the following sections. The fundamental principles of CE separations, the design of microchips and conductivity detection are discussed finding design rules for optimum sensitivity and maximum separation performance. The background information on the fundamentals of CE in this chapter is taken from textbooks on CE [5,6].

2.2 Fundamentals of capillary electrophoresis

2.2.1 Migration of ions in electric fields

The separation of ions by means of electrophoresis is based on the migration of charged species through an electrolyte solution under the influence of an externally applied electric field. Ions in solution experience an electrical force F_{ep} (N) equal to the product of the electrical field strength E (V/m), the electron charge e_0 (1.60×10^{-19} C) and the charge number z:

$$F_{ep} = ze_0E \tag{2.1}$$

This force acting on the ions results in their migration through the solution with anions and cations moving in opposite directions. As the ions move they experience a drag force F_{drag} (N) caused by friction with the electrolyte solution. For spherical ions the drag force can be calculated from the speed of movement v (m/s) via Stokes law. Assuming the ions have a radius r (m) (which includes the hydration sphere) and move through a medium with a viscosity η (Pa·s) the resulting drag force is:

$$F_{drag} = 6\pi\eta rv \tag{2.2}$$

Under equilibrium conditions the electrical force and the drag force are equal. Combining equations 2.1 and 2.2 results in the velocity of an ion in an electric field:

$$v = \frac{ze_0}{6\pi\eta r} E \tag{2.3}$$

The viscosity of a solution is temperature dependent and can be modeled for small changes in temperature by [7]:

$$\eta = \eta_0 \cdot e^{E_A / RT} \tag{2.4}$$

where E_A is the activity energy for viscous flow, R the molar gas constant (8.314 J/mol·K) and T the temperature (K).

The first term on the right hand side of Eq. 2.3 provides a measure of the ease with which a particular ion species can migrate through the medium and is referred to as the electrophoretic mobility μ ($m^2/V{\cdot}s$) of a species. Using the electrophoretic mobility Eq. 2.3 reduces to the generic form for the migration velocity of an ionic species:

$$v = \mu E \tag{2.5}$$

The electrophoretic mobilities of many substances have been experimentally determined and compiled [8]. In appendix B the mobilities for a selection of ionic species can be found that are used in this thesis. In practice the electrophoretic mobilities are influenced by various factors. These include the temperature of the solution (Eq. 2.4), the pH and the ionic strength. The degree of dissociation of a weakly acidic or basic analyte is a function of the pH of the solution. The effective mobility μ^{eff} ($m^2/V{\cdot}s$) of a species is therefore an average defined by its electrophoretic mobility at different charge numbers, where x is the fraction existing in the i^{th} form [8]:

$$\mu^{eff} = \sum_i x_i \mu_i \tag{2.6}$$

For a monovalent acid with an acid dissociation constant K_a the effective mobility as function of the pH is thus given by:

$$\mu^{eff} = \mu \frac{K_a}{[H^+] + K_a} \tag{2.7}$$

The ionic strength of the solution I (mol/L) also influences the effective mobility. The ionic strength is defined by the concentrations c (mol/L) of all the ions in solution:

$$I = \tfrac{1}{2} \sum_i z_i^2 \cdot c_i \tag{2.8}$$

For strong ions in a solution with an ionic strength between 1 and 100 mmol/L an empirical relation describes the mobility [9]:

$$\mu^{eff} = \mu e^{-0.77\sqrt{zI}} \tag{2.9}$$

For typical CE separations the temperature, pH and ionic strength of the solutions are defined by the experimental conditions and can be assumed stable. The electrophoretic mobilities can therefore be considered constant under defined conditions. Additional effects like interaction of species with the surface of the capillary also reduce the effective mobility, which is used in chapter 3 to examine the interaction of analytes with the capillary surface.

2.2.2 Electroosmotic flow

An important phenomenon in CE is the onset of an electroosmotic flow (EOF). Many materials, including glass, develop a charge at the surface when they come in contact with a protic solvent. For glass the surface charge develops from the protonation or deprotonantion of silanol groups (pKa~3.5). For polymers without any proton donating or accepting groups, traces of residual unreacted material in the bulk or charged substances adsorbed to the surface can result in a surface charge. To compensate the charge located at the surface the layer of solvent close to the surface is composed of an excess of oppositely charged ions, which is refered to as the electrical double layer (Fig. 2.1A). In this layer different regions can be distinguished. The first part of the double layer is composed of solvent molecules and dehydrated ions that are adsorbed onto the surface. The plane through the center of the ions is called the inner Helmholtz plane (IHP). Hydrated ions approach the surface corresponding to a distance defined by the radius of the hydration sphere. These non-specifically adsorbed ions define the outer Helmholtz plane (OHP) or Stern layer. These first two regions form the compact region of the double layer. The diffuse region starts at the outer Helmholtz plane and extends into the solution. In contrast to the compact layer, the ions in the diffuse region are still mobile. When an electric field is applied parallel to the surface, the ions in the diffuse layer migrate towards the oppositely charged electrode. As the ions move they drag the solvent along causing a bulk flow of the liquid, which is the EOF. The EOF velocity is zero at the shear plane, and reaches a maximum at a short distance from the surface. The flow profile can therefore be assumed uniform throughout if the capillary diameter is much larger than the electrical double layer thickness (typically between 1 and 100 nm).

The mobility of the EOF is determined by the surface charge density σ (C/m^2) and thickness of the double layer. Often the zeta potential ζ (V), which is the potential at the plane of shear, is used to characterize the double layer instead of the charge density (Fig. 2.1B). The mobility of the EOF is:

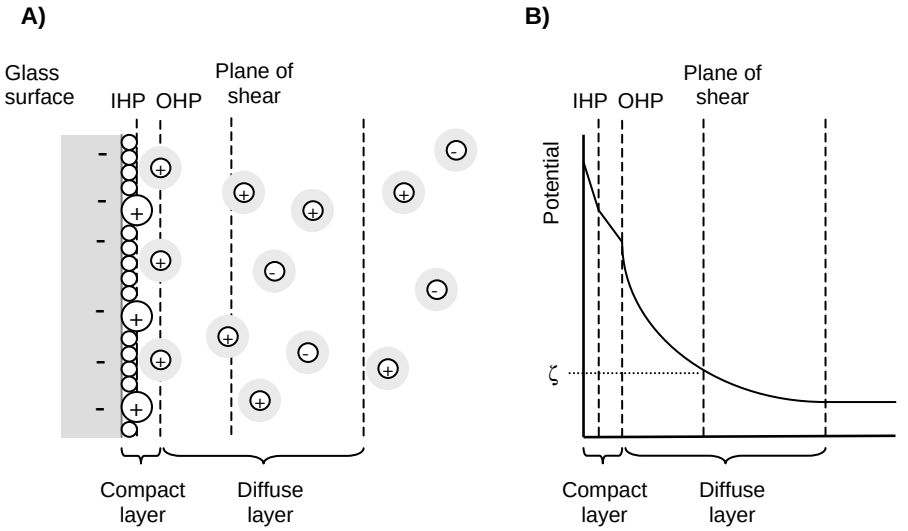

Figure 2.1: *A) Schematic representation of the interface between a glass surface and an aqueous solution and B) the potential in the different regions.*

$$\mu_{EOF} = \frac{\sigma}{\eta k} = \frac{\varepsilon_0 \varepsilon_r \zeta}{\eta} \tag{2.10}$$

where ε_0 and ε_r are the permittivity of vacuum (8.854×10^{-12} F/m) and relative permittivity of the electrolyte respectively. The Debeye length k^{-1} (m^{-1}), which is refered to as the thickness of the double-layer, is derived from the Debeye-Hückel theory:

$$k = \sqrt{\frac{2000F^2}{\varepsilon_0 \varepsilon_r RT} I} \tag{2.11}$$

where F is the Faraday constant (96,500 C/mol).

The EOF is used extensively on microchips to pump liquids through channel structures [10,11]. For some applications the EOF is an interfering side-effect and for other applications an EOF moving to the anode instead of the cathode may be desired. The use of an electrical field applied via an electrode on the outside of a capillary can be used to alter the ζ-potential enabling electrical control over the EOF [12]. A standard method to modify the EOF is by altering or shielding the surface charge using surface coatings [13-15]. These coatings are use in chapters three to seven to tune the EOF to the desired mobility or to shield the surface in order to prevent adsorption of analytes.

2.2.3 Capillary electrophoresis separation modes

Different types of separations by means of capillary electrophoresis can be distinguished. For inorganic ions, moving boundary electrophoresis (MBE), isotachophoresis (ITP) and capillary zone electrophoresis (CZE) are the most important separation modes. MBE and ITP are often used in combination with CZE. In a CZE separation a defined sample plug is introduced into one end of a capillary that is filled with background electrolyte (BGE) (Fig. 2.2A). Upon applying a potential difference between the ends of the capillary, the cationic species migrate towards the cathode and the anionic species to the anode. The analytes separate into zones with different mobility, which are detected at the end of the capillary (Fig. 2.2B). In ITP two different BGEs are used on both sides of the sample plug (Fig. 2.2E). The terminating electrolyte (TE) contains a BGE co-ion (an ion with the same charge sign as the analyte) that has a lower mobility than the ions in the sample. The leading electrolyte (LE) contains a BGE co-ion that has a higher mobility than the ions in the sample. Under these conditions an uninterrupted train of analyte zones form (Fig.

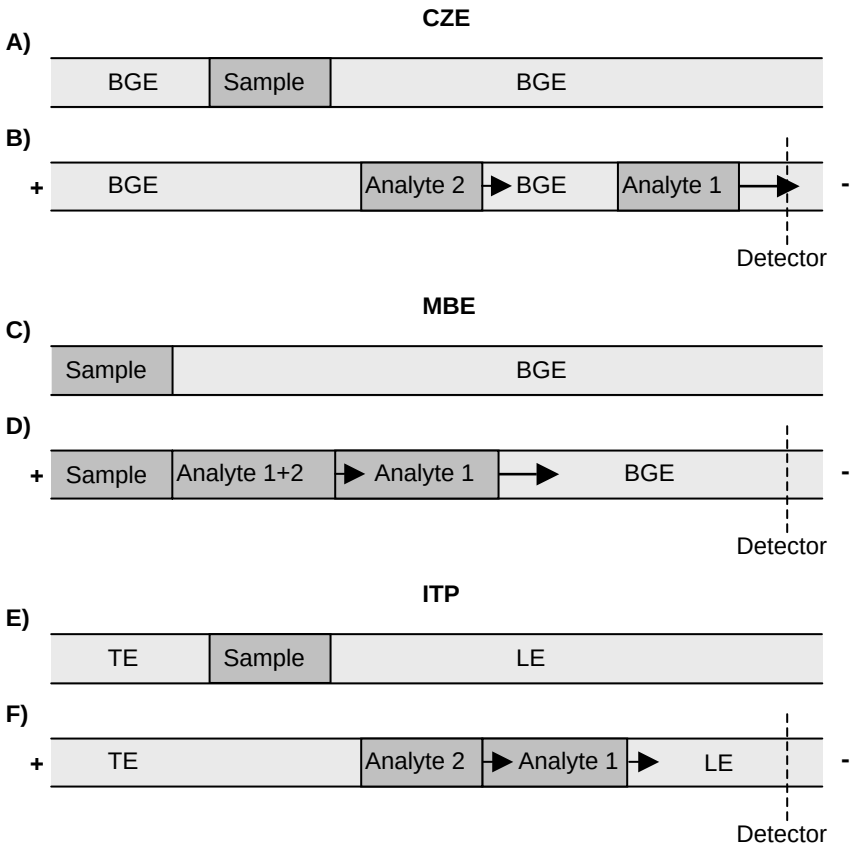

Figure 2.2: *Schematic representation of different capillary electrophoresis separation modes. A, C, E) starting situations, B, D, F) separation into zones. See the text for a description.*

2.2F). The difference with CZE is that the zones are not separated from each other by regions with BGE. In MBE the sample is not introduced as a plug, but is permanently present at the inlet of the capillary (Fig. 2.2C). Only a partial separation of the analytes occurs since apart from the leading analyte zone, all other zones contain a mixture of analytes. The MBE is an important part of the sample loading mechanism on a microchip and is discussed in detail in chapter 5. The actual separations in this thesis are all performed under CZE conditions.

2.3 Microchip design and separation performance

2.3.1 Sample loading and plug shaping

One of the differences between microchip CE and conventional CE is the method by which the sample plug is introduced into the capillary. In conventional instruments one end of the capillary is immersed in the sample solution. Sample is driven into the capillary by applying a pressure pulse (hydrodynamic injection) or by the use of EOF (electrokinetic injection) [16]. For a microchip separation a very short sample plug (<1 mm) needs to be introduced. To permit this, microchip CE devices typically employ a column coupling configuration of channels (Fig. 2.3A-H). The cross injector design and double-T in Fig. 2.3A,B are one of the earliest designs employed in microchip CE [17,18]. The sample plug is formed in the intersection of the channels using the EOF to drive sample from an inlet to a waste outlet (Fig. 2.4A). In order to prevent the sample from diffusing into the side channels an electric field from the side channels is used resulting in

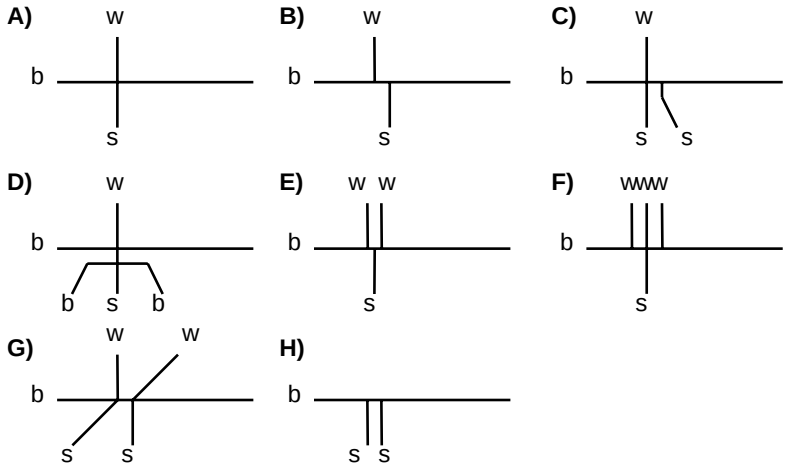

Figure 2.3: *Examples of sample injector types. A) cross, B) double-T, C) double-L, D) double cross, E) triple-T, F) multi-T, G) stacking type, H) π-injector. Sample inlet s, waste w and BGE inlet B are indicated.*

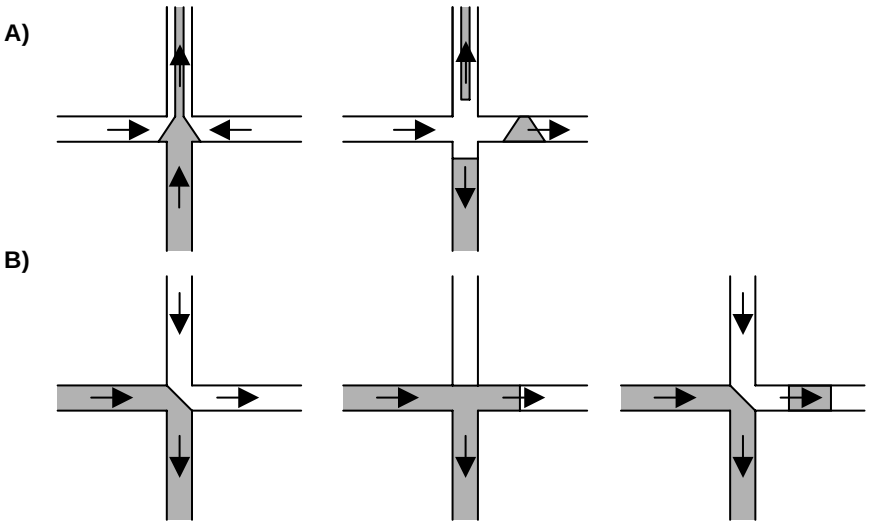

Figure 2.4: *Diagram of A) pinched sample loading and separation and B) gated injection. The sample solution is marked in grey and the background electrolyte in white. The arrows indicate the direction of the electrical field.*

a pinching effect [19]. When a sample plug is defined in the cross it is injected into the separation channel by changing the voltages applied to the fluid compartments. During the separation an electric field is used in the sample and waste channels pulling the sample away from the cross to prevent sample leaking into the separation channel. A particular advantage of this configuration is the possibility of heart cutting of zones from the sample channel, which is used in chapter 5. As the sample flows continuously through the cross, different fractions can be injected into the separation channel.

An alternative to the pinched injection is the gated injection [20]. In this approach the sample continuously flows through the cross even during the separation phase (see Fig. 2.4B). By changing the voltages the sample can be made to flow into the separation channel, whereby the length of the sample plug is defined by the duration of this step. The gated injection provides more flexibility over the length of the sample plug than a pinched injection, but is also more prone to a mobility-induced bias [21]. The mobility of a species has an effect on how much is injected, which makes the gated injection less suitable for quantitative analysis.

Over the years several refinements have been proposed to reduce leakage of sample from the cross into the separation channel and obtain better defined plugs. Examples are the double-cross [22], double-L [23], triple- and multi-T injection [24] and π-injector [25] (Fig. 2.3C-H). Also designs are made that enable a sample concentration enhancement

(Fig. 2.3G) [26]. The width of the channels leading to the cross offers another design parameter for optimization [27].

One of the advantages of electrokinetic injection is that flows are steered by applying electrical potentials to different points on the chip, which does not require mechanical components. Pressure driven injection with external pumps is also possible but is less practical because of the increased complexity [28,29]. A head-end injection mimics the injection procedure of conventional instruments but requires an autosampler to fill the microchip reproducibly [30]. Overall, the simple cross and double-T designs still are the most commonly used types owing to their simplicity. For all experiments in this thesis a double-T design is used, which provides a higher sensitivity than a cross because of the larger sample volume. The effect of the sample plug length on the separation performance is described in the next section.

2.3.2 Dimension of the microfluidic channels

The two main factors defining the microchip are the length of the separation channel and the length of the sample plug. In order to be able to compare different designs a measure to describe the performance is necessary. Following the definitions used in chromatographic separations the terms number of theoretical plates, plate height and resolution are used [31]. The plate number N is defined by the spatial variance of a zone σ^2 (m^2) after migrating a distance L (m):

$$N = \frac{L^2}{\sigma^2} \tag{2.12}$$

In analogy the plate height H (m) is given by:

$$H = \frac{L}{N} = \frac{\sigma^2}{L} \tag{2.13}$$

In the ideal case the broadening of a zone is the result of only molecular diffusion in the time interval t (s) before the analyte zone reaches the detector. The spatial variance resulting from the diffusion of an initially infinitely small zone with a diffusion coefficient D (m^2/s) is provided by the Einstein equation:

$$\sigma_{diff}^2 = 2Dt \tag{2.14}$$

Combining equations 2.5, 2.12 and 2.14 yields the plate number under ideal conditions:

$$N = \frac{\mu V}{2D} \tag{2.15}$$

This equation forms the basis of microchip CE. It shows that the separation efficiency is independent of the length of the separation channel under the conditions that the diffusion solely determines the spatial variance. The only experimentally accessible parameter is the applied voltage *V*.

The diffusion constant and electrophoretic mobility both involve movement through the medium and can be converted into one another:

$$D = \frac{\mu RT}{zF} \tag{2.16}$$

Equations 2.15 and 2.16 demonstrate that the plate number is also not affected by the mobility or diffusion constant since they cancel each other out. A more useful parameter to characterize the separation performance is the resolution R_s between two analyte peaks (see Fig. 2.5) that are separated by a distance Δx (m):

$$R_s = \frac{\Delta x}{4\sigma} = 1.18\frac{\Delta x}{w_{1/2}^{peak1} + w_{1/2}^{peak2}} \tag{2.17}$$

To calculate the resolution from experimental data it is easier to measure the width of the peak at half height, $w_{1/2}$, instead of the variance or the width at the baseline (w^1, w^2 in Fig. 2.5). Combining equations 2.5, 2.14 and 2.17 using the same diffusion constant for both analytes yields the theoretical resolution for a CE separation of two species:

$$R_s = \frac{1}{4}(\mu_1 - \mu_2)\sqrt{\frac{V}{D(\mu_1 + \mu_2 + 2\mu_{EOF})}} \tag{2.18}$$

The equations for plate number, plate height and resolution all indicate that the only way to increase the separating performance is to either increase the separation voltage or to

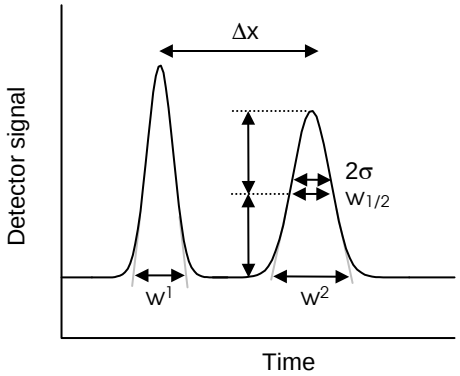

Figure 2.5: *Representation of the resolution in separation science.*

reduce the EOF. In reality diffusion is only one of many potential sources of dispersion. Also the length of the initial sample plug and the size of the detection area are not infinitely small. When these effects are taken into account it is possible to define a set of design rules for CE microchips that will provide the best performance.

The variance due to the finite length of the sample plug L_{inj} is described by [32]:

$$\sigma_{inj}^2 = \frac{L_{inj}^2}{12} \tag{2.19}$$

and similarly for the size of the detection region:

$$\sigma_{\mathrm{det}}^2 = \frac{L_{\mathrm{det}}^2}{12} \tag{2.20}$$

The spatial variance of an analyte peak is now given as the sum of the individual variances:

$$\sigma^2 = \sigma_{diff}^2 + \sigma_{inj}^2 + \sigma_{\mathrm{det}}^2 + \sigma_{\mathrm{int}}^2 \tag{2.21}$$

The last term σ_{int}^2 represents additional dispersion caused by interaction of the analytes with the capillary surface.

The resolution can thus be described as [33]:

$$R_s = \frac{L}{2} \frac{\frac{|\mu_2 - \mu_1|}{\mu_2 + \mu_1}}{\sqrt{\frac{2DLL_{cap}}{(\mu_i + \mu_{eof})V} + \frac{L_{inj}^2}{12} + \frac{L_{\mathrm{det}}^2}{12} + \sigma_{\mathrm{int}}^2}} \tag{2.22}$$

where L is the separation length and L_{cap} the total length of the capillary. It is now evident that the length of the separation channel in relation to the length of the sample plug does have an effect on the separation performance (Fig. 2.6). A calculation of the resolution between sodium and lithium shows that for baseline separation (R_s=1.5), the minimum required separation length is 3.5 mm based on a sample plug of 200 μm, 1000 V for the separation and an EOF mobility of 5×10^{-4} cm^2/V·s. The experiments performed in chapter 3, using a channel with a length of 2 cm, show that additional sources of dispersion can restrict the experimentally obtained resolution. Analyte adsorption in particular can severely restrict the performance.

For conventional CE separations fused silica capillaries ranging in length from a few decimeters up to a meter are used. It is possible to incorporate such a length onto a microchip by folding up the channel. However, the turns that are introduced are an additional source of zone broadening [34]. Although the dispersion can be kept to a minimum, following a couple of design rules (e.g. optimizing the turn radius and using narrow channels in the turns) [35], long channels are seldom used. One of the reasons is that the migration time increases due the longer migration distance while the migration velocity decreases due to the lower electrical field strength at the same voltage. This diminishes the benefits of microchip CE as a faster alternative to conventional systems. The separation channels on microchips therefore typically are shorter than 10 cm.

To calculate the electrical field strength in the channels and optimize the loading and separation voltages, the fluid channels can be modeled as a network of resistors [10]. The electric resistances R (Ω) of the four channels and the voltages V applied to the compartments define the potential V_j at the cross from which the field strength can then be calculated:

$$V_j = \frac{R_2R_3R_4V_1 + R_1R_3R_4V_2 + R_1R_2R_4V_3 + R_1R_2R_3V_4}{R_1R_2R_3 + R_2R_3R_4 + R_1R_3R_4 + R_1R_2R_4} \tag{2.23}$$

In order to reach high electrical field strengths in the separation channel, all other channels should have a low electrical resistance. This can be accomplished by making these channels as short as possible or with a large cross-sectional area. The microchips used in this thesis have an effective separation length of 2 cm and a total length of 2.6 cm between the fluidic compartments. Using 1000 V on the inlet compartment, 0 V on the outlet of the separation channel and 600 V on the two remaining compartments this provides a field strength of 330 V/cm for the chip design that will be discussed in chapter

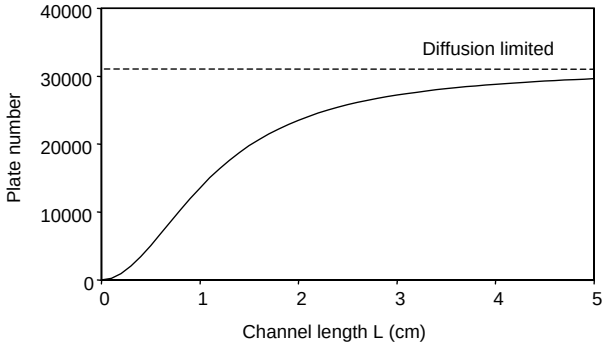

Figure 2.6: *Plate number for lithium as function of the length of the separation channel. The sample plug is 200 μm and the voltage is 1000 V.*

3. This magnitude of the electrical field strength is comparable to values reported for conventional CE.

The width and the depth of the channel also affect the performance, but in a more indirect manner. A hydrostatic pressure difference will cause a hydrodynamic flow during the separation. The flow profile has a parabolic shape, which produces additional dispersion of the zones. A pressure difference is avoided by filling all fluid compartments to the same height. However, since the channels are typically very short, the low hydrodynamic resistance can cause problems even for small pressure differences.

The variance produced in a time interval t due to the hydrodynamic flow in a channel with a square geometry is [36]:

$$\sigma_{siph}^2 = 3.36 \cdot 10^{-2} \frac{h^2 \rho^2 g^2 a^6 t}{\eta^2 L^2 D} \tag{2.24}$$

where h is the difference in height between the solution on both sides of the channel with length L and a height of $2a$, ρ is the density of the BGE and g is the gravitational constant. In another investigation that included the shape of etched channels it was found that wide and shallow channels cause less dispersion than narrow but high channels with the same cross-sectional area [37]. A hydrodynamic flow in microchips can also be induced by the surface tension of the solutions in the compartments and can be more significant than siphoning effects [38]. The use of fluidic compartments with a small diameter increases this effect.

The channel cross section also affects the electrical current through the channel, which is converted into Joule heating. The temperature gradient in the solution from the center of the capillary to the wall, where the heat is dissipated, causes different electrophoretic mobilities from the center outward. Petersen et al. derived an equation for the contribution of Joule heating to the plate height in a microchip modeled by two parallel plates at a distance d [39]:

$$H = \left(\frac{1713}{T^2} \right)^2 \frac{\mu E^5 \kappa^2 (0.5d)^6}{236.7 D k_b^2} \tag{2.25}$$

where k_b (W/m K) is the thermal conductivity off the BGE and κ (S/m) the electrical conductivity. Since the distance rises with the power of 6, a significant reduction of the plate height can be achieved by reducing the cross-section of the channels.

Roughness of the channel surface will also influence the performance due to local variations in the electrical field strength [40]. A comparison of smooth glass channels

made by chemical etching and relatively rough channels made by powderblasting (mechanical abrasion) showed a 7 to 9 times lower plate number for the latter method [41].

2.3.3 Electromigration dispersion

Electromigration dispersion (EMD) is, together with the diffusion, the most important source of band broadening. It originates from the fact that the analyte zones change the local electrical conductivity and hence the local electrical field strength. The migration velocity of a species is therefore a function of its concentration. As a result the zones develop a triangular shape shown schematically in Fig. 2.7. The larger the difference in mobility of the analyte ion and the BGE co-ion and the higher the analyte concentration in the sample, the stronger this type of dispersion is. In general the BGE will be optimized to minimize dispersion by selecting a co-ion with a mobility close to that of the analytes. However, for conductivity detection a large difference in mobilities is required for optimum sensitivity, which is discussed in section 2.4.2. Electromigration dispersion is therefore an important contributor to the peak broadening.

2.4 Detection methods for inorganic ions

A particular advantage of microchip technology is the integration of separation column and detection, which minimizes the dispersion ensuing from the dead volume. For conventional systems optical detection still is the favored method because it is applicable to most organic substances. Inorganic ions are best measured using conductivity detection, since many of these species cannot be detected directly with optical methods. Conductivity detection also suits the need for non-selective detection suitable for a universal point-of-care testing platform. More details on the design of integrated

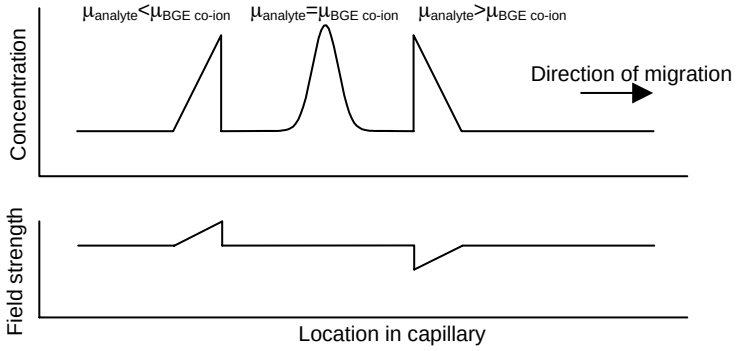

Figure 2.7: *Concentration distribution and local electrical field strength caused by electromigration dispersion and diffusion for three analytes with different mobilities.*

conductivity detection are given in section 2.4.2.

2.4.1 Detection methods compatible with capillary electrophoresis

A large variety of detection principles have been applied for inorganic ion analysis with CE. A selection of detection methods is presented in Table 2.1. For conventional CE the optical methods UV/Vis and fluorescence are the standard since most applications are developed for organic compounds. With optical methods the concentration can be measured without having to make contact with the solution. This prevents problems arising from the high-voltage used. In addition fluorescence is one of the most sensitive detection methods, while UV/Vis can be used without analyte labeling and adds an amount of selectivity by selection of the wavelength. The use of diode array detectors can help with identifying compounds. Optical detection can be integrated into microfluidic chips with the use of optical fibers and light emitting diodes [42-44]. However, many inorganic ions cannot be detected directly by optical methods. Indirect optical detection of such species is possible using absorbing species in the BGE [45,46]. The analyte displaces the absorbing species resulting in negative peaks in the signal.

Amperometric detection of redox active substances [47] and potentiometric [48] detection require no complex optics, which make these methods attractive for use in small portable instruments. Despite the very low detection limits that can be achieved with amperometric detection, these methods are not used very often. Interference by the electrical field required for the separation and the need for a stable reference electrode necessitate the use of special detectors. Using the high voltage electrode as a pseudo reference electrode eliminates the need for a real reference electrode [47], but the positioning of the working electrode and stability of the electrical field remain critical. Conductivity detection is a more straightforward choice, since all ionic species can be detected and the conductivity can be measured even from outside the capillary. On the other hand, compared to many other techniques it is challenging to achieve extremely low detection limits.

Table 2.1: *Detection methods for inorganic cations. Reproduced from ref 49.*

Detection method	*Detection limits* *Mass (mol)* *Conc. (mol/L)*	*Primary advantages*	*Primary drawbacks*
Indirect optical			
UV–Vis Absorption indirect by BGE	10^{-12}–10^{-14} 10^{-4}–10^{-6}	Universal	Relatively low sensitivity
Indirect by complexation	10^{-13}–10^{-15} 10^{-6}–10^{-8}	Sensitive	Requires derivatization
Fluorescence indirect by BGE	10^{-15}–10^{-18} 10^{-6}–10^{-9}	Sensitive, universal	Limited number of suitable fluorophores
Indirect by complexation	10^{-13}–10^{-17} 10^{-5}–10^{-7}	Sensitive, selective	Requires derivatization
Electrochemical			
Conductivity	10^{-14}–10^{-16} 10^{-4}–10^{-8}	Universal	Maintenance of electrodes
Potentiometry	10^{-13}–10^{-16} 10^{-3}–10^{-8}	Universal	Limited number of suitable ionophores
Amperometry	10^{-18}–10^{-20} 10^{-5}–10^{-11}	Sensitive, selective	Maintenance of electrodes
Direct optical			
ICP–OES	10^{-13}–10^{-16} 10^{-3}–10^{-8}	Selective	Sensitivity
Mass Spectrometry			
ESI–MS	10^{-16}–10^{-17} 10^{-8}–10^{-9}	Selective	Limited choice of buffer, sensitivity
ICP–MS	10^{-13}–10^{-16} 10^{-3}–10^{-8}	Sensitive, selective	Limited number of detectable elements
TOF–MS	10^{-13}–10^{-16} 10^{-3}–10^{-8}	Number of detectable elements	Sensitivity
Radioactivity	10^{-16}–10^{-20} 10^{-9}–10^{-13}	Selective	Requires long count times
X-ray fluorescence	10^{-13}–10^{-16} 10^{-3}–10^{-8}	Selective, number of detectable elements	Complex set-up and alignment
Photothermal	10^{-13}–10^{-16} 10^{-6}–10^{-7}	Sensitive, selective	Complex set-up and alignment

2.4.2 Conductivity detection

Conductivity detection is frequently used for microchip CE since it is relatively easily integrated into a chip device. The method is not selective and can be used for a wide range of analytes. The detection principle is based on the difference in electrical conductivity between the BGE and the analyte zones.

The conductivity κ (S/m) of a solution is given by:

$$\kappa = \Lambda c \tag{2.26}$$

Where the specific molar conductivity of the solution at infinite dilution Λ^0 (S·m^2/mol) is defined by the composition of the solution:

$$\Lambda^0 = \sum_i n_i z_i \lambda_i^0 \tag{2.27}$$

With n_i the number of moles of the i^{th} ion produced by dissociation of 1 mol of the species. The limiting equivalent ionic conductivity λ^0 (S·m^2/mol) is a constant that can be looked up in tables. There is a direct relation between the ionic conductivity and electrophoretic mobility via:

$$\lambda = zF\mu \tag{2.28}$$

The molar conductivity is also influenced by the concentration of the solution as given by the Debeye-Hückel-Onsager relation which is valid up to 20 mmol/L [7]:

$$\Lambda(c) = \Lambda^0 - (A + B\Lambda^0)\sqrt{c} \tag{2.29}$$

where the coefficient A describes the asymmetry or relaxation effect:

$$A = \frac{z^2 e_0 F^2}{3\pi\eta}\sqrt{\frac{2}{\varepsilon RT}} \tag{2.30}$$

and the coefficient B the electrophoretic effect:

$$B = \frac{qz^3 e_0 F}{24\pi\varepsilon RT}\sqrt{\frac{2}{\varepsilon RT}} \tag{2.31}$$

where q is 0.586 for monovalent electrolytes.

Whereas optical detection gives a signal directly proportional to the analyte concentration c_{A+}, the signal in conductivity detection depends on the concentration of all ions. The

conductivity is thus determined by the BGE co- and counter-ions, too. In effect, conductivity detection is a combination of indirect and direct detection, and is universally applicable. The conductivity signal ΔG (S), for an analyte A^+ in a BGE with co-ion E^+ and counter-ion E^- is under ideal conditions [50]:

$$\Delta G = \frac{c_{A^+} F}{10^{-3} K_{cell}} \left\{ \mu_{E^-} \left(1 - \frac{\mu_{E^+} \left(\mu_{A^+} + \mu_{E^-} \right)}{\mu_{A^+} \left(\mu_{E^+} + \mu_{E^-} \right)} \right) - \mu_{E^+} \frac{\mu_{E^+} \left(\mu_{A^+} + \mu_{E^-} \right)}{\mu_{A^+} \left(\mu_{E^+} + \mu_{E^-} \right)} + \mu_{A^+} \right\} \qquad (2.32)$$

where the cell constant K_{cell} is defined by the design of the detection cell, which is discussed in section 2.4.3. The term in Eq. 2.32 containing the mobilities provide guidelines for optimizing the BGE with respect to the sensitivity. The value of this part of the function is plotted in Fig. 2.8 for a fictive analyte with a mobility of 25×10^{-9} m^2/Vs. It shows that there is no signal at all for a BGE with a co-ion with the same mobility as the analyte. The signal increases for both faster and slower co-ion mobilities. However, under these conditions the EMD also increases as discussed in section 2.3.3 and a compromise between sensitivity and EMD has to be found. The BGE counter-ion has a limited effect, but the signal increases for counter-ions with a higher mobility.

In conclusion, conductivity detection is favorable for the detection of inorganic ions,

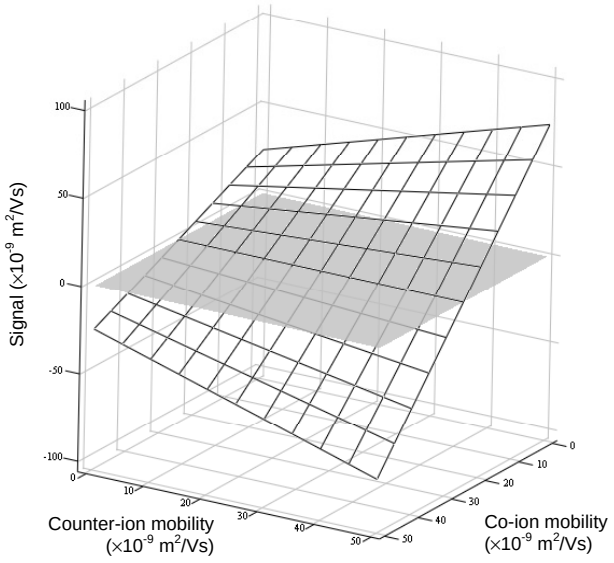

Figure 2.8: *Conductivity signal for a species with an electrophoretic mobility of 25×10^{-9} m^2/Vs as function of the BGE co- and counter-ion mobility. Calculated from Eq. 2.32 using the right hand term only.*

which typically have a high electrophoretic mobility. Complex optical equipment that would restrict the use of the system as a low-cost portable system is therefore not required. However, the choice of BGE is a compromise between sensitivity and electromigration dispersion. In chapter 3, simulations are performed, which demonstrate that for the analysis of inorganic ions the EMD attributes more to the dispersion than the diffusion. In practice however, additional dispersive affects such as interaction of analytes with the surface of the microchip bring about even more zone broadening than the EMD, which is also shown chapter 3. Section 2.4.3 discusses the details for implementing conductivity detection on the CE microchip.

2.4.3 On-chip electrolyte conductivity measurement

To measure the conductivity two electrodes are integrated into the chip that make contact with the solution. Several designs have been manufactured shown in Fig. 2.9A-E. The conductivity is derived from the electrical current I (A) that flows through the electrodes for a potential difference U (V) applied between them. The electrical resistance R (Ω) or conductance G (S) follows from Ohm's law:

$$R = \frac{1}{G} = \frac{U}{I} \tag{2.33}$$

The area of the electrodes in contact with the solution and the distance between them define the measuring cell with a certain cell constant K_{cell} (1/m). The relation between the electrical conductivity of the solution and the measured conductance is subsequently given by:

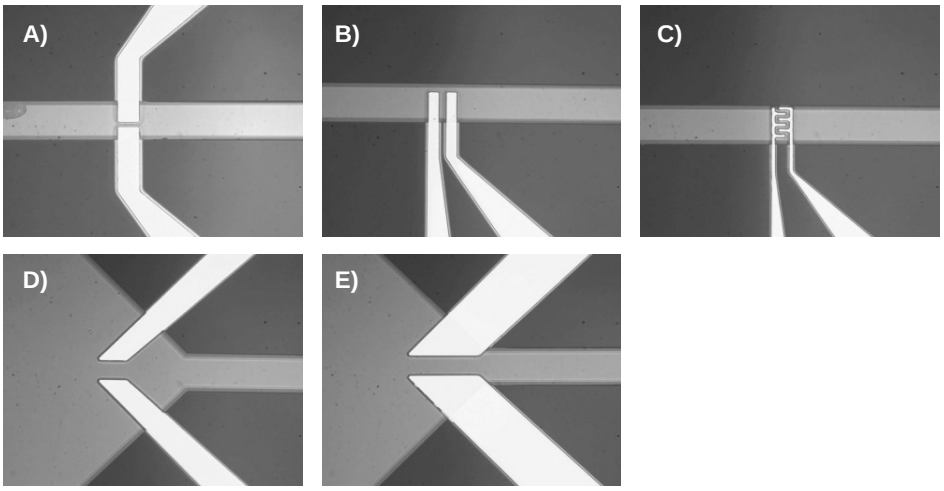

Figure 2.9: *Photographs of CE chips with different layouts of the conductivity detection electrodes (bright structure). The width of the channel is 56 μm in all chips.*

$$\kappa = K_{cell} G \tag{2.34}$$

For two parallel electrodes with an area A (m^2) at a distance d (m) as shown in Fig. 2.10A, the cell constant can be approximated by:

$$K_{cell} = \frac{d}{A} \tag{2.35}$$

Due to fringing of the electrical fields at the edges of the electrodes the experimentally determined cell constant will differ slightly. In many microchip devices the two electrodes are in the same plane since this is simpler to fabricate (Fig. 2.10B,C). For this layout the cell constant can be calculated from [51]:

$$K_{cell} = \frac{1}{(N-1)L} \frac{2K(k)}{K\sqrt{1-k^2}} \tag{2.36}$$

where N is the number of electrode fingers with a length L (cm) and width w (cm), $K(k)$ is the elliptical integral of the first kind:

$$K(k) = \int_0^1 \frac{1}{\sqrt{(1-x^2)(1-k^2x^2)}} dx \tag{2.37}$$

where for two fingers k is:

$$k = \frac{d}{d+w} \tag{2.38}$$

and for more than two fingers:

$$k = \cos\left(\frac{\pi}{2}\frac{w}{d+w}\right) \tag{2.39}$$

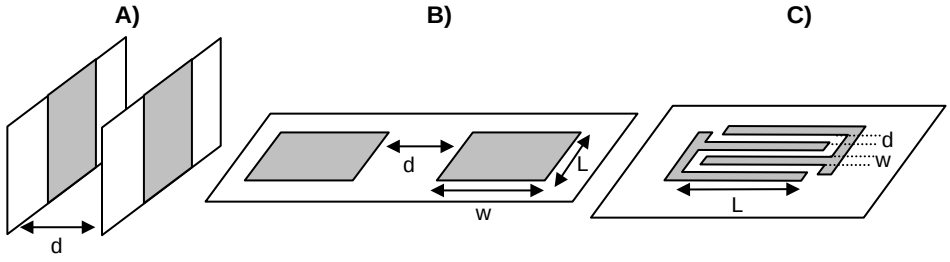

Figure 2.10: *Typical conductivity cell geometries. A) parallel, B) in-plane, C) interdigitated fingers.*

As shown by Eq. 2.32 the signal increases with smaller cell constants. As a rule of thumb for interdigitated electrodes, the cell constant decreases with smaller spacing and larger length. The optimum ratio between distance and width, d/w is 0.54 for finger electrodes [52]. The design with interdigitated electrodes in Fig. 2.9C will have a lower cell constant than a cell with two rectangular electrodes shown in Fig. 2.9A,B. The electrodes in Fig. 2.9D,E have a larger area but also a larger distance between them. In practice the designs A, B and D have a similar cell constant and also C and E. For microchips based on the design shown in Fig. 2.11A, with electrodes of different dimensions inside a microfluidic channel, the conductivity response was measured. Two solutions with different conductivity where flushed through the channel in succession. Figure 2.11B shows that the conductivity response scales linearly with the length *L* (the dimension parallel to the channel) of the electrode. The same behavior is observed for the distance *d* between the electrodes (Fig. 2.11C).

The electrical characteristics of the conductivity cell can be modeled by an electrical circuit shown in Fig. 2.12A [53]. The resistance of the electrolyte solution R_{el} is part of a complex circuit of capacitors and resistors. The electrical double layer at the surface of the electrodes forms a capacitance C_{DL} (F). The two electrodes itself also form a capacitor C_{cell} (F). When an electrochemical reaction takes place at the electrodes, a Faradaic

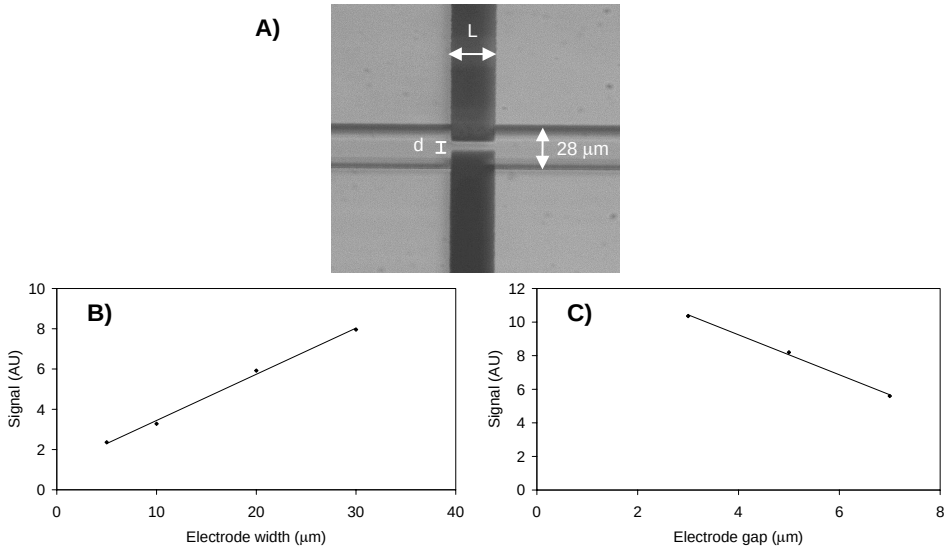

Figure 2.11: *A) Photograph of one of the test structures to measure the sensitivity of different electrode sizes. The electrode is shown in dark and the channel is 28 µm wide and 8 µm deep. B) Measured conductivity signal as function of the length of the electrodes with a constant electrode distance of 3 µm, C) signal as function of the electrode distance for electrodes 30 µm long. The signal is produced by flushing alternately 20 mmol/L MES/His (0.49 mS/m) and 0.7458 g/L KCl (1.32 mS/m) through the chip.*

current flows through the branch formed by the reaction resistance $R_{reaction}$, diffusion resistance $R_{diffusion}$ and diffusion capacitance $C_{diffusion}$. In practice an alternating voltage is used to capacitively couple the electric field into the solution via the double layer capacitance C_{DL}. This is achieved by using inert electrodes (e.g. platinum) and a low voltage (<1.2 V, the starting point of the electrolysis of water), which allows the electrical conductivity of the electrolyte solution to be measured without interference by Faradaic currents causing electrochemical reactions to take place. The equivalent model of the conductivity cell in Fig. 2.12A can therefore be simplified to the form shown in Fig. 2.12B.

The frequency f (Hz) dependent impedance Z (Ω) for this model is given by contributions from the impedances formed by the double layer capacitance C_{DL}, the electrolyte resistance R_{el} and the combination of the cell capacitance with any parasitic capacitances C_{cell} [54]:

$$Z = \frac{2}{j2\pi fC_{DL}} + \frac{R_{el}}{1 + j2\pi fR_{el}C_{cell}} \tag{2.40}$$

in which j is the imaginary unit.

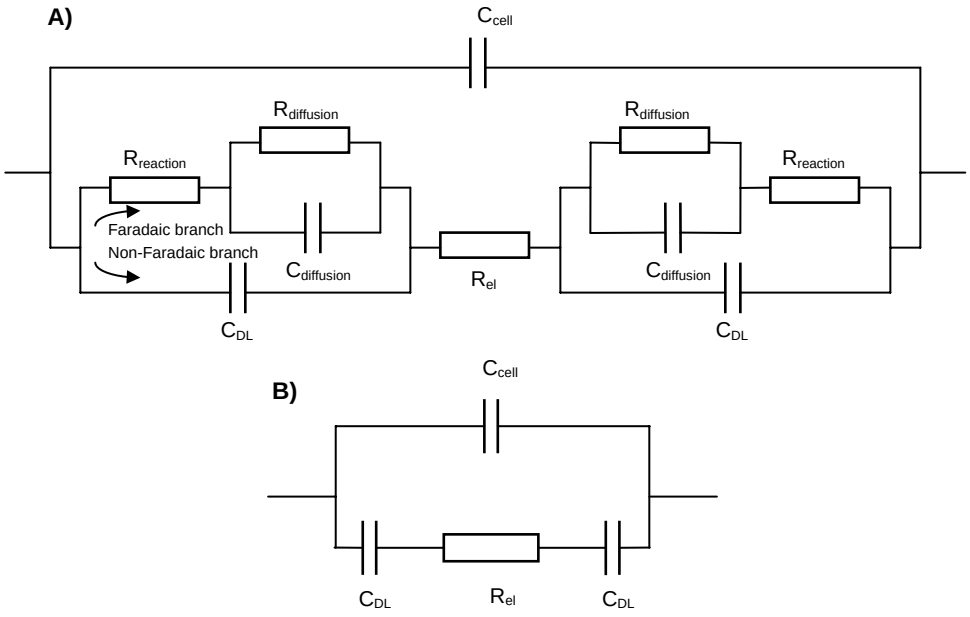

Figure 2.12: *A) Electrical equivalent circuit and B) simplified circuit of the detection cell.*

The cell capacitance follows from the cell constant and the relative permittivity ε_{el} of the electrolyte solution:

$$C_{cell} = \frac{\varepsilon_{el}\varepsilon_0}{K_{cell}} \tag{2.41}$$

The double layer capacitance is comprised of contributions by the Stern layer (approximately 20 μF/cm^2) and the diffusive layer. The latter can be calculated from the thickness of the diffusive layer (Debye length) [54]:

$$C_{DL} = C_{Stern} + C_{Diffuse} = C_{Stern} + A\sqrt{\frac{2\cdot 10^{-3} z^2 e_0^2 \varepsilon_{el}\varepsilon_0 c N_A}{kT}} \tag{2.42}$$

where k is Boltzman's constant (1.38×10^{-23} J/K) and N_A Avogadro's constant (6.022×10^{23} 1/mol). The impedance as function of the frequency calculated for various electrolyte resistances using Eq. 2.40 is shown in Fig. 2.13A. Only in a limited frequency range the impedance is determined mainly by the electrolyte resistance R_{el}. The conductance of the circuit (the real part of the solution of Eq. 2.40) is linear only in a limited range of conductivities (Fig. 2.13B). Deviation from linearity occurs due to the double layer capacitance at high solution conductivity and the cell capacitance at low conductivity. The conductivity of the electrolyte, the layout of the detection electrodes and the detector all have to be tuned to each other for maximum sensitivity and linearity.

Figure 2.14 shows the impedance spectra measured for the electrodes shown in Fig. 2.9A-E. Typical for the large electrodes is that there is a reduced effect of the double layer capacitance, while the interdigitated finger design measures the lowest electrolyte resistance. Because the capacitances in the design of Fig. 2.9D and E affect the measured

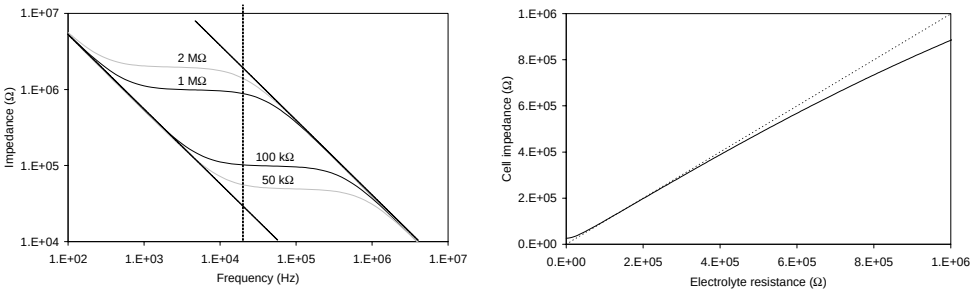

Figure 2.13: *A) Calculated impedance spectrum for various electrolyte resistances and B) cell impedance versus electrolyte resistance at a frequency of 20 kHz. C_{DL} is 600 pF and C_{Cell} is 4 pF and have been estimated from actual impedance measurements.*

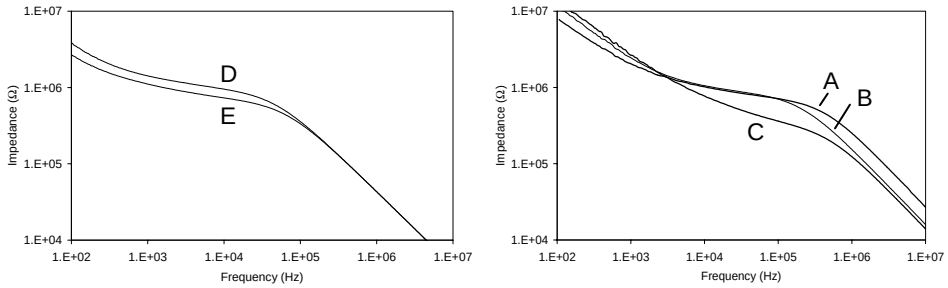

Figure 2.14: *Impedance spectra for chips with different electrode designs. The curves correspond with the electrode designs shown in Fig. 2.9. The chips are filled with a BGE consisting of 20 mmol/L MES/His and 1 mmol/L KCl.*

impedance less than in the other designs, the response of the detection cell based on this layout is linear over a wider frequency and concentration range. However, because of the larger cell constant this layout provides less sensitivity than for example the interdigitated electrodes shown in Fig. 2.9C.

2.4.4 Implementation of on-chip conductivity detection

Placing detection electrodes into an electrolyte solution to which up to 1000 V is applied necessitates full decoupling of the high-voltage circuit and detection electronics. Electrolysis will take place as soon as a DC current is able to flow from the high-voltage supply via the electrolyte solution through the detection electrodes and back to the high-voltage supply via ground. The gas formation coinciding with the electrolysis will subsequently interfere with the detection. One way to prevent this is to place the electrodes close to the end of the channel where the electrical potential is low. By connecting the high-voltage electrode in the outlet compartment to ground, the potential at the detection electrodes can never reach high values. The detector used in this thesis allows a potential of less than 10 V on the electrodes before it starts to conduct a current. By widening the channel at the end as is shown in Fig. 2.9D,E the potential in this section drops rapidly. Alternatively, the potential can be measured with an additional electrode so that the potential on the detection electrodes can be actively matched to the solution [55].

As is shown by Eq. 2.32 the highest sensitivity is obtained for a low cell constant, which requires the use of electrodes with a large area. However, a potential difference develops along the length of an electrode due to the electric field used for the CE separation. At a certain electrode size the potential difference reaches a certain threshold value resulting in the onset of oxidation reactions at one end and reduction at the other end of the electrode [56]. For example, when using an electrical field of 300 V/cm the electrodes should be smaller than 40 μm in order to obtain a voltage drop below the 1.2 V at which electrolysis

starts. Also when using electrodes that are at a different potential as in Fig. 2.9B the detector has to be constructed such that no DC current can pass between the electrodes.

The easiest way to decouple the detection electronics from the high-voltage is to isolate the electrodes from the electrolyte [57]. This contactless conductivity detection was originally used for conventional CE by placing metal electrodes around the fused silica capillaries [58]. To increase the sensitivity voltages of up to 500 V can be used and electrodes can be placed in the holder instead of on the chip making the chip much easier to fabricate [59]. Yet, the linearity and sensitivity are strongly influenced by the thickness and electrical properties of the insulating layer [60]. To eliminate the effect of the capacitance of the insulating layer, a four-electrode arrangement can be used [61]. This technique extends the working range to much lower detection frequencies. But still, to probe only a small sample volume the insulating layer has to be very thin, which can cause problems due to electrical breakdown. For example, a 30 nm silicon carbide film breaks down at 3 to 9 volt [55,62]. For short separation channels the size of the detection region has to be as small as possible so that it does not affect the separation resolution (Eq. 2.20). This means that only thin insulating layers can be used, which are prone to electrical breakdown. In this thesis contact detection is therefore used together with a custom-made detector and a high-voltage supply that are electrically decoupled. This permits the use of a simple chip design, while offering high sensitivity and linearity.

2.5 Background electrolyte

The main function of the BGE is to provide an electrically conductive medium that has buffering properties. Microchips generally have small fluid compartments, which can result in a rapid change of pH due to the electrolysis products accumulating in a restricted volume [63]. Changes in the pH alter the effective mobility of weak electrolytes and the mobility of the EOF. The species selected for the BGE should therefore exhibit excellent buffering capacity. For applications where the BGE enables the indirect detection of analytes, also the concentration of at least one of its constituents has to be measurable. In the case of conductivity detection, the main consideration for the selection of the BGE is the sensitivity, which is influenced by the mobility of the BGE ions (Eq. 2.32).

The BGE concentration needs to be optimized for minimal electromigration dispersion (EMD). At low BGE concentrations the EMD is excessive, while at high concentrations the Joule heating causes additional dispersion. A sufficiently high BGE also provides the conditions for sample stacking [64,65]. This is a process that occurs at the start of the separation when the ions migrate out of the sample matrix and into the BGE, resulting in a compression of the sample plug. Under most circumstances the sample solution has a lower conductivity than BGE solution. As a result the electrical field strength is higher in the sample plug than in the remainder of the capillary (Fig. 2.15A). The analytes quickly

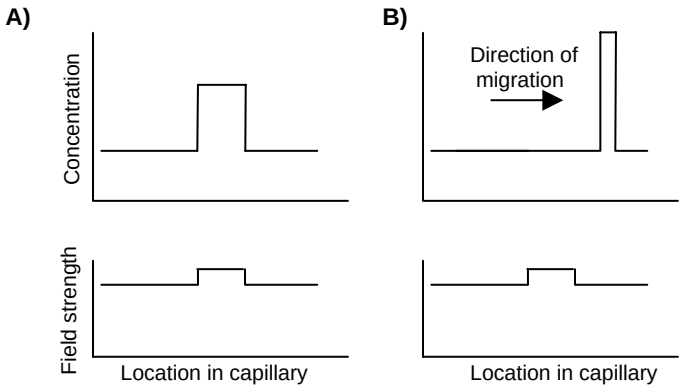

Figure 2.15: *Schematic representation of the stacking of a sample plug. A) Starting conditions, B) after stacking.*

migrate out of the sample plug and slow down as they enter the BGE. The analyte zone therefore is compressed into a smaller volume with an increased concentration (Fig. 2.15B). The ions in the original sample plug are displaced by ions from the BGE, but at a lower concentration. This resulting zone is detected as a negative peak in conductivity detection and is refered to as the water peak or EOF peak. Stacking typically is used to enable the injection of a large sample plug with a low analyte concentration, which is then automatically concentrated. In chapter 5 the opposite process is used to dilute samples with a high ionic strength.

In chapter 3 simulations are performed to optimize the BGE concentration. A BGE which is often cited for conductivity detection is an equimolar mixture of 2-(N-morpholino)ethanesulfonic acid (MES) and histidine (His). These substances have an almost identical pK_a, which means that both are buffering when put into solution together. Furthermore they have a low electrophoretic mobility which makes them suitable for sensitive conductivity detection. This BGE composition is therefore used in this work as the starting point for optimization of the microchip system.

2.6 Chip interfacing to the outside world

Very little has been published on the interface between the microchip and the outside world. Most designs require manual filling of the microchips with sample and BGE. The use of an autosampler, which is used for example by the Shimadzu MCE-2010 instrument provides repeatable liquid handling, but makes the instrument large and heavy. A flow-through microchip has been presented utilizing channels with a low flow resistance for automated sampling [66]. By using channels with a high flow resistance for the CE separation the dispersion can be kept to a minimum. Another design allows the sample

compartment to overflow with excess solution [67]. For point-of-care applications a microchip needs to be used only once. Sampling using a painless needle and an EOF pump has been demonstrated [68], but this device does not include a CE channel. Silicon microneedle arrays have been coupled to CE microchips, and promising first results were achieved [69,70]. However, actual sampling by puncturing the skin with the needles has not yet been demonstrated. In chapter 6 various new methods to sample blood onto the chip are investigated.

2.7 Conclusions

In order to design a CE microchip optimized for analyzing inorganic ions many factors need to be considered. The length of the sample plug and separation channel are important parameters affecting the separation efficiency. Channels in the order of a centimeter can be used for rapid separations when a sufficiently short sample plug is introduced by means of a double-T or cross injector. In order to minimize the dispersion due to hydrodynamic flow and Joule heating, the cross-sectional area of the channels should be as small as possible, without impeding the required volume or path length for detection.

The use of conductivity detection can provide a simple microchip without the need of complex optics. Contactless conductivity detection provides more freedom in the design and placement of the electrodes than the use of contact detection, but it may also reduce the sensitivity and resolution. The geometry of the electrodes measuring the conductivity is crucial for optimizing the sensitivity. The sensitivity improves for detection electrodes with a low cell constant. However, the space available inside the channel restricts the size of the electrodes.

Optimization of the BGE is a tradeoff between detection sensitivity and separation resolution. The sensitivity increases when a BGE co-ion is selected that has a much higher or lower electrophoretic mobility than the analyte. However, this also leads to increased electromigration dispersion. The use of high ionic strength BGEs provides conditions that enable sample stacking, resulting in a concentration enhancement, but can also enhance the dispersion due to increased Joule heating.

The complete chip design is therefore a compromise between separation speed, separation power and detection limits. The chip has to be designed to meet the desired operational criteria for the intended application. Based on the guidelines presented in this chapter a chip is designed and tested in chapter 3 for the analysis of inorganic ions.

2.8 References

1. JW Jorgenson and KD Lukacs "*Zone Electrophoresis in Open-Tubular Glass Capillaries"*, Anal. Chem. 1981, **53**, 1298-1302.
2. V Pacáková, P Coufal, K Štulik and B Gaš "*The importance of capillary electrophoresis, capillary electrochromatography, and ion chromatography in separations of inorganic ions"*, Electrophoresis 2003, **24**, 1883-1891.
3. WG Kuhr "*Capillary Electrophoresis"*, Anal. Chem. 1990, **62**, 403R-414R.
4. WG Kuhr and CA Monnig "*Capillary Electrophoresis"*, Anal. Chem. 1992, **64**, 389R-407R.
5. JP Landers (ed.) "*Handbook of capillary electrophoresis"*, 2nd edition, 1997, CRC Press
6. R Kuhn and S Hoffstetter-Kuhn. "*Capillary electrophoresis: principles and practice"*, 1st edition, 1993, Berlin, Springer-Verlag
7. PW Atkins. "*Concepts in physical chemistry"*, 1st edition, 1995, Oxford University Press
8. J Pospíchal, P Gebauer and P Bocek "*Measurement of Mobilities and Dissociation Constants by Capillary Isotachophoresis"*, Chem. Rev. 1989, **89**, 419-430.
9. W Friedl, JC Reijenga and E Kenndler "*Ionic strength and charge number correction for mobilities of multivalent organic anions in capillary electrophoresis"*, J. Chromatogr. A 1995, **709**, 163-170.
10. K Seller, Z Fan, K Fluri and DJ Harrison "*Electroosmotic Pumping and Valveless Control of Fluid Flow within a Manifold of Capillaries on a Glass Chip"*, Anal. Chem. 1994, **66**, 3485-3491.
11. SC Jacobson, TE McKnight and JM Ramsey "*Microfluidic Devices for Electrokinetically Driven Parallel and Serial Mixing"*, Anal. Chem. 1999, **71**, 4455-4459.
12. RBM Schasfoort, S Schlautmann, J Hendrikse and A Van den Berg "*Field-Effect Flow Control for Microfabricated Fluidic Networks"*, Science 1999, **286**, 942-945.
13. J Horvath and V Dolník "*Polymer wall coatings for capillary electrophoresis"*, Electrophoresis 2001, **22**, 644-655.
14. PG Righetti, C Gelfi, B Verzola and L Castelletti "*The state of the art of dynamic coatings"*, Electrophoresis 2001, **22**, 603-611.
15. EAS Doherty, RJ Meagher, MN Albarghouthi and AE Barron "*Microchannel wall coatings for protein separations by capillary and chip electrophoresis"*, Electrophoresis 2003, **24**, 34-54.
16. TT Lee and ES Yeung "*Compensating for Instrumental and Sampling Biases Accompanying Electrokinetic Injection in Capillary Zone Electrophoresis"*, Anal. Chem. 1992, **64**, 1226-1231.
17. DJ Harrison, A Manz, Z Fan, H Lüdi and HM Widmer "*Capillary Electrophoresis and Sample Injection Systems Integrated on a Planar Glass Chip"*, Anal. Chem. 1992, **64**, 1926-1932.

18. CS Effenhauser, A Manz and HM Widmer "*Glass Chips for High-speed Capillary Electrophoresis Separations with Submicrometer Plate Heights"*, Anal. Chem. 1993, **65**, 2637-2642.
19. SC Jacobson, R Hergenröder, LB Koutny, RJ Warmack and JM Ramsey "*Effects of Injection Schemes and Column Geometry on the Performance of Microchip Electrophoresis Devices"*, Anal. Chem. 1994, **66**, 1107-1113.
20. SC Jacobson, SV Ermakov and JM Ramsey "*Minimizing the Number of Voltage Sources and Fluid Reservoirs for Electrokinetic Valving in Microfluidic Devices"*, Anal. Chem. 1999, **71**, 3273-3276.
21. BE Slentz, NA Penner and F Regnier "*Sampling BIAS at Channel Junctions in Gated Flow Injection on Chips"*, Anal. Chem. 2002, **74**, 4835-4840.
22. L-M Fu, R-J Yang and G-B Lee "*Electrokinetic Focusing Injection Methods on Microfluidic Devices"*, Anal. Chem. 2003, **75**, 1905-1910.
23. L-M Fu and C-H Lin "*High-resolution DNA separation in microcapillary electrophoresis chips utilizing double-L injection techniques"*, Electrophoresis 2004, **25**, 3652-3659.
24. L-M Fu, R-J Yang, G-B Lee and H-H Liu "*Electrokinetic Injection Techniques in Microfluidic Chips"*, Anal. Chem. 2002, **74**, 5084-5091.
25. CA Emrich and RA Mathies "The π-injector: a new electrokinetic dispensing element for microdevice separations". In: Y Baba, S Shoji, and A Van den Berg, eds. Proceedings of micro total analysis systems 2002. Dordrecht: Kluwer academic publishers, vol. 2, 748-750
26. J Lichtenberg, E Verpoorte and NF De Rooij "*Sample preconcentration by field amplification stacking for microchip-based capillary electrophoresis"*, Electrophoresis 2001, **22**, 258-271.
27. CX Zhang and A Manz "*Narrow Sample Channel Injectors for Capillary Electrophoresis on Microchips"*, Anal. Chem. 2001, **73**, 2656-2662.
28. X Bai, HJ Lee, JS Rossier, F Reymond, H Schafer, M Wossner and HH Girault "*Pressure pinched injection of nanolitre volumes in planar micro-analytical devices"*, Lab on a Chip 2002, **2**, 45-49.
29. NY Lee, M Yamada and M Seki "*Pressure-Driven Sample Injection with Quantitative Liquid Dispensing for On-Chip Electrophoresis"*, Anal. Sci. 2004, **20**, 483-487.
30. RM Guijt, E Baltussen, G Van der Steen, RBM Schasfoort, S Schlautmann, HAH Billiet, J Frank, GWK Van Dedem and A Van den Berg " *New approaches for fabrication of microfluidic capillary electrophoresis devices with on-chip conductivity detection"*, Electrophoresis 2001, **22**, 235-241.
31. JC Giddings "*Generation of Variance, "Theoretical Plates," Resolution, and Peak Capacity in Electrophoresis and Sedimentation"*, Separation Science 1969, **4**, 181-189.
32. JC Sternberg "*Extracolumn contributions to chromatographic band broadening"*, Adv. Chromatogr. 1966, **2**, 206-270.

33. X Huang, WF Coleman and RN Zare "*Analysis of factors causing peak broadening in capillary zone electrophoresis"*, J. Chromatogr. 1989, **480**, 95-110.
34. CT Culbertson, SC Jacobson and JM Ramsey "*Dispersion Sources for Compact Geometries on Microchips"*, Anal. Chem. 1998, **70**, 3781-3789.
35. SK Griffiths and RH Nilson "*Design and Analysis of Folded Channels for Chip-Based Separations"*, Anal. Chem. 2002, **74**, 2960-2967.
36. A Cifuentes, MA Rodrigues and FJ García-Montelongo "*Rectangular capillary electrophoresis: study of some dispersive effects"*, J. Chromatogr. A 1996, **737**, 243-253.
37. D Dutta and DTJr Leighton "*Dispersion Reduction in Pressure-Driven Flow Through Microetched Channels"*, Anal. Chem. 2001, **73**, 504-513.
38. HJ Crabtree, ECS Cheong, DA Tilroe and CJ Backhouse "*Microchip Injection and Separation Anomalies Due to Pressure Effects"*, Anal. Chem. 2001, **73**, 4079-4086.
39. NJ Petersen, RPH Nikolajsen, KB Mogensen and JP Kutter "*Effect of Joule heating on efficiency and performance for microchip-based and capillary-based electrophoretic separation systems: A closer look"*, Electrophoresis 2004, **25**, 253-269.
40. GW Slater and P Mayer "*Electrophoretic resolution versus fluctuations of the lateral dimensions of a capillary"*, Electrophoresis 1995, **16**, 771-779.
41. Q-S Pu, R Luttge, JGE Gardeniers and A Van den Berg "*Comparison of capillary zone electrophoresis performance of powder-blasted and hydrogen fluoride-etched microchannels in glass"*, Electrophoresis 2003, **24**, 162-171.
42. S Qi, X Liu, S Ford, J Barrows, G Thomas, K Kelly, A McCandless, K Lian, K Goettert and SA Soper "*Microfluidic devices fabricated in poly(methyl methacrylate) using hot-embossing with integrated sampling capillary and fiber optics for fluorescence detection"*, Lab on a Chip 2002, **2**, 88-95.
43. K Uchiyama, W Xu, J Qiu and T Hobo "*Polyester microchannel chip for electrophoresis – incorporation of a blue LED as light source"*, Fresenius J. Anal. Chem. 2001, **371** , 209-211.
44. ML Chabinyc, DT Chiu, JC McDonald, AD Stroock, JF Christian, AM Karger and GM Whitesides "*An Integrated Fluorescence Detection System in Poly(dimethylsiloxane) for Microfluidic Applications"*, Anal. Chem. 1 A.D.
45. P Doble and PR Haddad "*Indirect photometric detection of anions in capillary electrophoresis"*, J. Chromatogr. A 1999, **834**, 189-212.
46. I Haumann, J Boden, A Mainka and U Jegle "*Simultaneous determination of inorganic anions and cations by capillary electrophoresis with indirect UV detection"*, J. Chromatogr. A 2000, **895**, 269-277.
47. MA Schwarz, B Galliker, K Fluri, T Kappes and PC Hauser "*A two-electrode configuration for simplified amperometric detection in a microfabricated electrophoretic separation device"*, Analyst 2001, **126**, 147-151.

48. J Tanyanyiwa, S Leuthardt and PC Hauser "*Conductimetric and potentiometric detection in conventional and microchip capillary electrophoresis"*, Electrophoresis 2002, **23**, 3659-3666.
49. C Vogt and GL Klunder "*Separation of metal ions by capillary electrophoresis - diversity, advantages, and drawbacks of detection methods"*, Fresenius J. Anal. Chem. 2001, **370**, 316-331.
50. MU Katzmayr, CW Klampfl and W Buchberger "*Optimization of conductivity detection of low-molecular-mass anions in capillary zone electrophoresis"*, J. Chromatogr. A 1999, **850**, 355-362.
51. W Olthuis, W Streekstra and P Bergveld "*Theoretical and experimental determination of cell constants of planar-interdigitated electrolyte conductivity sensors"*, Sens. Actuators B 1995, **24-25**, 252-256.
52. GR Langereis "An integrated sensor system for monitoring washing processes" 1999 PhD Thesis
53. P Jacobs, A Varlan and W Sansen "*Design optimisation of planar electrolytic conductivity sensors"*, Med. & Biol. Eng. & Comput. 1995, **33**, 802-810.
54. B Timmer, W Sparreboom, W Olthuis, P Bergveld and A van den Berg "*Optimization of an electrolyte conductivity detector for measuring low ion concentrations"*, Lab on a Chip 2002, **2**, 121-124.
55. J Bastemeijer, W Lubking, F Laugere and M Vellekoop "*Electronic protection methods for conductivity detectors in micro capillary electrophoresis devices"*, Sens. Actuators B 2002, **83**, 98-103.
56. A Arora, JCT Eijkel, WE Morf and A Manz "*A Wireless Electrochemiluminescence Detector Applied to Direct and Indirect Detection for Electrophoresis on a Microfabricated Glass Device"*, Anal. Chem. 2001, **73**, 3282-3288.
57. J Lichtenberg, NF De Rooij and E Verpoorte "*A microchip electrophoresis system with integrated in-plane electrodes for contactless conductivity detection"*, Electrophoresis 2002, **23**, 3769-3780.
58. B Gaš, M Demjanìnko and J Vacík "*High-frequency contactless conductivity detection in isotachophoresis"*, J. Chromatogr. 1980, **192**, 253-257.
59. J Tanyanyiwa and PC Hauser "*High-voltage contactless conductivity detection of metal ions in capillary electrophoresis"*, Electrophoresis 2002, **23**, 3781-3786.
60. F Laugere, GW Lubking, A Berthold, J Bastemeijer and MJ Vellekoop "*Downscaling aspects of a conductivity detector for application in on-chip capillary electrophoresis"*, Sens. Actuators A 2001, **92**, 109-114.
61. F Laugere, RM Guijt, J Bastemeijer, G van der Steen, A Berthold, E Baltussen, P Sarro, GWK van Dedem, M Vellekoop and A Bossche "*On-Chip Contactless Four-Electrode Conductivity Detection for Capillary Electrophoresis Devices"*, Anal. Chem. 2003, **75**, 306-312.
62. A Berthold, F Laugere, H Schellevis, CR De Boer, M Laros, RM Guijt, PM Sarro and MJ Vellekoop "*Fabrication of a glass-implemented microcapillary electrophoresis*

device with integrated contactless conductivity detection", Electrophoresis 2002, **23**, 3511-3519.

63. MS Bello "*Electrolytic modification of a buffer during a capillary electrophoresis run"*, J. Chromatogr. A 1996, **744**, 81-91.
64. JL Beckers and P Boček "*Sample stacking in capillary zone electrophoresis; Principles, advantages and limitations"*, Electrophoresis 2000, **21**, 2747-2767.
65. ZK Shihabi "*Stacking in capillary zone electrophoresis"*, J. Chromatogr. A 2000, **902**, 107-117.
66. S Attiya, AB Jemere, T Tang, G Fitzpatrick, K Seiler, N Chiem and DJ Harrison "*Design of an interface to allow microfluidic electrophoresis chips to drink from the fire hose of the external environment"*, Electrophoresis 2001, **22**, 318-327.
67. Q Fang, G-M Xu and Z-L Fang "*A High-Throughput Continuous Sample Introduction Interface for Microfluidic Chip-based Capillary Electrophoresis Systems"*, Anal. Chem. 2002, **74**, 1223-1231.
68. A Oki, M Takai, H Ogawa, Y Takamura, T Fukasawa, J Kikuchi, Y Ito, T Ichiki and Y Horiike "*Healthcare Chip for Checking Health Condition from Analysis of Trace Blood Collected by Painless Needle"* , Jpn. J. Appl. Phys. 2003, **42**, 3722-2727.
69. EX Vrouwe, R Luttge, and A van den Berg "Sampling for point-of-care analysis of whole blood with microchip CE". In: T Laurell, J Nilson, K Jensen, DJ Harrison, and JP Kutter, eds. Proceedings of micro total analysis systems 2004. Cambridge: The Royal Society of Chemistry, vol. 1, 503-505
70. R Luttge, HJGE Gardeniers, EX Vrouwe, and A van den Berg "Microneedle array interface to CE on chip". In: MA Northrup, KF Jensen, and DJ Harrison, eds. Proceedings of micro total analysis systems 2003. San Diego: Transducers Research Foundation, vol. 1, 511-514

Chapter 3

Capillary electrophoresis of metal ions in glass microchips

In this chapter the separation performance of capillary electrophoresis chips made from glass is evaluated. The experimental results obtained for the analysis of alkali metal solution show restricted performance compared to electrophoresis simulations. The problem is identified as an interaction of the analytes with the glass surface, resulting in peak tailing and the splitting of single analyte peaks. The separation is optimized using a surface coating or the addition of 0.5 mmol/L potassium to the background electrolyte, which provides baseline separation of solutions containing potassium, sodium and lithium. Furthermore the effect of annealing the chips on the performance is investigated. Five batches of chips made in consecutive months show an aging effect resulting in a reduction of the electroosmotic flow (EOF) over time. The EOF is restored by the annealing step, which also reduces surface roughness measured by atomic force microscopy. The annealed chips also provide better separating performance than chips that were used as received.

3.1 Introduction

Microchips for capillary electrophoresis (CE) can be manufactured from a variety of materials. Important is that the material is electrically insulating and impermeable to water. Predominantly glass is used, but polymers quickly became popular because of the potential to rapidly replicate devices using hot embossing, injection molding or lithography [1,2]. Poly(dimethylsiloxane) [3], poly(methyl methacrylate [4], polycarbonate [5], cyclic olefin polymers [6], SU-8 [7], polyimide [8] each have unique material properties that make them suitable for different applications. The processes for manufacturing microfluidic chips from plastics are however not established as well as they are for glass. Especially the integration of well-defined metal electrodes that are needed for the conductivity detection is difficult. The manufacture of glass microfluidic chips evolved from silicon processing technology, which has been perfected over the years to make ever-smaller integrated circuits for electronic applications. All processes that are needed to manufacture glass chips are available in the Mesa$^+$ cleanroom facilities. In this thesis glass chips are used to prove the principles for measuring inorganic ions in complex mixtures, e.g. blood, with microchip CE. Subsequently, the concepts can be transferred to manufacture plastic microchips for a commercialized product.

3.2 Simulation of microchip CE separations

Chapter 2 presented guidelines to predict the performance of CE microchips. Yet, to accurately describe peak shapes more complex algorithms are required [9-13]. Computer programs that simulate CE separations offer a convenient way of evaluating the

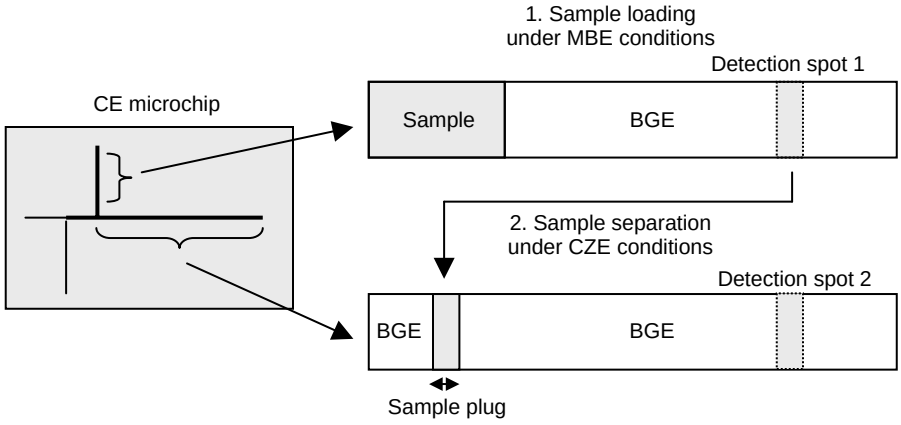

Figure 3.1: *Diagram of the simulation of the sample loading under MBE conditions and the subsequent separation under CZE conditions.*

performance of microchip separations. For example, the freeware program Simul [14] solves a set of nonlinear partial differential equations [15] in order to calculate the spatial distribution of any number of ionic species inside a capillary during electromigration processes. This includes the simulation of isotachophoresis, zone electrophoresis (CZE) and moving boundary electrophoresis (MBE) conditions. However, a CE microchip consists of a column-coupling configuration of two channels and the software does only allow simulating a single channel. The sample loading and separation therefore have to be simulated separately. The sample loading is simulated under MBE conditions discussed in chapter 2. The concentrations of analytes at the end of the first simulation in detection region 1 in Fig. 3.1 are used as the starting conditions for the simulation of the CZE separation.

The sample loading is simulated for a mixture containing 1 mmol/L potassium, sodium and lithium chloride, which is used to test the performance of the microchips. The background electrolyte (BGE) consists of a mixture with 20 mmol/L 2-(N-morpholino)ethanesulfonic acid (MES) and 20 mmol/L histidine (His). The EOF is included in the simulation using a mobility value estimated from experimental data. For the electrical field strength a value is used that is half the field strength, which was calculated for the microchip. At higher values numerical instabilities appear in the simulation due to the fact that the sample is not buffering, causing difficulties with the calculation of the pH. Figure 3.2 shows the composition of the solution at the detection point over time. At the start of the sample loading there is only BGE in the detection region. Potassium has the highest electrophoretic mobility and arrives at the detection region after 2.6 seconds. Sodium and lithium follow in 3.5 and 4.0 seconds, respectively.

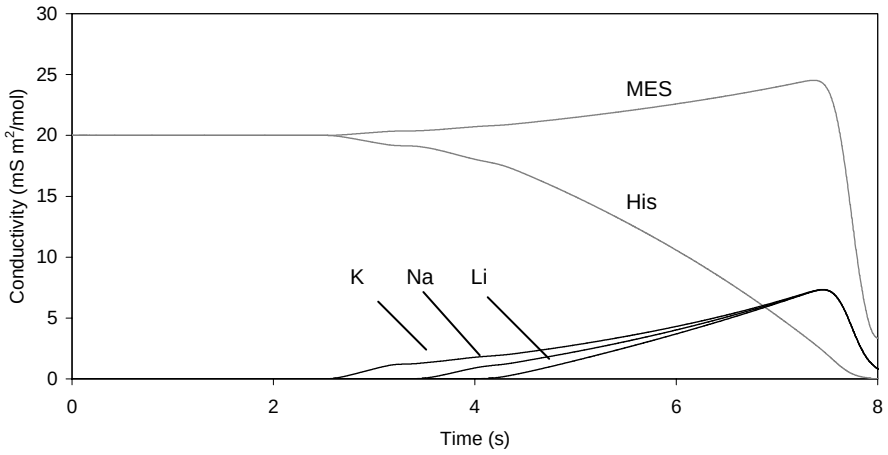

Figure 3.2: *Simulation of the composition of the contents in the double-T (detection spot 1 in Fig. 3.1) of a microchip during the sample loading step. The sample is a mixture of 1 mmol/L KCl, NaCl and LiCl in water. The BGE contains 20 mmol/L MES/His. Capillary length is 11 mm, field strength 164 V/cm and EOF mobility* 40×10^{-9} m^2/Vs. *The simulations are performed using an unreleased beta-version of Simul [16].*

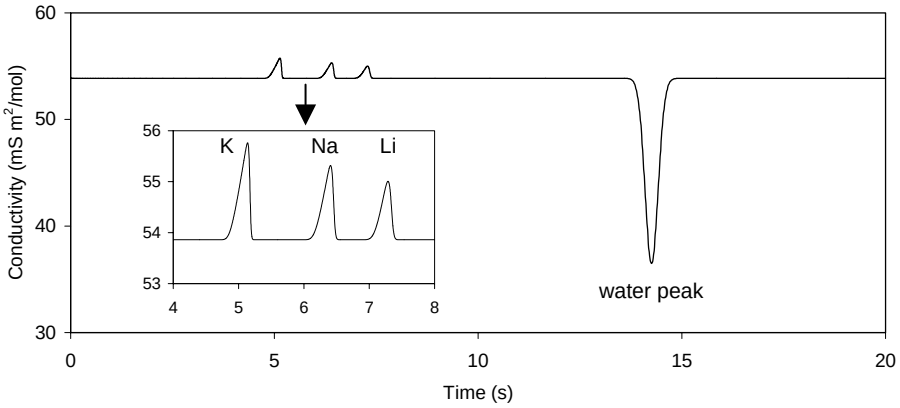

Figure 3.3: *Simulation of the CZE separation with conductivity detection (detection spot 2 in Fig. 3.1) based on the sample plug composition simulated in Fig. 3.2. Injection plug length is 200 μm, channel length 26.5 mm, field strength 337 V/cm and EOF mobility 40×10^{-9} m^2/Vs.*

The concentration of the three analytes gradually increase over time due to a sample stacking process [17], which is described in detail in chapter 5. Superimposed on the migration is an electroosmotic flow that pumps the sample through the capillary without being stacked. After approximately eight seconds the sample reaches the detector shown by the sudden drop in the concentration of the analytes. From this moment on the composition of the solution in the detector remains unchanged and the capillary is filled with a homogeneous solution. The composition of the solution at the end of the simulation consists of 0.562 mmol/L potassium, sodium and lithium and 1.68 mmol/L MES. This is significantly lower than the initial 1 mmol/L in the sample. The reason for this is that the chloride counter-ion in the sample does not migrate into the channel and is replaced by MES counter-ions from the BGE to maintain electroneutrality. This displacement of ions is accompanied by a change in the concentration [17], which is discussed in chapter 5.

The concentration of the analytes received at the end of the simulation of the loading process are entered into the program to simulate the CZE separation step using a sample plug with a length of 200 μm. Figure 3.3 shows the resulting electropherogram of this simulation. The electromigration dispersion dominates the diffusion resulting in peaks with a triangular shape instead of a symmetrical Gaussian profile. The separation channel with a length of 2 cm provides baseline separation of the alkali metals within 10 seconds. In the experimental work the microchips have the same separation length and Fig. 3.3 will be used as the benchmark for the comparison of the experimental separation results in the following sections.

The software can also aid in an initial optimization of the separation. Due to the non-linearity of CE separations caused by the combined effects of sample stacking, diffusion

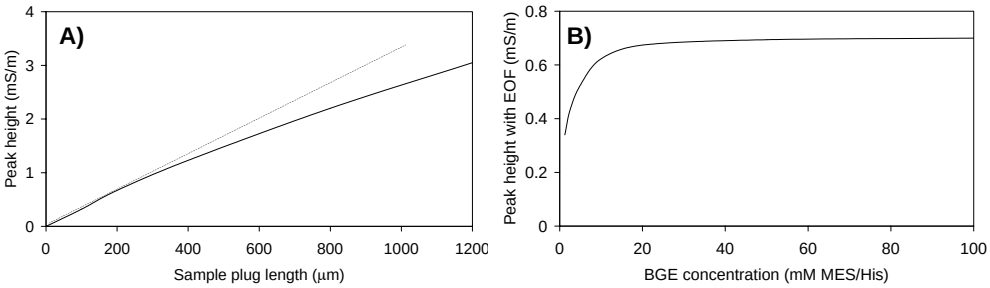

Figure 3.4: *A) Simulated effect of the sample plug length on the conductivity signal height of the lithium peak (solid line). B) The effect of the BGE concentration on the conductivity signal height of lithium using a 200 µm sample plug. Conditions as in Fig. 3.3.*

and electromigration dispersion, it is not possible to analytically calculate the concentration distribution of all species involved. For example, Eq. 2.32 describes the peak height for conductivity detection, but only includes the analyte concentration and the mobilities of the ions involved. The effect of the sample plug length on the height of the peaks can only be simulated (Fig. 3.4A). The same holds for optimization of the BGE concentration. Figure 3.4B shows that for separating a sample containing 1 mmol/L potassium, sodium and lithium a BGE electrolyte with a concentration higher than 20 mmol/L MES/His should be used for maximum sensitivity. At lower concentrations the peaks rapidly become broader resulting in a reduced signal height. The main factor contributing to the broadening is the increased electromigration dispersion at low BGE concentrations, while diffusion is dominant at high BGE concentrations. In the experiments a concentration of at least 20 mmol/L MES/His is therefore used.

Overall, the simulation of electrophoretic separations offers an excellent method to find relatively quickly the optimum background electrolyte composition and the length of the separation channel for a certain size of the sample plug. From the simulations alone it is however difficult to predict how the different parameters affect the separation result. Therefore an effective optimization is only possible with the knowledge of the fundamental electromigration processes as they were discussed in chapter 2.

3.3 Capillary electrophoresis on glass microchips

3.3.1 Manufacture of glass chips

The layout of the CE microchips used in this study is shown in Fig. 3.5A. The design was optimized for the analysis of inorganic ions based on a critical evaluation of the parameters affecting the performance described in chapter 2. A separation length of 2 cm was opted for together with a double-T of 200 μm, which were shown suitable by the simulations in the previous section. The channels with dimensions of 8×56 μm provide a high flow resistance to minimize the peak dispersion due to hydrodynamic flow. Embedded platinum electrodes provide a means for detecting the zones at the end of the separation channel. The manufacture was initially performed in-house using process parameters as described in appendix C. With the need for improved manufacturing the microchips were custom fabricated by a company that is specialized in microfabrication of fluidic chips (Micronit, Enschede, The Netherlands). The choice of processing steps during manufacture can have a substantial influence on the performance leading to changes in surface composition and roughness. This can lead to additional band broadening and a reduced separation resolution (Eq. 2.22). Important for the surface characteristics of the channels in this work is that they are etched into glass (Borofloat) with dilute hydrofluoric acid solutions. Figure 3.5B shows a cross-section of an etched channel. The electrodes for conductivity detection are made on a second glass wafer by sputtering platinum (approximately 200 nm) on a tantalum adhesion layer (approximately

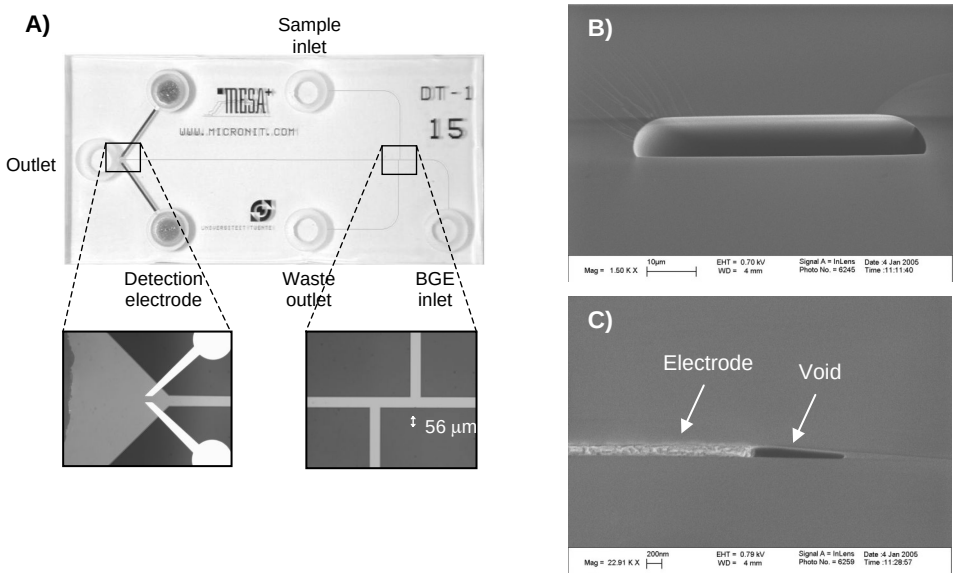

Figure 3.5: *Photograph of A) the CE chip with a magnification of the electrodes for conductivity detection and the double-T. B) SEM picture of a cross-section through the channel and C) cross-section through the embedded electrode showing a void at the edge.*

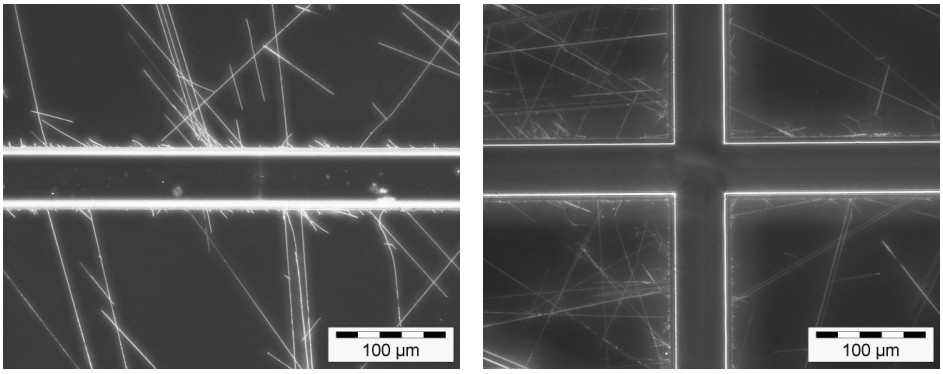

Figure 3.6: *Photograph of the channels in a glass microchip after one hour in 5% NaOH at 95°C. Microscope image under darkfield illumination. The channel in the right picture is filled with liquid, resulting in less light scattering on the edge of the channel.*

10 nm). The electrodes are deposited in a shallow recess that is etched in the wafer so that the electrodes do not protrude. A flat wafer surface is essential to bond the wafer with the microfluidic channels and the electrode wafer. The thickness of the electrodes is critical to keep the void between the metal and the cover wafer is as small as possible. However, a small gap around the electrodes as shown in Fig. 3.5C is difficult to avoid without switching to more complex manufacturing processes. Any hydrodynamic flow of electrolyte through the gap, which in this figure is approximately 150 nm × 1 µm, will be very limited due to the high flow resistance and can be neglected.

3.3.2 Entry tests of glass microchips

In order to determine the reproducibility of CE chips from different batches, one wafer containing 18 chips was made every month for a total of five months. The yield of microchips passing optical inspection ranges from 60 to 80% per batch. Bonding defects between the two glass wafers are the most common problem. On some chips there are point defects were the width of the channel is locally reduced or wider. More disturbing is the presence of scratches. With darkfield microscopy the scratches are barely visible. When the chips are immersed for one hour in a 5% sodium hydroxide solution at 95°C many more scratches become visible (Fig. 3.6). The apparent width of the scratches after etching is approximately 1.6 µm while the length can exceed 1 mm. The etch rate of the glass in the NaOH solution is estimated at 0.84 µm/h based on the loss of mass measured. This is a typical value for borosilicate glass. For example Pyrex 7740, which is also a borosilicate glass with a similar composition to Borofloat, etches with 0.66 µm/h in 30% KOH at 80°C [18].

From each of the five wafers the chips at positions 1 and 15 (see Fig. 3.7) are used to continue testing. To test the electrodes for conductivity detection the chips are filled with 20 mmol/L MES/His BGE and an impedance spectrum is recorded (Hewlett Packard 4194A impedance analyzer). The spectra in Fig. 3.8A,B shows that for chips from the same wafer the impedances are almost identical. Between wafers there is a variation from 1.06 to 1.30 MΩ at 10 kHz. This variation resulting from different cell constants, will also affect the peak heights measured during the electrophoretic separations. The existence of a small variation in cell constants indicates that there is a small error in the alignment of the electrode and channel wafer, affecting the area of the electrode in contact with the solution. Also the roughness of the electrodes, affecting the double layer capacitance can

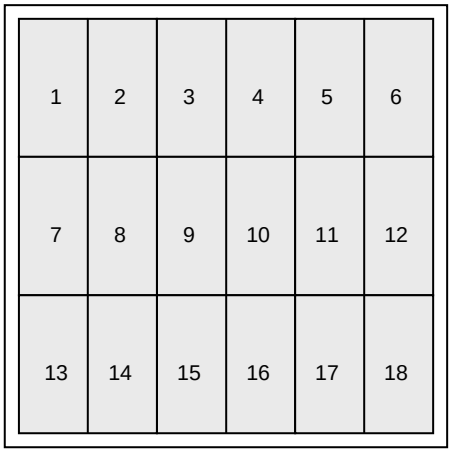

Figure 3.7: *Position of the 18 chips on the 10-inch wafer.*

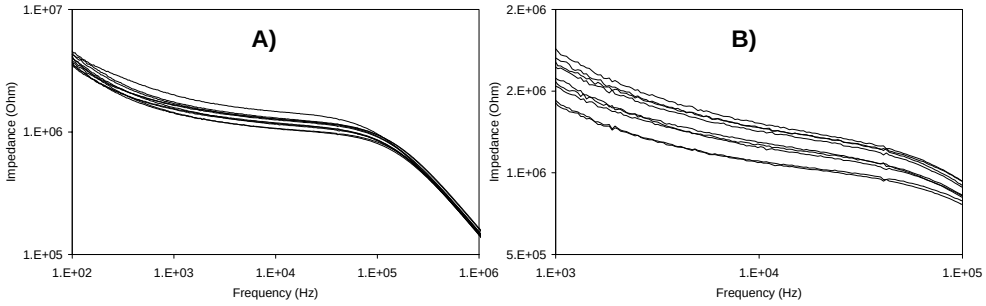

Figure 3.8: *A) Impedance spectra measured for ten chips from five wafers. B) enlarged section of A. The chips are filled with 20 mmol/L MES/His BGE.*

Table 3.2: *Sequence of voltages applied to the four compartments during the sample loading and separation. The field strengths in the channels are calculated using Eq. 2.23.*

Time (s)	Sample (V) (V/cm)	BGE (V) (V/cm)	Waste (V) (V/cm)	Outlet (V) (V/cm)
60	1000 (328)	800 (182)	0 (672)	1000 (164)
40	600 (69)	1000 (472)	600 (69)	0 (334)

have an effect on the impedance. The linear frequency range, in which the electrolyte resistance dominates the capacitive effects, extends from approximately 3 kHz to 40 kHz. For the experiments therefore a frequency of 25 kHz is used throughout.

3.3.3 Separation of calibration mixtures

To assess the performance of the microchips for separating metal ions by CE an aqueous solution containing 1 mmol/L potassium, sodium and lithium chloride is used. Separations are performed on ten chips that were characterized by the impedance analyzer, using 20 mmol/L MES/His as BGE. An optimized voltage sequence as given in Table 3.2 is used for the pinched sample loading and separation by means of a computer-controlled high-voltage power supply (CU 411, IBIS Technologies, Hengelo, The Netherlands). The conductivity is measured using a custom-made conductivity detector (Sprenkels Consultancy, Lelystad, The Netherlands) using a measuring voltage of 400 mV_{pp} at 25 kHz. Compared to the simulations shown in Fig. 3.3 section 3.2, the separating performance of the microchips in Fig. 3.9 is severely limited. The peaks of potassium and sodium overlap almost completely and lithium is only partially separated. There is some variation between the chips though, with batch 1 performing better than any of the other four. In contrast, the results for chips from the same wafer are very similar. Even the position of the water peak is nearly identical for chips from the same wafer while there is significant variation between wafers. This indicates that the state of the channel surface is not consistent. The variation in performance can be a result of different conditions during

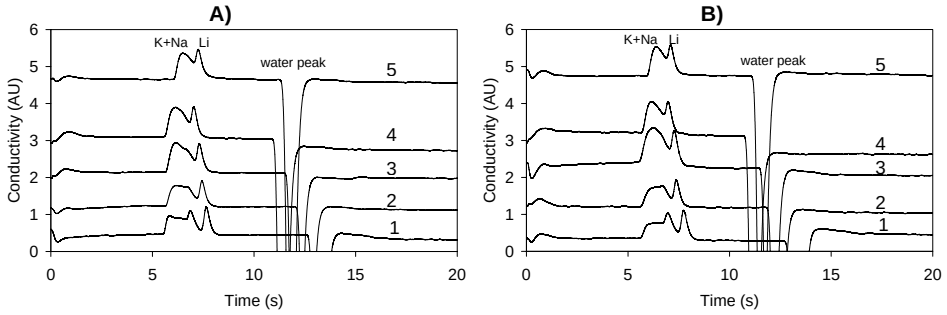

Figure 3.9: *Separation of 1 mmol/L K, Na and Li on 10 chips from A) position 1 and B) position 15 on the wafer (see Fig. 3.7). The numbers indicate the batch from which the chips originate, in the order of manufacturing. BGE 20 mmol/L MES/His.*

the manufacturing but it can also be an effect of the channel surfaces becoming contaminated during storage. Fused silica capillaries are typically preconditioned to obtain a reproducible surface condition by flushing with NaOH solutions [19]. The chips were used as received without any treatment to avoid the risk of contaminating the channels. The last two steps in the manufacture process are a cleaning step and the annealing at more than 500°C for bonding the wafers. Hence the chips should be clean directly after manufacture. In figure 3.9 a trend is observed for batch 1 to 4 indicating a reduced EOF for older chips (the batches are numbered in the order as they were received). The only exception is batch 5 which has an EOF mobility between those of batches 3 and 4. This trend is an indication that the condition of the glass surface changes over time resulting in a lower zeta potential. Possibly the surface slowly becomes contaminated with organic material. Further evidence for this conclusion is provided in section 3.3.5 where a temperature treatment of the microchips results in an increase in EOF.

By performing separations using solutions with only a single analyte instead of a mixture, the shapes of individual peaks can be evaluated better. The potassium peak in Fig. 3.10A exhibits significant tailing, which is more clearly seen at high concentrations. The sodium peak in Fig. 3.10B appears to split up in a double peak at a sample concentration higher than 1 mmol/L. Also the peak has some tailing, but this is less pronounced than for the potassium peak. The lithium peak in Fig. 3.10C displays a small bump at the leading edge, but has overall the best peak shape. The tailing of analyte peaks can be explained by interaction of the analytes with the channel surface [20]. The effective mobilities calculated from the electropherograms are lower than literature values (Fig. 3.11A-C) indicating the presence of a chromatographic retention mechanism of the ions. The decreasing mobility observed at higher sample concentrations is caused by the fact that the migration times used to calculate the mobilities are measured at the maximum of the peak. When the peak is not symmetrical an error is introduced. This is the case for increasing sample concentrations as the electromigration dispersion becomes more apparent. For this situation the use of a Haarhoff-Van der Linde function fitted to the data should provide a better estimate of the actual migration time [21]. The drop seen in the mobility of sodium in the MES/His BGE (Fig. 3.11B) is caused by the splitting of the peak. At low sodium concentration the faster of the two apparent peaks provides the highest signal while at a concentrations of 1.5 mmol/L and higher the slower peak dominates.

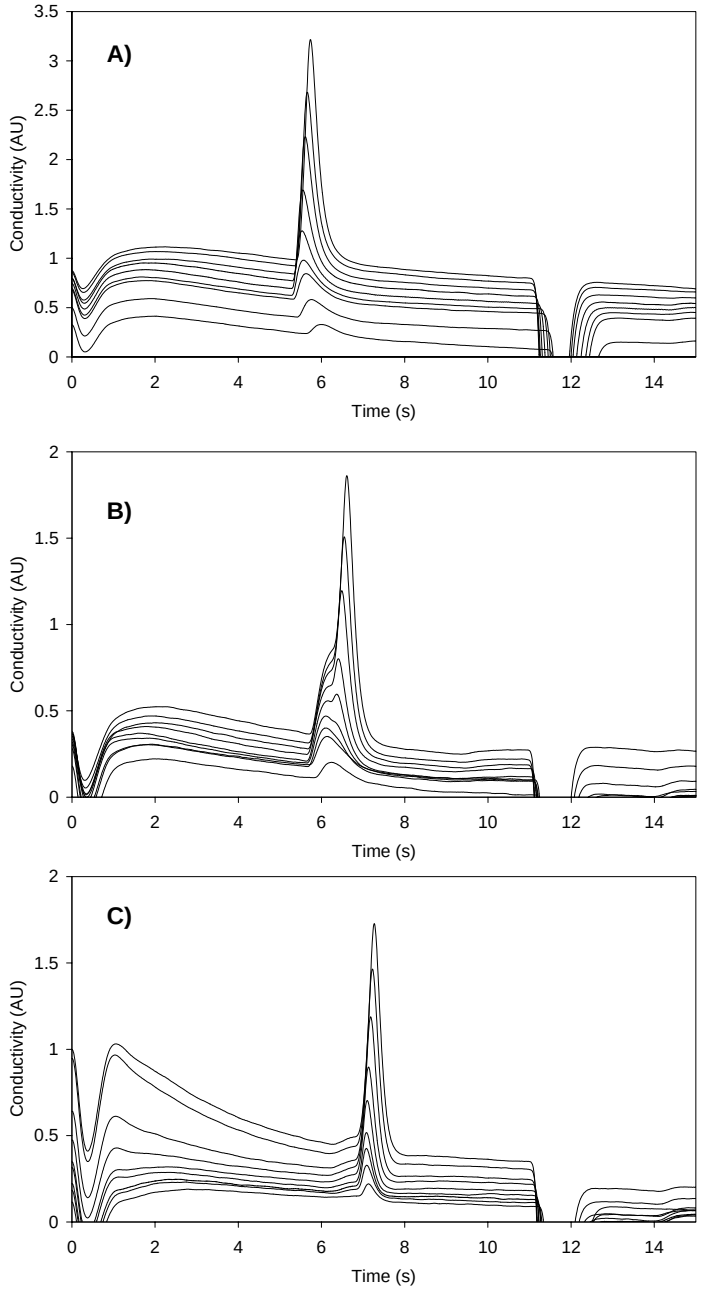

Figure 3.10: *Separations of A) potassium, B) sodium and C) lithium standards at concentrations of 0.25, 0.5, 0.75, 1.0, 1.5, 2.0, 3.0, 4.0 and 5.0 mmol/L. The negative peak observed at 11.5 s is the water peak. BGE 20 mmol/L MES/His.*

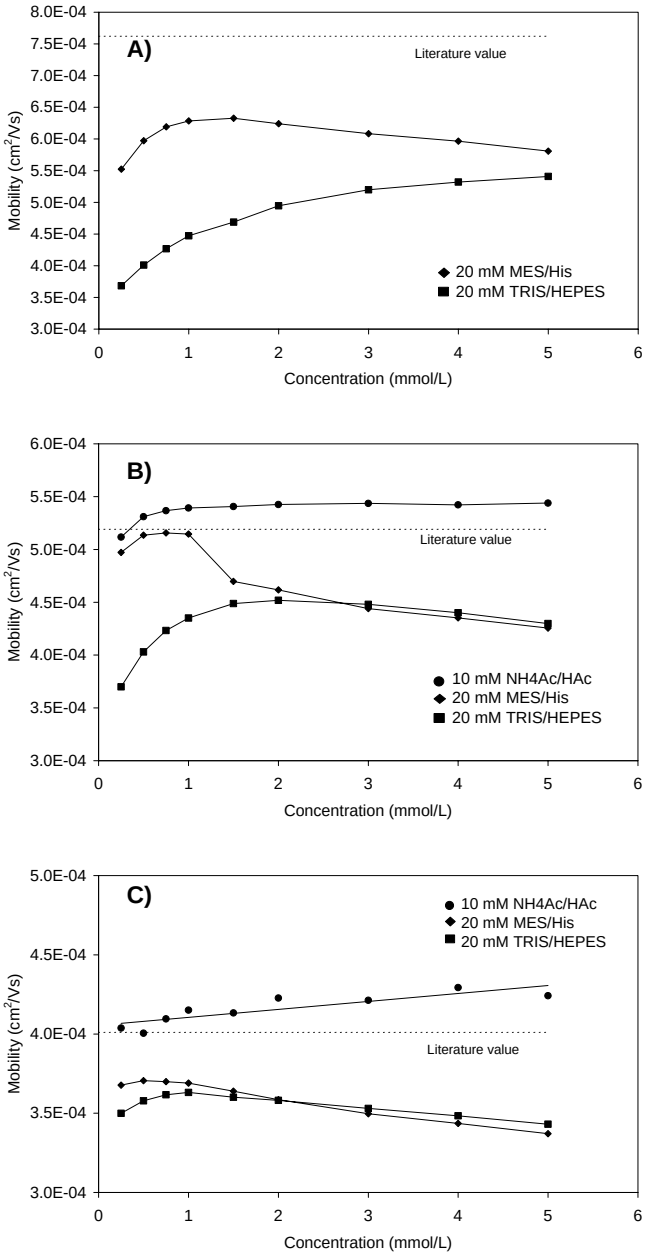

Figure 3.11: *Effective electrophoretic mobilities of A) potassium, B) sodium and C) lithium measured as function of the sample concentration and BGE composition. The dotted lines mark the literature values.*

The use of a BGE with a low pH (ammonium acetate, pH 4.8) provides higher effective mobilities than MES/His (pH 6.0) and Tris/HEPES (pH 7.8), shown in Fig. 3.11A-C. This trend is the result of the lower charge density on the glass surface due to less deprotonation of the silanol groups at higher pH. Consequently, the interaction of analytes with the surface reduces leading to a better separation and peak shape in the ammonium acetate BGE (Fig. 3.12A). However, potassium cannot be determined with conductivity detection under these conditions since it has the same mobility as ammonium. As a result the potassium zone has the same conductivity as the BGE (Eq. 2.32). In the MES/His BGE and TRIS/HEPES BGE (Fig. 3.12B,C) the peaks are much wider at the baseline than in the ammonium acetate BGE, which make these BGEs less suitable for the separation of alkali metals. However, the MES/His BGE has a lower electrical conductivity than an equal concentration ammonium acetate resulting in less Joule heating. Also ammonium acetate has the disadvantage that potassium cannot be detected. The next section therefore describes approaches to improve the performance of the microchips for analyzing potassium, sodium and lithium in the MES/His BGE.

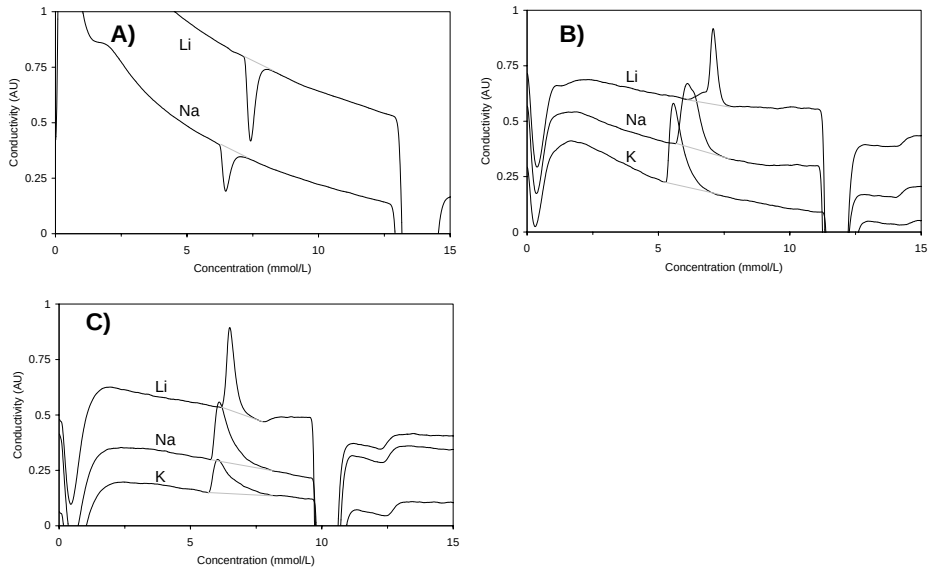

Figure 3.12: *Separation of 1 mmol/L potassium, sodium and lithium respectively. The BGE is A) 10 mmol/L NH_4Ac/HAc, B) 20 mmol/L MES/His and C) 20 mmol/L TRIS/HEPES. Potassium was not measured in ammonium acetate BGE.*

3.3.4 Optimization of the microchip performance

Interaction of analytes with the surface can be suppressed by applying a coating on the glass surface [22,23]. A chip with a polyacrylamide (PAAm) coating (see section 4.3.4 for the coating procedure) provides an excellent separating performance (Fig. 3.13C). The peaks have a clear triangular shape and resemble the simulation in Fig. 3.3 much more than all previous experiments. The peaks are also much higher due to the fact that the sample loading is governed by the electromigration of analytes instead of the EOF which is suppressed by the coating. The simulation in Fig. 3.2 showed that under these conditions the sample stacking results a sample plug with an analyte concentration that is higher than when using the EOF for the sample loading. The use of a chip with a monolayer of 3-(trimethoxysilyl)propyl methacrylate, which forms the basis onto which the PAAm is grafted, gives only a slight improvement over the chip without a coating (Fig. 3.13A,B). The presence of a water peak indicates that the glass surface is still largely exposed to the solution. Dynamic coatings can sometimes provide an alternative to a permanent coating like PAAm [24]. The main advantage is that the coating material is added to the BGE eliminating the time consuming procedure needed to prepare a permanent coating. However, a dynamic coating provided by adding 0.01% (w/v) (hydroxypropyl)methyl cellulose (HPMC) to the BGE did not result in significantly better peak shapes (separation not shown). Although HPMC effectively reduces the EOF, a property that is used in chapter 5, it does not sufficiently shield the glass surface from the inorganic ions.

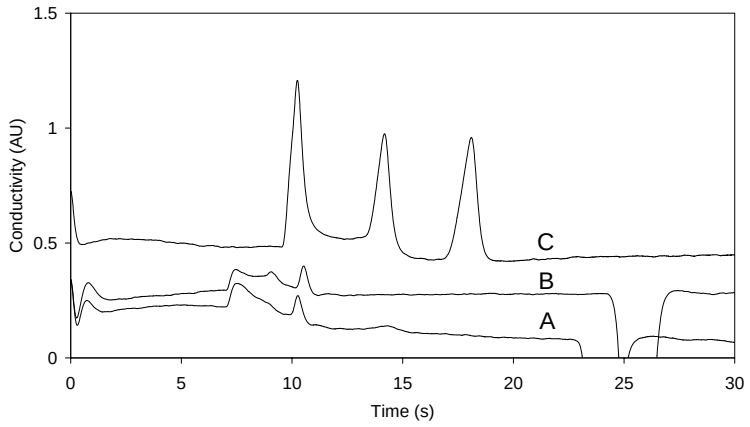

Figure 3.13: *Electropherograms of 1 mmol/L K, Na, Li. A) bare glass chip, B) after treating with 3-(trimethoxysilyl)propyl methacrylate and C) coated with polyacrylamide. BGE 20 mmol/L MES/His.*

Adsorption of proteins onto fused silica can be reduced by adding alkali metals to the BGE at a concentration of more than 300 mmol/L [25]. The mechanism is believed to be a competition between the metal ions and proteins for cation exchange sites at the surface. However, the authors also describe that the high ionic strength of the BGE causes problems due to Joule heating. For the microchip separations a significant resolution improvement already takes place when a small amount of potassium chloride in the order of 0.5 mmol/L is added to the BGE (Fig. 3.14). The mechanism appears to be a saturation of the surface with potassium, reducing the interaction of analytes with the glass. This principle is used again in chapter 7 to measure metal ions on an uncoated chip. However, care has to be taken with making changes to the BGE since a BGE with two co-ions will generate a system peak [26,27]. A simulation of the separation of 1 mmol/L sodium and lithium in a BGE with 0.5 mmol/L potassium displays a negative system peak at the

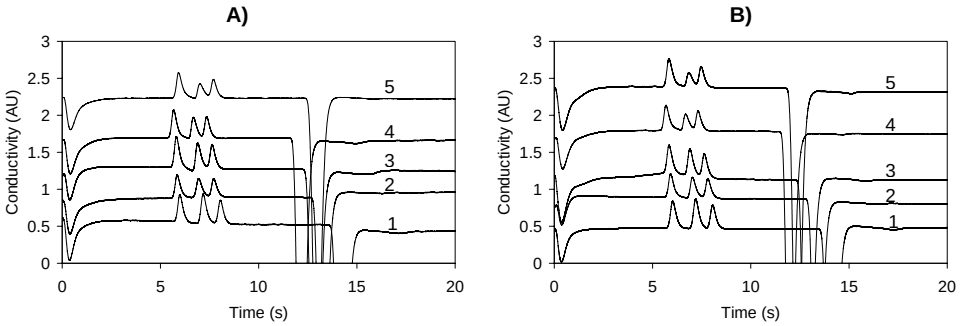

Figure 3.14: *Separation of 1 mmol/L K, Na, Li. A) chips from position 1 on the wafer and B) position 15 on the wafer (see Fig. 3.7). The chips are the same as in Fig. 3.9. The numbers indicate the batch from which the chips originate. The BGE is a mixture of 20 mmol/L MES/His and 0.5 mmol/L KCl.*

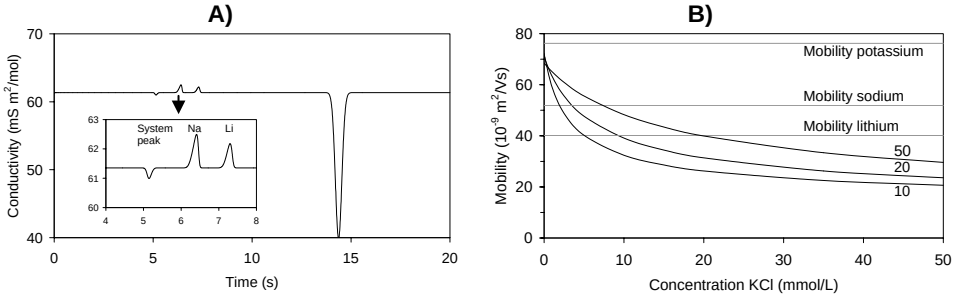

Figure 3.15: *A) Appearance of a system peak simulated for a sample with 1 mmol/L Na and Li. BGE 20 mmol/L MES/His with 0.5 mmol/L KCl. B) Mobility of the system peak calculated with Peakmaster for a BGE consisting of 10, 20 or 50 mmol/L MES/His and a varying amount of KCl. The dotted lines indicate the literature mobility values.*

position where potassium would normally be (Fig. 3.15A). The freeware program Peakmaster [14,28] provides a quick means of calculating the position of system peaks and can be used for optimization of the BGE without having to resort to time-consuming simulations. Fig 3.15B shows the position of the system peak as function of the potassium concentration and for 10, 20 and 50 mmol/L MES/His BGE. At a low potassium concentration the system peak lies close to the analyte peak of potassium, but it shifts to a lower mobility at higher concentrations. Furthermore, the size of the system peak depends on the composition of the sample and increases with increasing sample concentration. It will therefore be difficult to quantitate potassium or any other analyte that overlaps with the system peak. When the anayte peak and system peak have a similar mobility they can even influence each other leading to excessive dispersion or peaks with a zigzag or resonance pattern as shown in Fig. 3.16 [29].

The addition of potassium to the BGE not only reduces the tailing resulting in sharper potassium peaks (Fig. 3.17A), but also eliminates the splitting of the sodium (Fig. 3.17B) and lithium peaks (Fig. 3.15C) into peaks with two maxima. The addition of sodium (Fig. 3.18A-C) or lithium (Fig. 3.19A-C) to the BGE is less effective than potassium. This is consistent with the decreasing affinity of alkali metals for silica surfaces from potassium to sodium and lithium [30]. The appearance of a system peak at different positions depending on which metal is added to the BGE is also observed in Fig. 3.17B,C and 3.18C. The addition of lithium does interfere with the peak shapes of potassium and sodium, but does not give rise to a negative system peak (Fig. 3.19A-C).

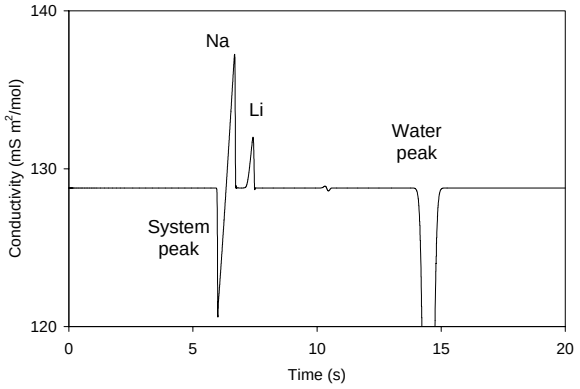

Figure 3.16: *Formation of a resonance pattern simulated with Simul for the separation of 1 mmol/L K, Na,Li in a BGE consisting of 20 mmol/L MES/His and 5 mmol/L KCl.*

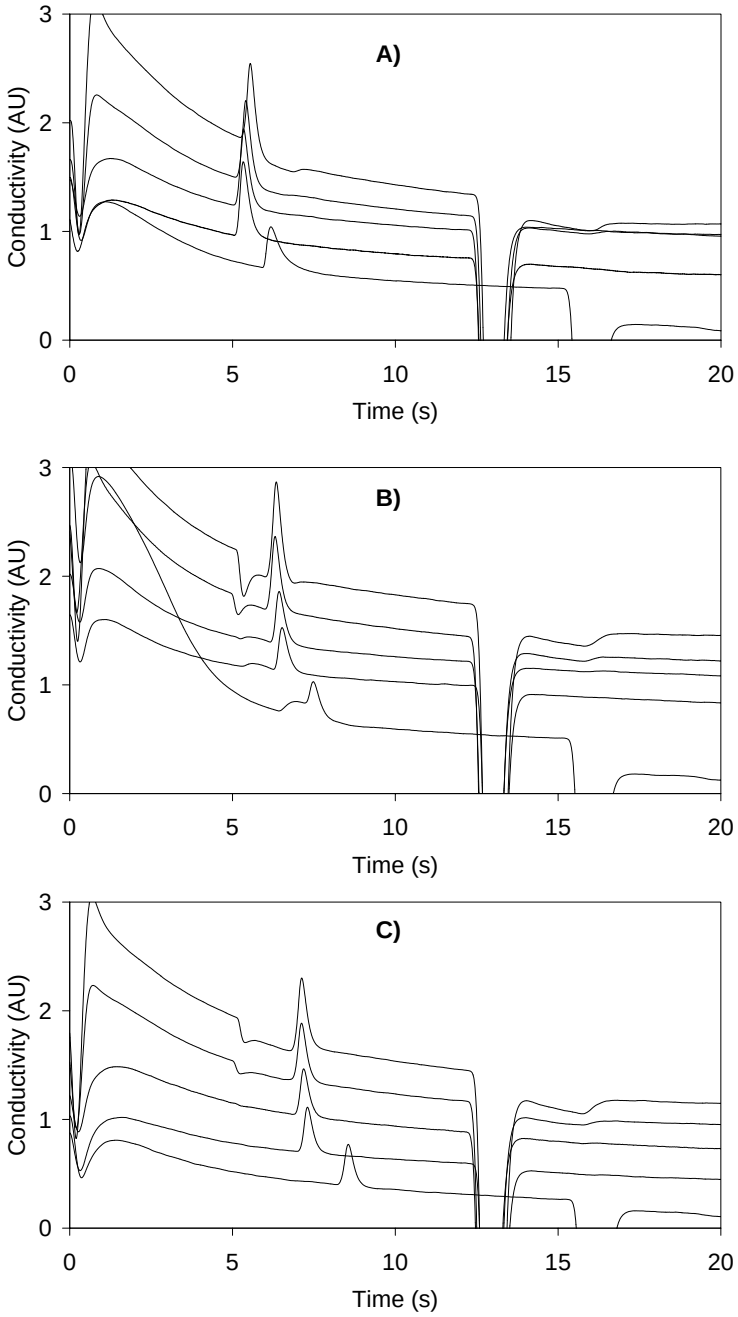

Figure 3.17: *Separations of 1 mmol/L A) potassium, B) sodium, C) lithium in a BGE consisting of 20 mmol/L MES/His with the addition of 0, 0.05, 0.1, 0.5 and 1.0 mmol/L potassium respectively (bottom to top curve).*

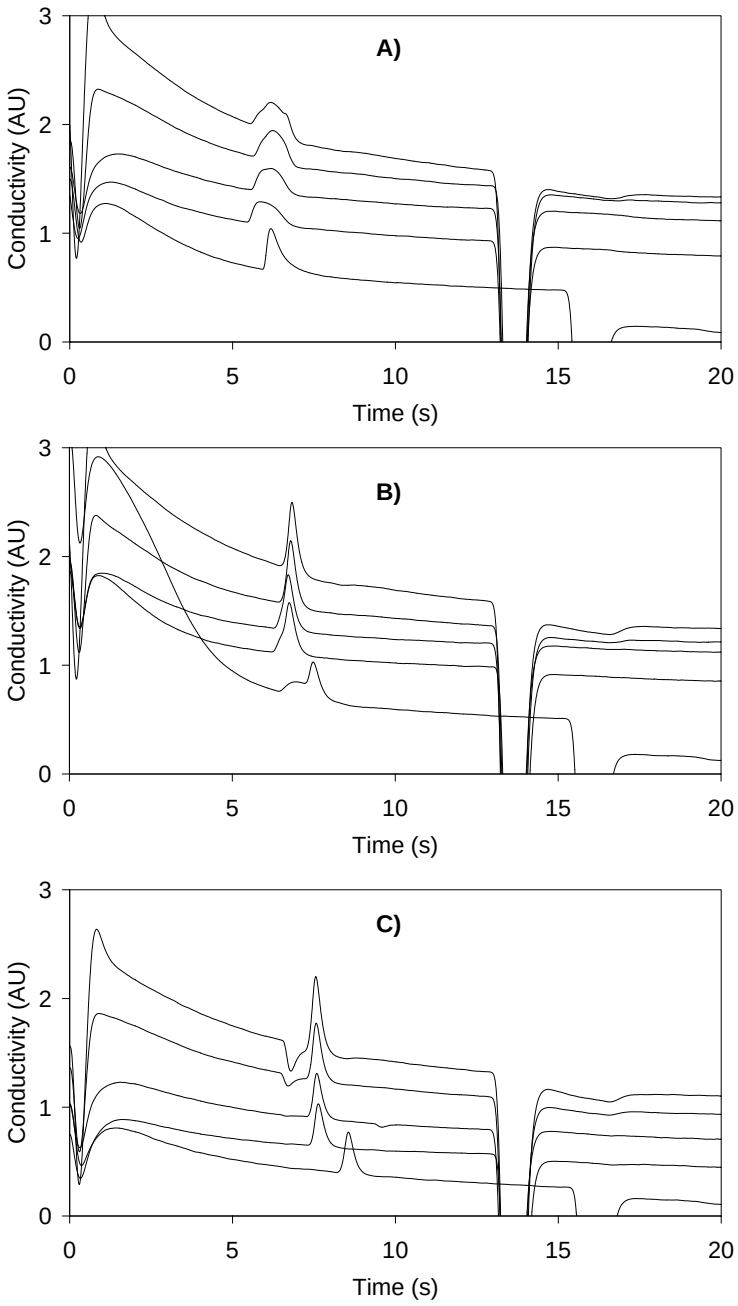

Figure 3.18: *Separations of 1 mmol/L A) potassium, B) sodium, C) lithium in a BGE consisting of 20 mmol/L MES/His with the addition of 0, 0.05, 0.1, 0.5 and 1.0 mmol/L sodium respectively (bottom to top curve).*

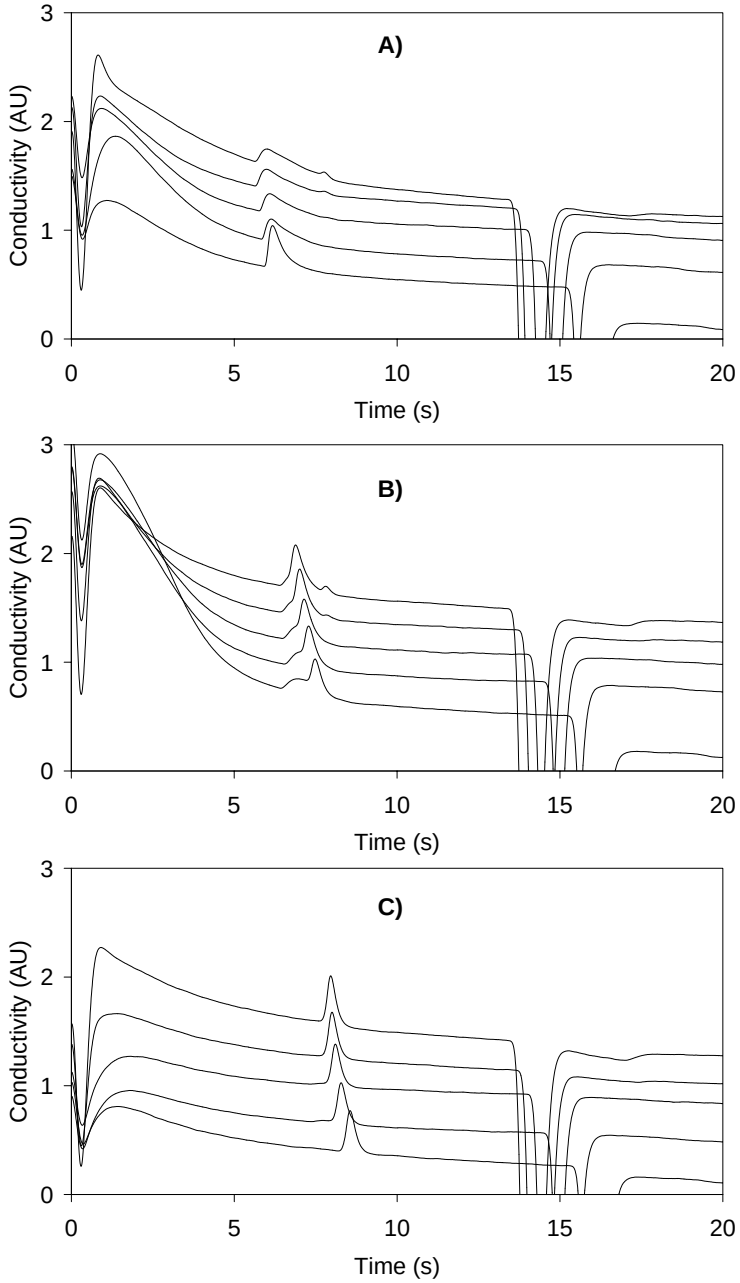

Figure 3.19: *Separations of 1 mmol/L A) potassium, B) sodium, C) lithium in a BGE consisting of 20 mmol/L MES/His with the addition of 0, 0.05, 0.1, 0.5 and 1.0 mmol/L lithium respectively (bottom to top curve).*

3.3.5 Surface characterization

If the restricted separation performance is indeed an interaction effect then the surface roughness should have a significant effect on the performance by increasing the area exposed to the BGE. One of the chips that had a bond defect was opened to expose the separation channel. An atomic force microscopy (AFM) scan of the bottom of the HF-etched channel shown in Fig. 3.20A reveals a significant roughness (average roughness ra=3.7 nm). Fused silica capillaries for example have a roughness on the inside of only 0.28 to 0.67 nm [31]. An annealing step at a sufficiently high temperature can significantly reduce the surface roughness of glass [32]. Although the chips have been annealed during manufacture to bond the two wafers, the temperature may not have been optimized to reduce roughness. To study the effect of an extra annealing step on the

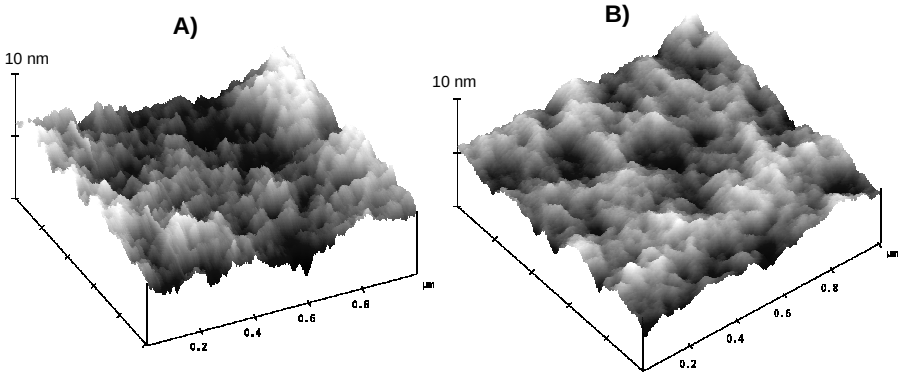

Figure 3.20: *AFM scan of the bottom of the bottom of an HF-etched channel. A) microchip as received, B) after annealing for one hour at 600°C.*

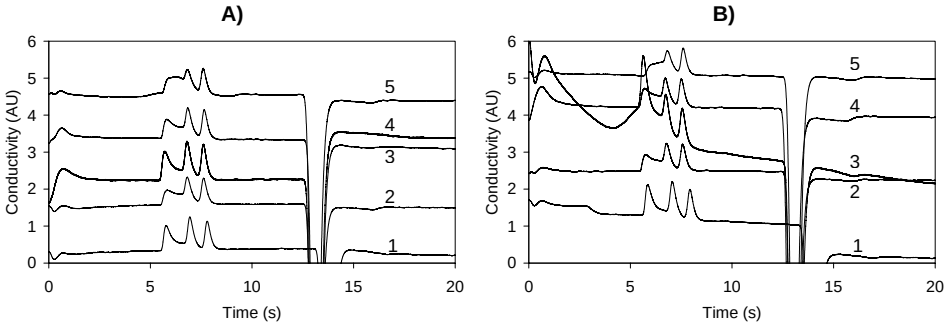

Figure 3.21: *Separation of 1 mmol/L K, Na, Li after annealing the chips for 1 hour at 600°C. A) chips from position 1 on the wafer and B) position 15 on the wafer (see Fig. 3.7). The chips and conditions are the same as in Fig. 3.9. The numbers indicate the batch from which the chips originate.*

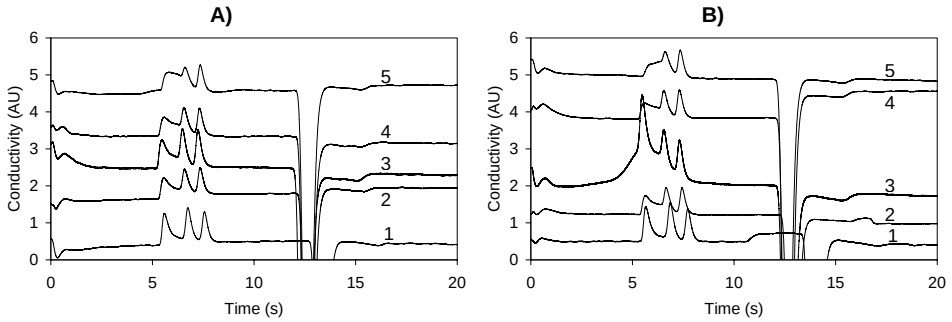

Figure 3.22: *Separation of 1 mmol/L K, Na, Li after reannealing the chips used in Fig. 3.21 for another 2 hours at 600°C. A) chips from position 1 on the wafer and B) position 15 on the wafer (see Fig. 3.7). The separation conditions are the same as in Fig. 3.9. The numbers indicate the batch from which the chips originate.*

surface roughness, the chips were placed in a furnace at 600°C for 1 hour. The temperature was raised above the annealing point of Borofloat glass at 560°C (the temperature defined as the point above which the internal stresses of glass are substantially released within a few minutes) but well below the softening point at 820°C (at this temperature the glass cannot support its own weight). The AFM scan indeed shows a decreased roughness (ra=1.7 nm, Fig. 3.20B), while optical inspection shows no obvious deformation of the channels. The separations of the calibration mixture performed on the annealed chips (Fig. 3.21) show improvement compared to the same chips before annealing (Fig. 3.9). The EOF peaks overlap for all chips with the exception of batch 1, reversing the apparent ageing effect seen for the untreated chips in Fig. 3.9. The glass from batch 1 might have slightly different material properties, if it originates from a different glass batch. Another annealing step for 2 hours at 600°C does not result in any further significantly improved separation performance (Fig. 3.22). In comparison with the results obtained by adding potassium to the BGE the effect of annealing on the separation resolution is less pronounced.

A new wafer was processed to further investigate the effect of surface roughness on the separations. On each chip a test structure was included in the design, consisting of an etched channel that was exposed via an opening in the top wafer. This allows the roughness to be measured with AFM without having to open up the chip, which would ruin the chip for performing separations. The average roughness measured for 13 chips is 1.19 nm with a relative standard deviation (RSD) of 9.3% (Fig. 3.23 and 3.24). The chips were subsequently annealed for 3.5 hours at 640°C. The roughness decreased considerably to 0.24 nm (RSD 20%, n=6), which is comparable to the roughness of fused silica capillaries. The separations of the alkali metals on the annealed chips shown in Fig. 3.25B are only slightly better than on the chips that were used as received (Fig. 3.25A). Also compared to the separations using the previous five batches of chips after annealing

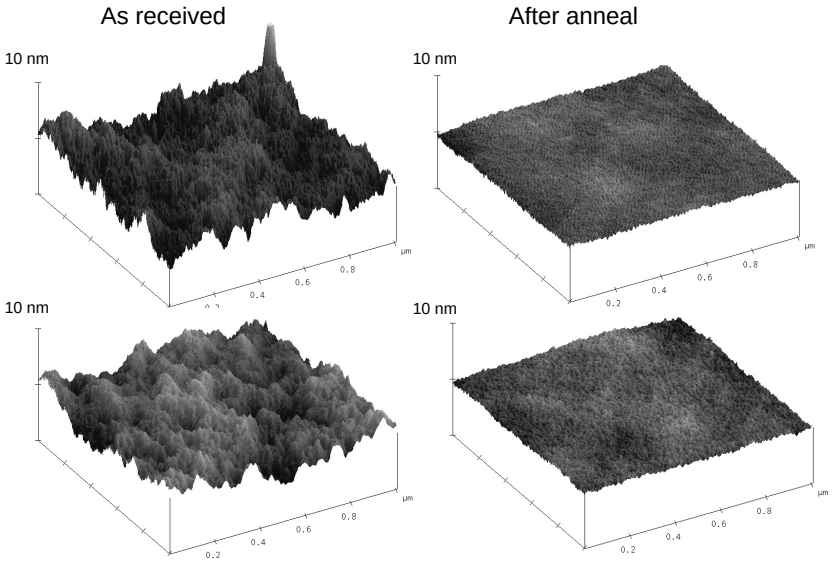

Figure 3.23: *AFM scans of the bottom of an HF-etched channel for two chips as received and after annealing for 3.5 hours at 640°C.*

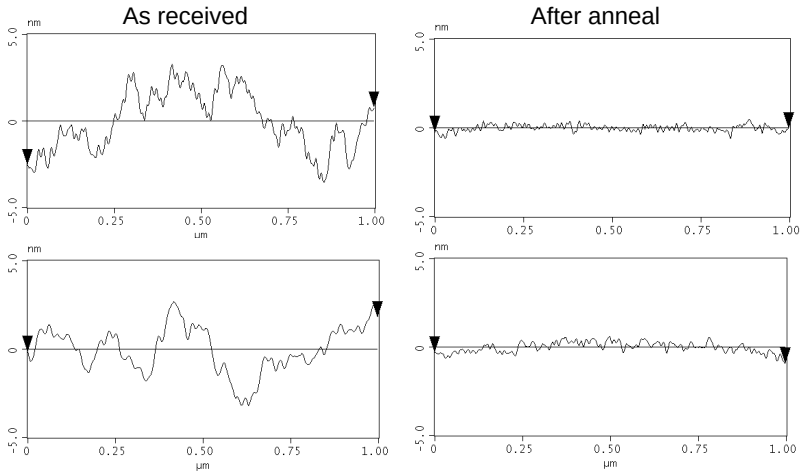

Figure 3.24: *Cross-sections of the AFM surface profiles corresponding to the two chips shown in Fig. 3.23.*

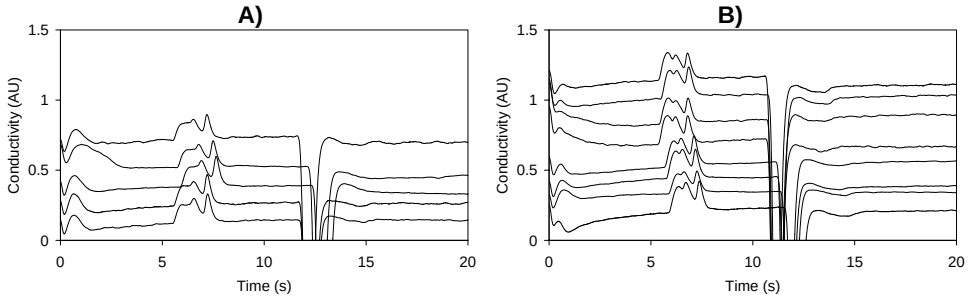

Figure 3.25: *Separation of 1 mmol/L potassium, sodium and lithium on 13 chips. A) chips that were used as received and B) chips that had been annealed for 3.5 hours at 640°C first. Separation conditions as in Fig. 3.9.*

(Fig. 3.21) the resolution is limited. This indicates that the surface roughness is not decisive for the separation performance, but that there are other factors present. Yet, at this point it is not clear what causes the difference in the performance between batch 1, batches 2 to 5, and the new batch. The manufacturer was instructed to keep the process exactly the same for all batches. However, the glass wafers could have come from different lots and have slightly different compositions.

The water peaks in Fig 3.25A,B cluster in both figures into two sets. This is caused by the fact that some experiments were performed in an air-conditioned room at approximately 21°C and the remainder immediately afterwards in an unconditioned environment where the temperature was considerably higher. On average the electroosmotic mobility shows an increase from 5.31×10^{-4} cm^2/Vs (RSD 2.6%, n=5) for the chips as received to 5.76×10^{-4} cm^2/Vs (RSD 3.3%, n=8) after the anneal step. When only the measurements performed in one environment are used, the relative standard deviations are only 1% or less. This shows that the experimental conditions are similar when changing to a different chip. Although the chips are manually filled with BGE and sample, this does not significantly reduce the precision of the measured migration times.

Overall, annealing reduces the surface roughness and has a positive effect on the separation. The chips appear to age, of which the effect is reversed by the temperature treatment. Still, there is a difference in performance from batch-to-batch while chips from the same wafer show similar performance (Fig. 3.21 and 3.22).

Another method to characterize the surface is by measuring the EOF. There is a strong correlation between the condition of the channel surface and the mobility of the EOF. However, care has to be taken to interpret EOF values since the EOF is affected by adsorption of contaminants onto the surface and temperature during the experiments as was observed in the previous section. Also changes in the chemical composition of the glass can have an effect. Still, the EOF is a useful indication of the condition of the microchips. A more detailed study of the EOF can also provide information on the adsorption of alkali metals to the surface. The mobility of the EOF is governed by the surface charge density and the thickness of the electrical double layer (Eq. 2.10). Since the surface charge is affected by the adsorption of cations from the solution the EOF can be modeled according to [33]:

$$\mu_{EOF} = \frac{\sigma}{\eta(1 + K_{wall}[M^+])}\left(d_0 + \frac{1}{K'\sqrt{[M^+]}}\right) \tag{3.1}$$

where σ is the density of ionized silanol groups on the surface, d_0 the thickness of the compact layer, K_{wall} the equilibrium constant for adsorption and $[M^+]$ the concentration of a monovalent cationic species in the BGE. The last term in Eq. 3.1 represents the Debeye length with K' 3.2×10^9 $m^{-1}(mol/L)^{-1/2}$. The EOF mobility was measured for a range of BGEs consisting of the chloride salts of the alkali metals cesium, potassium, sodium and lithium respectively. These solutions were prepared at concentrations between 1 and 100 mmol/L, without the addition of buffering species. As the sample an electrolyte solution

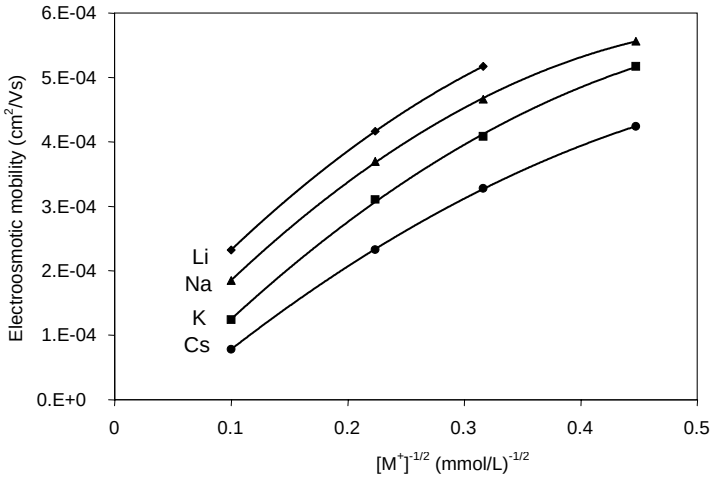

Figure 3.26: *Dependency of the electroosmotic mobility on the concentration and type of BGE cation. Electrolyte solutions are prepared from the chloride salts.*

diluted to 0.5 mmol/L was used. A separation of the diluted electrolyte solution results in only a water peak, which is used to calculate the mobility of the EOF (Fig. 3.26). At high electrolyte concentrations the mobility of the EOF differs by a factor of more than two between a cesium and lithium BGE. The Debeye-Hückel model for the EOF (Eq. 2.10) only has an ionic strength dependency and does not take the composition of the electrolyte into account. This result demonstrates that the metal ions indeed adsorb onto the glass surface and alter the separation conditions.

3.3.6 Peak shape distortions caused by surface interaction

The peak tailing due to adsorption is a phenomenon well-known in separation science. The splitting of peaks is more difficult to understand. Under certain circumstances ions can exhibit a schizophrenic migration behaviour [34] resulting in a splitting of peaks as experienced in Fig. 3.10. The origin of this phenomenon is a transition from a fronting to a tailing migration or vice versa. This can occur under certain conditions when the mobility of an ion is not constant. This can for example be caused by a pH dependency [11,35,36]. Figure 3.27 shows an example simulating an analyte species that produces a fronting peak at high concentration and a tailing peak at low concentration. A similar distortion can occur for a BGE with two co-ions [37]. In the experiments the mobility of the analytes is independent of the pH and the distortion occurs with a BGE with a single co-ion. There is however a dependency of the concentration on the mobility as shown in Fig. 3.11A-C. With increasing concentration the analytes have a higher mobility (neglecting the decreasing mobility produced by the error made in determining the migration time as discussed in section 3.3.3). At the same time the electromigration dispersion causes a lower mobility for higher concentrations. Hence the conditions for a schizophrenic behaviour, i.e. two opposed dispersive effects, are present (Fig. 3.28). In capillary electrochromatography separations these conditions can provide anomalously high separation performance [38,39]. A theory combining the properties of electrophoresis and chromatography showed that the combination of dispersive effects can indeed exist

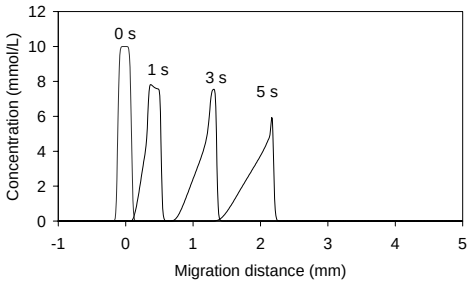

Figure 3.27: *Simulated evolution of the peak shape during migration after 1, 3 and 5 seconds respectively. Imaginary species with a mobility of 20×10^{-9} m^2/Vs and a pK_a of 7. The counter ion is 10 mmol/L sodium and the BGE consists of 10 mmol/L sodium / MES. The simulation using Simul was based on an example of schizophrenic peak distortion in ref.11.*

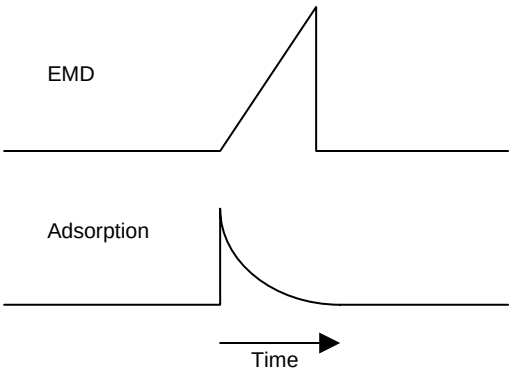

Figure 3.28: *Schematic representation of the evolution of different peak profiles from an initially rectangular plug due to electromigration dispersion and reversible adsorption.*

[40]. It is however a transient effect and it depends strongly on the conditions whether the effect is observed. For potassium the interaction with the surface dominates, while for lithium the electromigration dispersion is more dominant. Only for sodium the effects are more balanced, making the peak splitting visible.

3.4 Conclusions

Software for simulating CE separations can assist in the initial optimization of the separation conditions. In addition it forms a point of reference for the microchip separations. The interaction of alkali metals with the surface of the glass chips is a problem and results in restricted performance. Only when the interaction is reduced via a surface coating or a BGE additive, the baseline separation of potassium, sodium and lithium on the glass chip is possible. The addition of potassium to the BGE offers an efficient method to restrict the dispersion. However, the formation of a system peak can interfere with the quantitation of analytes. AFM scans of the surface of HF-etched channels showed that the surface is relatively rough compared to fused silica capillaries, which reduces the separation performance. Annealing the chips at 640°C significantly reduces the roughness, yet the separation performance increases only slightly. Although conditions can be found that are suitable for the separation of alkali metal ions, the choice of glass as the substrate material is not ideal. Coating the surface with polyacrylamide provides excellent separation performance, which suggests that polymer chips are better suited for separating alkali ions.

3.5 References

1. H Becker and C Gärtner "*Polymer microfabrication methods for microfluidic analytical applications"*, Electrophoresis 2000, **21**, 12-26.
2. A De Mello "*Plastic fantastic"*, Lab on a Chip 2002, **2**, 31N-36N.
3. DC Duffy, JC McDonald, OJA Schueller and GM Whitesides "*Rapid Prototyping of Microfluidic Systems in Poly(dimethylsiloxane)"*, Anal. Chem. 1998, **70**, 4974-4984.
4. J Wang, M Pumera, MP Chatrathi, A Escarpa, R Konrad, A Griebel, W Dörner and H Löwe "*Towards disposable lab-on-a-chip; Poly(methylmethacrylate) microchip electrophoresis device with electrochemical detection"*, Electrophoresis 2002, **23**, 596-601.
5. Y Liu, D Ganser, A Schneider, R Liu, P Grodzinski and N Kroutchinina "*Microfabricated Polycarbonate CE Devices for DNA Analysis"*, Anal. Chem. 2001, **73**, 4196-4201.
6. S Benetton, J Kameoka, A Tan, T Wachs, H Craighead and JD Henion "*Chip-based P450 drug metabolism coupled to electrospray ionization-mass spectrometry detection"*, Anal. Chem. 2003, **75**, 6430-6436.
7. Y-J Chuang, F-G Tseng, J-H Cheng and W-K Lin "*A novel fabrication method of embedded micro-channels by using SU-8 thick-film photoresists"*, Sens. Actuators A 2003, **103**, 64-69.
8. JS Rossier, C Vollet, A Carnal, G Lagger, V Gobry, HH Girault, P Michel and F Reymond "*Plasma etched polymer microelectrochemical systems"*, Lab on a Chip 2002, **2**, 145-150.
9. FEP Mikkers "*Concentration Distributions in Capillary Zone Electrophoresis: CZE in a Spreadsheet"*, Anal. Chem. 1999, **71**, 522-533.
10. H Poppe "*Overloading and Interaction Phenomena in Electrophoretic Separations"*, Anal. Chem. 1992, **64**, 1906-1919.
11. P Gebauer and P Bocek "*Predicting Peak Symmetry in Capillary Zone Electrophoresis; The Concept of the Peak Shape Diagram"*, Anal. Chem. 1997, **69**, 1557-1563.
12. JL Beckers "*Calculation of the composition of sample zones in capillary zone electrophoresis; II. Simulated electropherograms"*, J. Chromatogr. A 1995, **696**, 285-294.
13. RA Mosher, D Dewey, W Thormann, DA Saville and M Bier "*Computer Simulation and Experimental Validation of the Electrophoretic Behavior of Proteins"*, Anal. Chem. 1989, **61**, 362-366.
14. http://www.natur.cuni.cz/~gas/
15. C Schwer, B Gaš, F Lottspeich and E Kenndler "*Computer Simulation and Experimental Evaluation of On-Column Sample Preconcentration in Capillary Zone Electrophoresis by Discontinuous Buffer Systems"*, Anal. Chem. 1993, **65**, 2108-2115.
16. Personal communication, B Gaš, Charles University, Prague, Czech Republic

17. JL Beckers and P Bocek "*Sample stacking in capillary zone electrophoresis; Principles, advantages and limitations"*, Electrophoresis 2000, **21**, 2747-2767.
18. KR Williams, K Gupta and M Wasilik "*Etch Rates for Micromachining Processing - Part II"*, Journal of Microelectromechanical Systems 2003, **12**, 761-778.
19. T Ehmann, K Bächmann, L Fabry, H Rüfer, M Serwe, G Ross, S Pahlke and L Kotz "*Capillary preconditioning for analysis of anions using indirect UV detection in capillary zone electrophoresis Systematic investigation of alkaline and acid prerinsing techniques by designed experiments"*, J. Chromatogr. A 1998, **816**, 261-275.
20. SV Ermakov, MY Zhukov, L Capelli and PG Righetti "*Wall adsorption in capillary electrophoresis Experimental study and computer simulation"*, J. Chromatogr. A 1995, **699**, 298-313.
21. GL Erny, ET Bergström, DM Goodall and S Grieb "*Predicting Peak Shape in Capillary Zone Electrophoresis; a Generic Approach to Parametrizing Peaks Using the Haarhoff-Van der Linde (HVL) Function"*, Anal. Chem. 2001, **73**, 4862-4872.
22. J Horvath and V Dolník "*Polymer wall coatings for capillary electrophoresis"*, Electrophoresis 2001, **22**, 644-655.
23. EAS Doherty, RJ Meagher, MN Albarghouthi and AE Barron "*Microchannel wall coatings for protein separations by capillary and chip electrophoresis"*, Electrophoresis 2003, **24**, 34-54.
24. PG Righetti, C Gelfi, B Verzola and L Castelletti "*The state of the art of dynamic coatings"*, Electrophoresis 2001, **22**, 603-611.
25. JS Green and JW Jorgenson "*Minimizing adsorption of proteins on fused silica in capillary zone electrophoresis by the addition of alkali metal salts to the buffers"*, J. Chromatogr. 1989, **478**, 63-70.
26. B Gaš and E Kenndler "*System zones in capillary zone electrophoresis"*, Electrophoresis 2005
27. JL Beckers, P Gebauer and P Bocek "*Why robust background electrolytes containing multivalent ionic species can fail in capillary zone electrophoresis"*, J. Chromatogr. A 2001, **916**, 41-49.
28. M Jaroš, K Vèeláková, I Zusková and B Gaš "*Optimization of background electrolytes for capillary electrophoresis; II. Computer simulation and comparison with experiments"*, Electrophoresis 2002, **23**, 2667-2677.
29. JL Beckers, P Gebauer and P Bocek "*System zones in capillary zone electrophoresis"*, Electrophoresis 2001, **22**, 3648-3658.
30. RL Smith and DJ Pietrzyk "*Liquid Chromatographic Separation of Metal Ions on a Silica Column"*, Anal. Chem. 1984, **56**, 610-614.
31. R Barberi, M Giocondo, R Bartolino and PG Righetti "*Probing the inner surface of a capillary with the atomic-force microscope"*, Electrophoresis 1995, **16**, 1445-1450.
32. H Wensink, S Schlautmann, MH Goedbloed and MC Elwenspoek "*Fine tuning the roughness of powder blasted surfaces"*, J. Micromech. Microeng. 2002, **12**, 616-620.

33. K Salomon, DS Burgi and JC Helmer "*Evaluation of fundamental properties of a silica capillary used for capillary electrophoresis"*, J. Chromatogr. 1991, **559**, 69-80.
34. P Gebauer, C Desiderio, S Fanali and P Bocek "*"Schizophrenic" behavior of zones in capillary zone electrophoresis: Explanation of an old problem"*, Electrophoresis 1998, **19**, 701-706.
35. SV Ermakov, MY Zhukov, L Capelli and PG Righetti "*Experimental and Theoretical Study of Artifactual Peak Splitting in Capillary Electrophoresis"*, Anal. Chem. 1994, **66**, 4034-4042.
36. SV Ermakov, MY Zhukov, L Capelli and PG Righetti "*Artifactual Peak Splitting in Capillary Electrophoresis. 2. Defocusing Phenomena for Ampholytes"*, Anal. Chem. 1995, **67**, 2957-2965.
37. P Gebauer, P Borechká and P Bocek "*Predicting Peak Symmetry in Capillary Zone Electrophoresis. Background Electrolytes with Two Co-ions; Schizophrenic Zone Broadening and the Role of System Peaks"*, Anal. Chem. 1998, **70**, 3397-3406.
38. J Ståhlberg "*The Theory for Zone Migration in Electrochromatography"*, Anal. Chem. 1997, **69**, 3812-3821.
39. AM Enlund, ME Andersson and G Hagmar "*Peak compression effects in capillary electrochromatography"*, J. Chromatogr. A 2004, **1044**, 153-158.
40. MS Bello, MY Zhukov and PG Righetti "*Combined effects of non-linear electrophoresis and non-linear chromatography on concentration profiles in capillary electrophoresis"*, J. Chromatogr. A 1995, **693**, 113-130.

Chapter 4

Determination of lithium in whole blood with microchip capillary electrophoresis*

In this chapter a method is introduced which enables the measurement of cations including lithium directly in whole blood. The electrokinetic transport of red blood cells inside the capillary electrophoresis microchip is studied to find sample loading conditions suitable for the analysis of lithium without injecting any blood cells into the separation channel. A comparison is made between bare glass chips and chips coated with polyacrylamide, showing the behavior of the cells under different electroosmotic flow conditions. Blood samples collected from a finger stick are analyzed on the microchip with only the addition of an anticoagulant.

* This chapter is based on papers in Electrophoresis 2004, 25, 1660-1667 and Ned.Tijdschr.Klin.Chem.Labgeneesk. 2004, 29, 295-296

4.1 Introduction

Direct analysis of whole blood without any sample pretreatment is still a largely unexplored field in separation science. Its complex matrix makes the analysis of even serum or plasma a nontrivial analytical problem. At the present state of microfluidic chip technology, it is possible to combine sample treatment steps with separation methods on a single chip. However, few devices have been developed that fully exploit the combination of multiple functionalities in so-called micro total analysis systems (μTAS) [1,2]. Instead of developing advanced multifunctions on chip, here we demonstrate that the measurement of alkali metals in a drop of whole blood can be performed on a capillary electrophoresis (CE) microchip with a standard double T-injector [3] applying the principles of column coupling.

Under normal dietary conditions lithium is not present in the human body in a significant amount. However, lithium salts are widely used in the treatment of manic-depressive mood disorder. It has been shown to very effectively suppress mood swings, either as a single drug or in combination with antidepressants. To reach an effective lithium concentration in plasma of 0.5 to 1.2 mmol/L, the required daily lithium dosage can vary considerably between patients, ranging from 10 to 80 mmol [4]. Changes in the rate of excretion, for example due to increased perspiration in the summer will affect the lithium concentration in plasma. In addition, the therapeutic index, i.e. the ratio between the toxic concentration (approximately 1.6 mmol/L) and the therapeutic concentration, is very low. This makes monitoring of the lithium concentration in blood a critical issue in order to prevent adverse side-affects throughout the treatment.

4.2 Measuring whole blood with microchip CE

4.2.1 Standards of clinical analysis

Routine clinical methods for the determination of alkali metals in plasma or serum include flame emission spectroscopy, atomic absorption spectrometry and potentiometry with ion selective electrodes. Though these techniques provide accurate results, there is currently no point-of-care test for lithium commercially available. Both patients and physicians would therefore welcome a lithium analyzer that provides an almost instantaneous result without any sample preparation while reducing the necessary amount of sample to a single drop. Commercially, there are a few point-of-care tests available that actually do measure directly in whole blood. Examples are the common glucose meter and the more sophisticated i-STAT clinical analyzer [5]. The first instrument uses amperometry to measure the enzymatic conversion of glucose on the electrodes. The i-STAT system utilizes disposable cartridges with different detection principles (e.g., miniaturized ion selective electrodes (ISE), conductivity and amperometry) to measure a range of blood components. It determines the alkali metals potassium and sodium with ISEs, but there is no sensor for lithium. Although it is possible to measure lithium with a conventional ISE

there is ongoing research finding suitable ionophores with sufficiently high selectivity with respect to the high concentration of sodium [6]. A more generic method, for example separation by capillary electrophoresis, has the advantage that a multitude of ions can be measured simultaneously on the same device without the need for selective detection.

4.2.2 On-chip removal of blood cells

In the clinical laboratory the first step of almost any blood test is to remove the cells to obtain either plasma or serum. Therefore, errors caused by continuing cell metabolism or cell lysis are avoided. One of the problems of working with blood in microfluidic devices is the vast amount of cellular material in blood (Fig. 4.1A,B). Blood contains approximately five million red blood cells per microliter, accounting for approximately 40% of the total blood volume. Platelets take up another 6% of the volume or 250,000 cells per microliter and the white blood cell count is approximately 7,000 per microliter.

There has been research conducted towards the fabrication of micromachined devices that are capable of preparing plasma from whole blood on-chip. One way to generate plasma is to put the whole chip in a centrifuge after collecting a blood sample [8]. Alternatively, a blood sample can be pumped through a filtration structure to remove cellular material. Weirs and micropost structures have been used to trap white blood cells [9] and lateral percolation filters have been machined in silicon [10]. Dielectrophoresis can be used to trap cells in an electrical field, which also allows the cells to be released again on command [11,12]. Another approach is utilized by the T-sensor or filter, which does not trap the cells but relies on diffusion of analyte ions and molecules into an acceptor solution, which is then analyzed [13]. In this chapter the electromigration of the blood cells will be used to obtain a cell-free fraction.

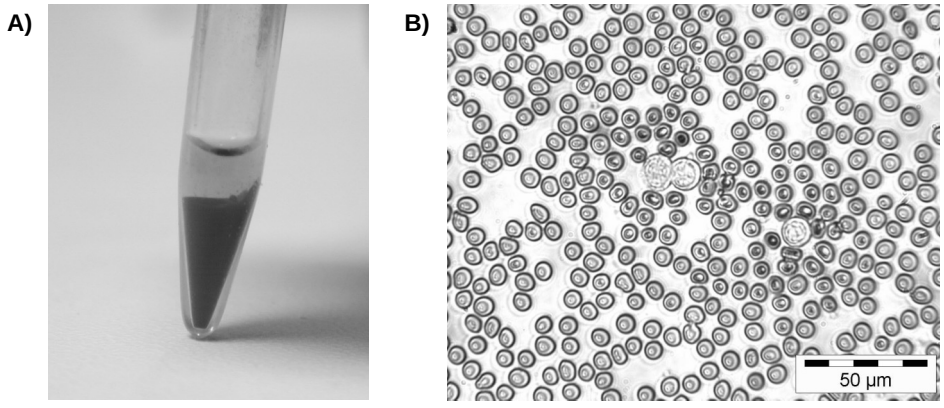

Figure 4.1: *A) Separation of whole blood in a cell fraction and plasma by centrifugation, B) blood smear stained with a Giemsa stain (mixture of eosin and methylene blue in methanol [7]).*

4.2.3 Microchip analysis of lithium in blood

Once plasma or serum is available, the separation by CE is still not trivial. The high sodium and chloride background concentrations of around 140 mmol/L and 105 mmol/L respectively remain as a problem. Compared to most CE background electrolytes (BGE), blood has a much higher ionic strength and this mismatch between sample and BGE can result in extensive dispersion. The analysis of lithium with conventional CE was therefore performed on 20 or 50 times diluted serum [14]. Alternatively, Everaerts and Gebauer showed, that there are conditions under which minor components can still be determined in an excess of matrix [15,16]. This process of sample self-stacking relies on transient isotachophoretic conditions at the beginning of the separation changing to zone electrophoresis towards the end. There, the matrix ion serves as either leading or terminating ion with the BGE co-ion as its complement. Sample components with a mobility between that of the matrix component and the BGE co-ion are determined with high efficiency [17]. This method has been applied for example to the analysis of organic acids in undiluted serum [18].

Besides the high ionic strength there are other interfering components in serum. Proteins can cause problems in CE due to wall adsorption altering the separation conditions when performing multiple runs. These adsorption effects have to be studied for method development but may not be a critical parameter for a single-use disposable device. Also many types of surface coatings can be found in literature to reduce the adsorption problem of proteins during CE separations [19].

Microchip electrophoresis of alkali ions in aqueous samples has been shown before, including the separation of lithium [20-24]. The challenge is to develop this further and use the specific advantages that chip technology offers to measure these ions in whole blood. In order to prevent interference from blood cells it will be necessary to avoid injecting them into the separation channel. The concern is that cells that enter the separation channel will lyse, releasing their contents. In this study we present for the first time the direct measurement of whole blood by microchip capillary electrophoresis. The relatively low electrophoretic mobility of the blood cells, compared to the alkali metals, is used to receive a cell-free sample plug in the double-T of a typical CE microchip. The sample plug is subsequently separated and the lithium concentration is determined.

4.3 Materials and methods

4.3.1 Reagents

Standards containing sodium, potassium and lithium were prepared by dissolving the chloride salts (Merck, Darmstadt, Germany) in deionized water (Millipore). To model clinically relevant concentrations aqueous solutions were prepared with 0.5 and 1 mmol/L lithium in the presence of 150 mmol/L sodium while for the calibration curve the lithium

concentration was extended to 5 mmol/L. For the CE experiments a background electrolyte consisting of 50 mmol/L 2-(N-morpholino)ethanesulfonic acid (MES, Sigma, Steinheim Germany) and 50 mmol/L histidine (His, Fluka, Buchs, Switzerland) with a pH of 6.1 was used. In certain experiments 200 mmol/L glucose (Sigma) was added to adjust the osmotic strength of the BGE. Glucose does not increase the electrical conductivity of the BGE and should therefore not interfere with the separation or detection of alkali ions.

4.3.2 Blood samples

Blood was obtained performing a finger stick on a volunteer using Haemolance (HaeMedic AB, Sweden) disposable lancets. Approximately 30 µl of blood was collected with a pipette and transferred to a plastic tube. For experiments requiring whole blood 10 µl of 80.6 mmol/L sodium citrate (Sigma) was added to prevent the sample from coagulating. To obtain serum the sample was allowed to clot for 10 minutes. The serum was collected after centrifuging the sample for 10 minutes at 11,500 g (Biofuge Pico, Heraeus, Germany). From each sample an aliquot of 18 µl was spiked with 2 µl of 20 mmol/L lithium just before the start of an experiment in order to obtain a concentration of 2 mmol/L. To visualize the plug formation a positively charged fluorescent dye (rhodamine 123, Fluka) was added to the samples at a concentration of 1 mmol/L when required.

4.3.3 Microfabricated CE chips

Figure 4.2A shows a Borofloat glass chip with a double-T injector that was purchased

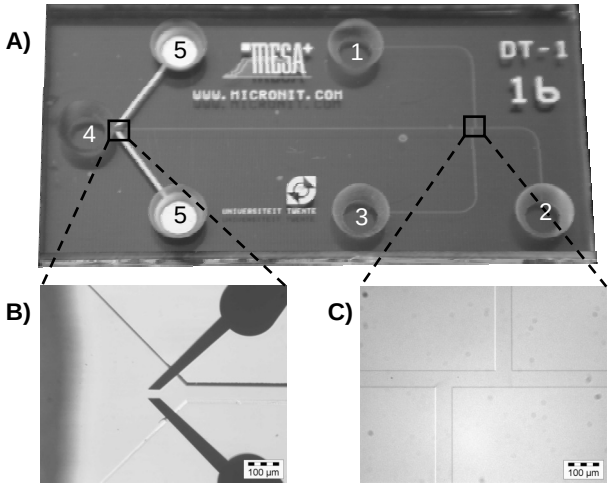

Figure 4.2: *A) Photograph of the microchip with dimensions 3 cm × 1.5 cm. With sample compartment (1) background electrolyte compartment (2), waste compartment (3), outlet compartment (4) and detection electrodes (5). B) Close-up of the end of the channel with the conductivity detection electrodes and C) double-T injector.*

from Micronit Microfluidics BV (Enschede, The Netherlands). All channels were etched to a depth of 8 μm and a top width of 56 μm using hydrofluoric acid. The same figure also shows close-ups of the conductivity detection electrodes (Fig. 4.2B) and the double-T injector (Fig. 4.2C). The length of the separation channel from the T-injector to the detection electrodes was 2 cm while the T-intersection had a length of 200 μm. The detection electrodes consisted of a layer of thin film platinum, which was in direct contact with the electrolyte inside of the channel. The chips were placed in a holder made from Delrin™ consisting of a bottom support plate with an opening below the chip. A cover plate with platinum wires inserted into the fluidic compartments for electrical contacts to the high-voltage supply was placed on top of the chip. The holder containing the chip was placed on an inverted microscope stage (Leica DM/IRM, Wetzlar, Germany) to follow the filling of the channels with BGE and to track the blood cells during the separation experiments.

4.3.4 Surface coating

All experiments were performed on coated glass chips unless specified otherwise. Chips were coated with polyacrylamide according to the procedure of Hjertén for fused silica capillaries [25]. In brief, the chip was filled with a solution of 40 μl 3-(trimethoxysilyl)propyl methacrylate (Aldrich) in 10 ml water adjusted to pH 3.5 with acetic acid (Merck) and allowed to react overnight. The channels were subsequently washed with water and filled with a mixture of 3% (w/v) acrylamide (Aldrich), 0.1% (v/v) N,N,N',N'-tetramethylethylenediamine (Sigma) and 0.1% (w/v) potassium persulfate (Aldrich) in water. During the polymerization reaction the chip was covered with a microscope slide to prevent inhibition by oxygen from the air. After 30 minutes the solution was removed and channels were washed with water after which the chip was ready for use.

4.3.5 Capillary electrophoresis on microfabricated chips

For the CE experiments a computer controlled high voltage power supply (CU 411, IBIS Technologies BV, Hengelo, The Netherlands) with four independently controllable positive voltage outputs and a custom-made AC-conductivity detector (Sprenkels Consultancy, Lelystad, The Netherlands) were used. The detector signal was recorded with a data acquisition card (DAQCard 6036E, National Instruments, Austin, TX, USA). An in-house written software package combined the control of the power supply, acquisition of data from the detector and the subsequent data processing.

A pinched sample loading procedure was used to fill the double-T with sample. The voltages were set to 1000 V at the sample compartment and at the outlet (1 and 4 in Fig. 4.2A), to 0 V at the waste (3) and to 800 V at the background electrolyte compartment (2). These settings were maintained for 15 seconds on an uncoated chip and for 60 seconds on the coated microchip. To initiate the separation the voltages were switched at the background electrolyte compartment to 1000 V, at the sample and waste to 600 V, and at

the outlet to 0 V. The separation was performed for 60 seconds on the uncoated chip and for 120 seconds on the coated chip. Throughout the experiment the red blood cells were tracked to determine the distance they traveled inside the channels and to verify whether they remain intact. The platelets and white blood cells were not observed under these conditions.

4.4 Results and discussion

4.4.1 Sample loading and electrokinetic transport of red blood cells in uncoated channels

The first experiments were performed on a microchip without coating. Under physiological conditions red blood cells (RBC's), white blood cells and platelets all have a negative net charge. This is due mainly to glycoproteins on the cell surface terminating in a sialic acid group. Since the cells have a charge, they migrate through capillaries in the presence of an electrical field [26]. The heterogeneity between individual cells for example has been used to determine the electrophoretic mobility of single RBC's [27]. On-chip manipulation of RBC's has been demonstrated too, showing the possibility to lyse cells by mixing them with a stream of sodium dodecyl sulfate [28]. Also microchip immunoelectrophoresis of RBC's has been performed [29]. However in all these papers the authors used RBC's removed from the blood plasma and resuspended in buffer or at least diluted the blood sample in order to minimize interference from proteins and to obtain a suitable cell concentration.

In order to explain how the cells can be excluded from the cross or T-injector of the microchip without any additional features for sample preparation a closer look to the sample loading is required. Typically, the sample plug in the double-T of a microchip is formed using the EOF to drive the sample through the channels. In general, also a voltage is applied to the remaining compartments to prevent leakage of sample into the separation channel, thus creating the conditions for full plug shaping [30]. The mobility of the EOF in glass channels is 4.2×10^{-4} cm^2/Vs, calculated from the EOF peak in our microchip CE experiments using a clean chip. Electrophoretic mobility values of red blood cells have been reported between -1.6×10^{-4} cm^2/Vs and -3.0×10^{-5} cm^2/Vs [26,28]. Since the EOF exceeds the migration velocity of the cells, the cells will enter the sample channel during the sample loading and consequently they will eventually fill also the double-T. However, for the measurement of relatively fast ions such as sodium and lithium the sample loading does not have to be maintained that long, which gives the opportunity to start the separation before the cells reach the double-T.

For example, consider the situation depicted in Fig. 4.3A, showing the sample loading that has progressed for a certain time. From the start of the loading the bulk of the sample moves towards the injector because of the EOF (zone α). Cations migrate out of the EOF driven sample bulk and form additional leading zones (i.e. zones β and γ). Completely at the front, there is a zone containing only the fastest sample component, in this case potassium. This zone is followed by moving boundary zones in the order of decreasing mobility [31]. Since different zones form, a cell-free fraction can be selected for separation by switching to the separation phase at the correct time (Fig. 4.3B). When switching too late to the separation phase, also slow moving components such as the blood cells in zone α are injected into the separation channel. On the contrary when the sample loading is too short lithium has not reached the injector. An estimation of the minimal loading time for lithium based on its electrophoretic mobility is 4.5 seconds to reach the injector at zero EOF conditions. Normally during CE on glass chip the ions experience a co-migrating EOF, which would make the net flow of the analytes even faster. By observing the migration of red blood cells into the channels the maximum allowable sample loading time can be determined.

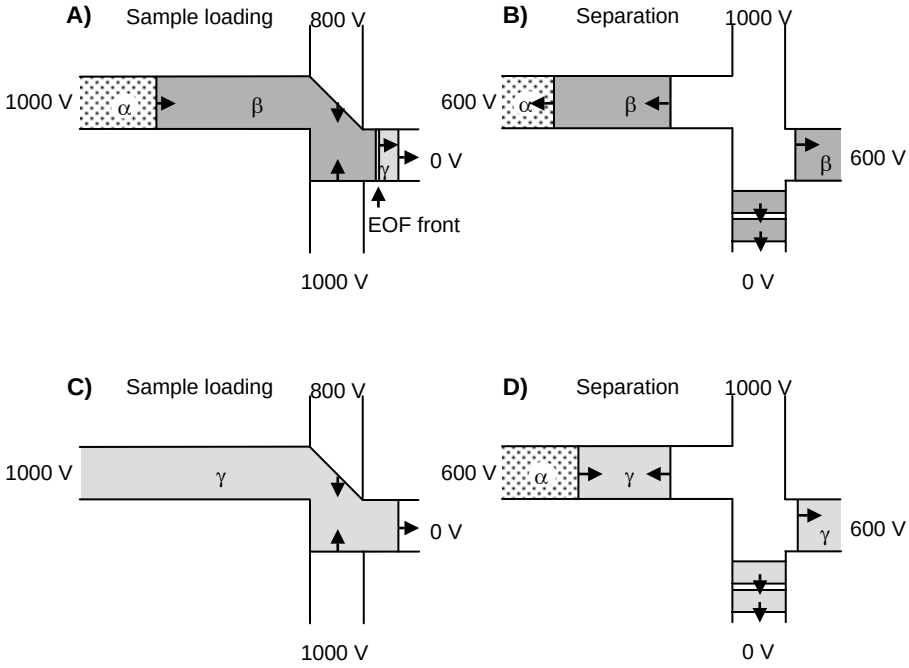

Figure 4.3: *Schematic representation of the sample loading and separation procedure in uncoated channels (A, B) and coated channels (C, D). Zone α: containing blood cells, β: EOF driven zone free from cells, γ: cations migrated out of the sample zone. Sample compartment is on the left of the picture, background electrolyte on the top, waste on the right and outlet compartment is on the bottom. The arrows indicate the direction of migration.*

On the uncoated chip, the experiments show that the cells are indeed pumped from the sample compartment into the sample channel during the loading step (Fig. 4.4). Using the chip for the first time with whole blood, the cells almost reached the double-T in the loading time of 15 seconds as selected for this experiment. During the separation the cells ought to be pumped out of the sample channel again, however, a significant number adhered to the surface. In addition, these cells were exposed to the low osmotic strength BGE during the separation step, which caused them to lyse. Also a few cells were seen to travel into the opposite direction compared to the majority. This was probably caused by mobility differences between individual cells combined with local variations in the EOF due to adsorption of proteins on the channel surface. After the experiment any cells that were still inside the channels were flushed out manually using a hydrodynamic flow of BGE. In a subsequent run the cells travel only half the distance during the loading indicating that proteins were adsorbed during the first run, reducing the EOF (see section 2.2.2 for fundamentals on EOF). It was also observed that this protein layer decreased the interaction between cells and the channel wall minimizing the risk for cell lysis during the separation run.

In all separation runs the sodium peak was clearly identified, but lithium could not be resolved sufficiently (Fig. 4.5B). For the calibration solutions consisting of an aqueous mixture of 150 mmol/L sodium and 2 mmol/L lithium the peaks were not resolved at all (Fig. 4.5A). The difference in peak height between calibration and blood is proof for variations in the sample loading conditions leading to sample plugs with a different size or composition. All these factors together prompted us to continue the experiments with microchips that had a defined coating on the surface of the channels in order to obtain more stable conditions.

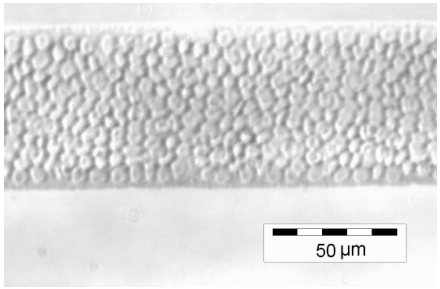

Figure 4.4: *Red blood cells as observed in the experiments entering the sample channel of an uncoated device during sample loading. This photograph is taken from a device with slightly wider channels than used for all other experiments.*

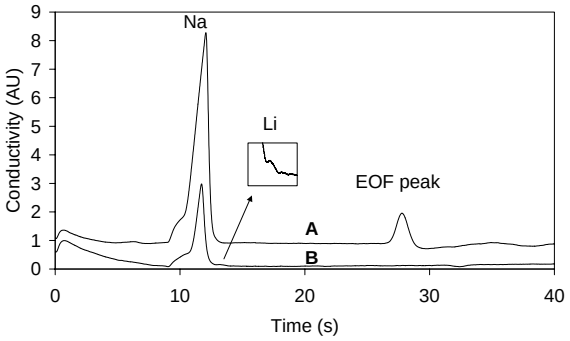

Figure 4.5: *Separation on an uncoated device of A) aqueous calibration mixture containing 150 mmol/L sodium, 5 mmol/L potassium and 2 mmol/L lithium, B) whole blood spiked with 2 mmol/L lithium. Background electrolyte 50 mmol/L MES/His.*

4.4.2 Sample loading and electrokinetic transport of red blood cells in coated channels

When applying EOF suppression the net direction of the cells reverses as the mobility of the cells exceed that of the EOF. Under these conditions the cells do not enter the channels during the sample loading and cells that are in the channels, e.g. from a previous experimental run, will even migrate out (Fig. 4.3C). However, when a pull-back field is used during the separation, cells will now enter the sample channel (zone α in Fig. 4.3D). Depending on the duration of the separation and the electric field strength inside the channels, cells can eventually reach the double-T. Once reached the double-T, they continue to move towards the BGE compartment thus do not enter the separation channel and travel towards the detection region. Yet this could interfere with subsequent experiments.

In general, if the EOF is faster than the mobility of the cells, the cells are always surrounded by blood plasma. In contrast if the cells and bulk flow move in opposite directions, the cells can also migrate out of the blood matrix into the background electrolyte. For example when there is a residual EOF, the cell-depleted blood is pumped into the sample channel during the loading step while the cells themselves remain in the sample compartment. During the separation this blood matrix is again pumped out of the sample channel, but know the cells enter the sample channel and at some point will cross the interface between the blood matrix and background electrolyte. Consequently, when the osmotic strength of the background electrolyte is not matched to blood, cells can lyse. To prevent this 200 mmol/L glucose is added to the background electrolyte for the experiments with whole blood.

The loading experiments using whole blood samples on a coated device clearly showed that the EOF indeed has been suppressed substantially as cells did not enter the sample

channel. Only during the separation when a small pull-back field is used cells slowly migrated down the channel. In this case the cells traveled approximately 2 mm within the 120 seconds of separation. At the moment the next run was started, all cells quickly migrated out without any adhering to the coated surface. Also for repeated injections there was no indication of changes in the behavior of the cells. It was observed that cells being exposed to the BGE during the separation step still showed some degree of swelling, however, there was no sign of cell lysis using the glucose modified BGE.

To summarize, the net transport of cells can be tuned by changing the surface conditions of the channels. The use of a polyacrylamide coating results in reproducible behavior of the red blood cells for at least three consecutive runs using whole blood.

4.4.3 Quantitation of lithium in serum and whole blood

During the separation of aqueous calibration mixtures on a coated chip potassium, sodium and lithium peaks were identified (Fig. 4.6A,B). Also when using serum and whole blood samples (Fig. 4.7) the separation on the coated chip is superior compared to the uncoated chips (Fig. 4.5). The higher efficiency can be attributed in part to the reduction of the EOF, which generally results in a better separation. But also the concentration of analytes in the sample plug can be affected by the suppressed EOF leading to less dispersion as described in chapter 5. Another important conclusion is that also under conditions of suppressed EOF the pinched plug shaping works well as shown in Fig. 4.8. The length of the sample plug dispensed from the 200 μm double-T increases due to diffusion to approximately 350 μm.

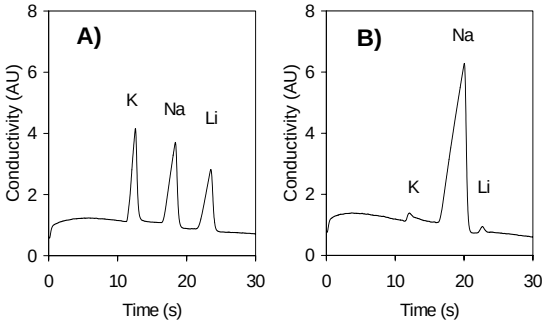

Figure 4.6: *Separation of aqueous calibration mixtures on a coated chip. A) 1 mmol/L of potassium, sodium and lithium. B) 150 mmol/L sodium, 5 mmol/L potassium and 2 mmol/L lithium. Background electrolyte 50 mmol/L MES/His.*

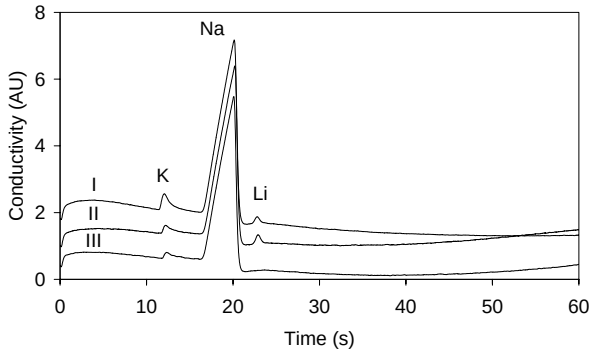

Figure 4.7: *Separation of blood on a coated device. I) serum spiked with 2 mmol/L lithium, II) whole blood spiked with 2 mmol/L lithium, III) whole blood without spiking. Background electrolyte 50 mmol/L MES/His with 200 mmol/L glucose.*

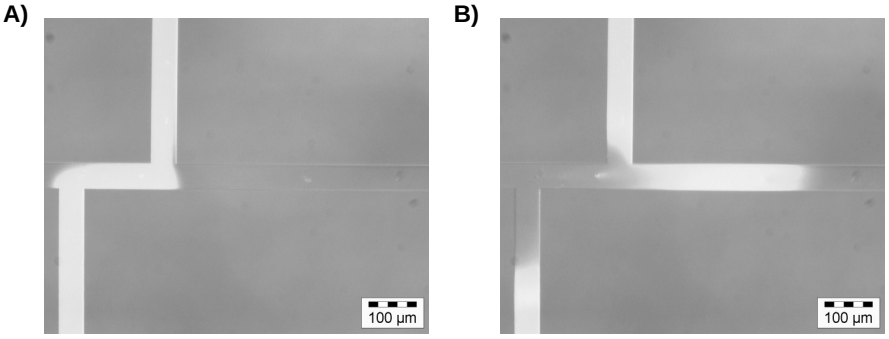

Figure 4.8: *Sample plug formation in the double-T of a chip coated with polyacrylamide (A) and subsequent injection into the separation channel (B). Whole blood sample with 1 mmol/L rhodamine 123.*

For the quantitation of lithium only the coated chips were used. At this point it is important to realize that the sample loading and formation of the sample plug is solely based on the electromigration of ions instead of pumping the sample through the double-T by EOF. This has some consequences for the actual composition of the sample plug injected into the separation channel. Whereas with EOF loading the composition of the sample plug is similar to the bulk of the sample, now with only electromigration the concentration of sample components changes in a way described by Kohlrausch [32]. With the electromigration as transport mechanism the cations from the sample displace the BGE co-ions. The initial BGE concentration and the sample matrix composition therefore determine the final sample concentration inside the channels, regardless of the concentration in the sample. In fact what happens is that sample is either stacked or destacked during the loading. Since the blood sample has a higher ionic strength than the

BGE, the sample plug should consist of diluted sample. These effects were verified by examining the calibration curve of an aqueous mixture of sodium and lithium, which showed a nonlinear behavior (Fig. 4.9A). For the concentration of lithium in the sample plug this means that it is more diluted when the sample contains a larger amount of sodium. For quantitation it is therefore necessary to correct for this matrix effect using an internal standard. Figure 4.9B shows that the ratio between the sodium and lithium peak area scale linearly with the sodium concentration. The blood sodium concentration is fairly stable between 135 and 145 mmol/L and can be used as a readily present internal standard. In the calibration curve of lithium in a background of 150 mmol/L sodium (Fig. 4.10), sodium was therefore used as internal standard by dividing the peak area of lithium by that of sodium to correct for changes in the loading conditions. This also presents us with the interesting opportunity to report sodium-lithium ratios instead of absolute lithium concentrations. It has been argued that sodium-lithium ratios reflect the patients' condition better [33]. This only requires knowledge about the relative detector sensitivity for sodium and lithium without having to perform a calibration needed to determine absolute values.

From the calibration experiments (Fig. 4.10) the relative lithium/sodium sensitivity was calculated, which was used to calculate the lithium concentration in the spiked blood samples. For the calibration standards a factor of 1.18 was determined. In order to calculate the lithium concentration, it was assumed that the plasma sodium concentration in prepared blood samples containing sodium citrate (see section 3.2), was 148 mmol/L. From the composition of blood as described in the introduction the second assumption was that the volume of plasma is 55% of whole blood and that there is no exchange of components between cells and plasma. Spiking a blood sample of 18 µl with 2 µl of 20 mmol/L lithium chloride therefore theoretically results in a value of 3.36 mmol/L lithium. The experimental results show a lithium concentration of 2.7 mmol/L with a RSD of 2.1% (n=3) calculated from the electropherograms. Hence, the recovery of lithium from whole blood is 81%. We can expect changes in the concentration profile of a whole blood

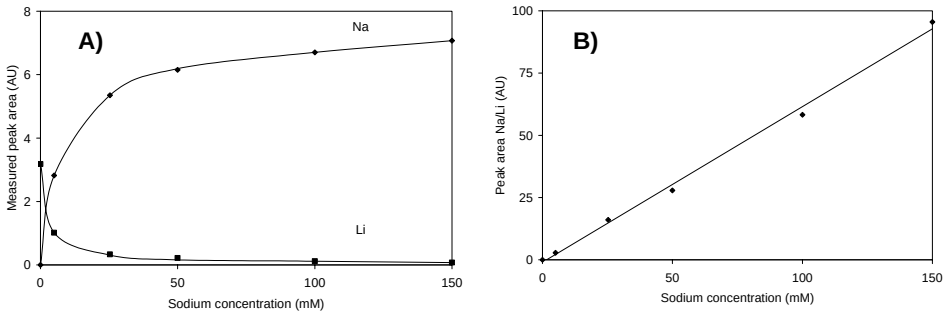

Figure 4.9: *A) Calibration curve for aqueous sodium standards containing 2 mmol/L lithium and B) the ratio of the peak areas as function of the sodium concentration.*

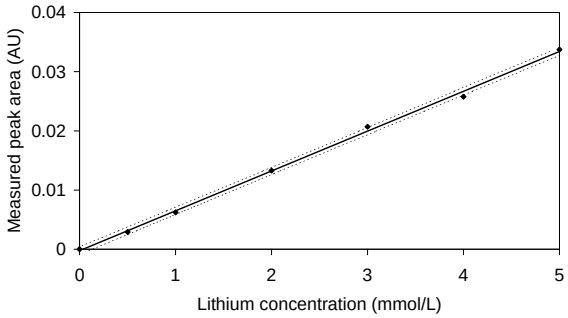

Figure 4.10: *Calibration curve for lithium in a fixed matrix of 150 mmol/L sodium. The dotted lines denote the 95% confidence intervals.*

sample, due to the uptake of lithium by cells. The experiment was therefore repeated using serum as sample. This sample also was spiked to result a lithium concentration of 2 mmol/L. The concentration calculated from that experiment was 1.8 mmol/L with a detection limit of 0.4 mmol/L for lithium defined as three times the low frequency noise level. Thus in this case lithium was also not fully recovered. Using an average of 140 mmol/L sodium as the internal standard the error on the lithium concentration can be estimated to be up to 4%. The error in the measured peak area does also not sufficiently explain the error of approximately 10% on the recovery for the serum sample. Depending on the choice of buffer system the concentration profile of ions in the sample plug may be influenced by the ions in the sample matrix as it was demonstrated for sodium (Fig. 4.9) and does not necessarily represent the original concentration ratios of the serum sample. To investigate the sources of error in detail more experiments are necessary. It is furthermore interesting to note that the potassium peak in the serum sample is higher than in the whole blood sample (Fig. 4.7), which can indicate that not all the cells stayed intact during the described non-clinical sample treatment for serum. However, this measurement was performed on a single sample only.

4.5 Conclusions

The presented experiments demonstrate that it is possible to measure alkali metal ions in a sample as complex as whole blood with a microfluidic glass chip. Even a bare glass chip without a coating might be suitable for single-use, although the current device did not have sufficient resolving power. The chip coated with polyacrylamide provided stable results over repeated injections with no adhesion of red blood cells to the channel surface and increased resolution for the separation of sodium and lithium. The voltage sequence in respect to the exact timing of loading and separation to prevent injection of blood cells was found to be not critical. The use of polymer microchips instead of glass is also an option since an EOF is not required.

Lithium was determined in whole blood diluted only with anticoagulant. Since a matrix effect occurs it is absolutely necessary to use an internal standard for quantitation. In serum the detection limit for lithium is with 0.4 mmol/L above the quantitation limit of 0.2 mmol/L that is desirable for clinical use. The main limitation for further optimization is the restriction of the dynamic range of the detector. Thus, increasing the sensitivity would only result in exceeding the working range of the detector which has been reached already for the sodium peak. Therefore the aim will be to reduce baseline noise by improving the detector electronics and to increase sensitivity for lithium compared to that of sodium by the choice of an appropriate background electrolyte.

Measurements on calibration samples in the clinically relevant range were presented. The next step towards the final application will be to measure in blood samples obtained from patients being on lithium therapy and compare the results obtained from the microchip with routine clinical methods. A larger supply of sample taking into account the variation from one individual to another will give us the opportunity to focus more on the quantitative aspects in order to improve the lithium recovery. Especially, the sample loading process under conditions of suppressed EOF needs to be studied in greater detail. The process of sample stacking and destacking under moving boundary electrophoresis conditions during the sample loading is discussed in the chapter 5.

4.6 References

1. A van den Berg and TSJ Lammerink "*Micro Total Analysis Systems; Microfluidic Aspects, Integration Concept and Applications"*, Topics in Current Chemistry 1998, **194**, 21-49.
2. E Verpoorte "*Microfluidic chips for clinical and forensic analysis"*, Electrophoresis 2002, **23**, 677-712.
3. CS Effenhauser, A Manz and HM Widmer "*Glass Chips for High-speed Capillary Electrophoresis Separations with Submicrometer Plate Heights"*, Anal. Chem. 1993, **65**, 2637-2642.
4. A Amdisen "*Monitoring of lithium treatment through determination of lithium concentration"*, Danish medical bulletin 1975, **22**, 277-291.
5. KA Erickson and P Wilding "*Evaluation of a Novel Point-of-Care System, the i-STAT Portable Clinical Analyzer"*, Clin. Chem. 1993, **39**, 283-287.
6. P Bühlmann, E Pretsch and E Bakker "*Carrier-Based Ion-Selective Electrodes and Bulk Optodes. 2. Ionophores for Potentiometric and Optical Sensors"*, Chem. Rev. 1998, **98** , 1593-1687.
7. L Weiss (ed). "*Cell and tissue biology. A textbook of histology."*, 6th edition, 1988, München, Urban&Schwarzenberg

8. A Oki, M Takai, H Ogawa, Y Takamura, T Fukasawa, J Kikuchi, Y Ito, T Ichiki and Y Horiike "*Healthcare Chip for Checking Health Condition from Analysis of Trace Blood Collected by Painless Needle"*, Jpn. J. Appl. Phys. 2003, **42**, 3722-2727.
9. P Wilding, LJ Kricka, J Cheng, G Hvichia, MA Shoffner and P Fortina "*Integrated Cell Isolation and Polymerase Chain Reaction Analysis Using Silicon Microfilter Chambers"*, Anlytical Biochemistry 1998, **257**, 95-100.
10. B He, L Tan and FE Regnier "*Microfabricated Filters for Microfluidic Analytical Systems"*, Anal. Chem. 1999, **71**, 1464-1468.
11. J Auerswald and HF Knapp "*Quantitative assessment of dielectrophoresis as a micro fluidic retention and separation technique for beads and human blood erythrocytes"*, Microelectronic Engineering 2003, **67-68**, 879-886.
12. PRC Gascoyne and J Vykoukal "*Particle separation by dielectrophoresis"*, Electrophoresis 2002, **23**, 1973-1983.
13. BH Weigl, J Kriebel, KJ Mayes, T Bui and P Yager "*Whole Blood Diagnostics in Standard Gravity and Microgravity by Use of Microfluidic Structures (T-Sensors)"*, Mikrochim. Acta 1999, **131**, 75-83.
14. X Huang, MJ Gordon and RN Zare "*Quantitation of Li^+ in serum by capillary zone electrophoresis with an on-column conductivity detector"*, J. Chromatogr. 1988, **425**, 385-390.
15. JL Beckers and FM Everaerts "*Isotachophoresis with two leading ions and migration behaviour in capillary zone electrophoresis; II. Migration behaviour in capillary zone electrophoresis"*, J. Chromatogr. 1990, **508**, 19-26.
16. P Gebauer, W Thormann and P Bocek "*Sample self-stacking in zone electrophoresis Theoretical description of the zone electrophoretic separation of minor compounds in the presence of bulk amounts of a sample component with high mobility and like charge"*, J. Chromatogr. 1992, **608**, 47-57.
17. J Boden and K Bächmann "*Investigation of matrix effects in capillary zone electrophoresis"*, J. Chromatogr. A 1996, **734**, 319-330.
18. V Dolník and J Dolníková "*Capillary zone electrophoresis of organic acids in serum of critically ill children"*, J. Chromatogr. A 1995, **716**, 269-277.
19. J Horvath and V Dolník "*Polymer wall coatings for capillary electrophoresis"*, Electrophoresis 2001, **22**, 644-655.
20. A Berthold, F Laugere, H Schellevis, CR De Boer, M Laros, RM Guijt, PM Sarro and MJ Vellekoop "*Fabrication of a glass-implemented microcapillary electrophoresis device with integrated contactless conductivity detection"*, Electrophoresis 2002, **23**, 3511-3519.
21. RM Guijt, E Baltussen, G Van der Steen, RBM Schasfoort, S Schlautmann, HAH Billiet, J Frank, GWK Van Dedem and A Van den Berg " *New approaches for fabrication of microfluidic capillary electrophoresis devices with on-chip conductivity detection"*, Electrophoresis 2001, **22**, 235-241.

22. J Lichtenberg, NF De Rooij and E Verpoorte "*A microchip electrophoresis system with integrated in-plane electrodes for contactless conductivity detection"*, Electrophoresis 2002, **23**, 3769-3780.
23. M Pumera, J Wang, F Opekar, I Helínek, J Feldman, H Löwe and S Hardt "*Contactless Conductivity Detector for Microchip Capillary Electrophoresis"*, Anal. Chem. 2002, **74**, 1968-1971.
24. J Tanyanyiwa, EM Abad-Villar, MT Fernández-Abedul, A Costa-Garcìa, W Hoffmann, AE Guber, D Herrmann, A Gerlach, N Gottschlich and PC Hauser "*High-voltage contactless conductivity-detection for lab-on-chip devices using external electrodes on the holder"*, Analyst 2003, **128**, 1019-1022.
25. S Hjertén "*High-performance electrophoresis; Elimination of electroendosmosis and solute adsorption"*, J. Chromatogr. 1985, **347**, 191-198.
26. S Kitagawa, O Nozaki and T Tsuda "*Study of the relationship between electrophoretic mobility of the diabetic red blood cell and hemoglobin A1c by using a mini-cell electrophoresis apparatus"*, Electrophoresis 1999, **20**, 2560-2565.
27. AR Minerick, AE Ostafin and H-C Chang "*Electrokinetic transport of red blood cells in microcapillaries"*, Electrophoresis 2002, **23**, 2165-2173.
28. PCH Li and DJ Harrison "*Transport, Manipulation, and Reaction of Biological Cells On-Chip Using Electrokinetic Effects"*, Anal. Chem. 1997, **69**, 1564-1568.
29. T Ichiki, T Ujiie, S Shinbashi, T Okuda and Y Horiike "*Immunoelectrophoresis of red blood cells performed on microcapillary chips"*, Electrophoresis 2002, **23**, 2029-2034.
30. LL Shultz-Lockyear, CL Colyer, ZH Fan, KI Roy and DJ Harrison "*Effects of injector geometry and sample matrix on injection and sample loading in integrated capillary electrophoresis devices"*, Electrophoresis 1999, **20**, 529-538.
31. CJ Backhouse, HJ Crabtree and DM Glerum "*Frontal analysis on a microchip"*, Analyst 2002, **127**, 1169-1175.
32. F Kohlrausch "*Ueber Concentrations-Verschiebungen durch Electrolyse im Inneren von Lösungen und Lösungsgemischen"*, Ann. Phys. Chem. 1897, **62**, 209-239.
33. E Metzger, R Dohner, W Simon, DJ Vonderschmitt and K Gautschi "*Lithium/Sodium Ion Concentration Ratio Measurements in Blood Serum with Lithium and Sodium Ion Selective Liquid Membrane Electrodes"* , Anal. Chem. 1987, **59**, 1600-1603.

Chapter 5

Microchip analysis of lithium in blood using moving boundary electrophoresis and zone electrophoresis*

The determination of inorganic cations in blood plasma is demonstrated using a combination of moving boundary electrophoresis (MBE) and zone electrophoresis. The sample loading performed under MBE conditions is studied with the focus on the quantitative analysis of lithium. A concentration adjustment takes place when the sample components migrate into the chip during the sample loading. Using a heart-cutting method a diluted sample plug is subsequently separated with capillary zone electrophoresis. The excessive dispersion that is typical for samples with a high ionic strength is thereby prevented. The method can be easily applied to other commercially available capillary electrophoresis microchips under the condition that the electroosmotic flow is suppressed. For the first time the lithium concentration is determined in blood plasma from a patient on lithium therapy without off-chip sample pretreatment. Using a microchip with conductivity detection, a detection limit of 0.1 mmol/L is obtained for lithium in a 140 mmol/L sodium matrix.

* This chapter has been accepted for publication in Electrophoresis

5.1 Introduction

Microfluidic systems for capillary electrophoresis (CE) have become the most studied analytical devices in the field of lab-on-a-chip for genomics and proteomics [1-3]. A less investigated application of these devices may be found in clinical diagnostics, with its challenges of reliability, ease-of-use and biosafety. Particularly for the measurement of blood electrolytes, microfluidic capillary electrophoresis systems can offer solutions applying their unique features to reduce sample volumes, operator handling and specimen transport. These aspects make microchip capillary electrophoresis a powerful tool for a wide range of clinical measurements, including the ones at the point of care. In this paper the quantitative analysis of blood with microchip CE is discussed with the focus on the determination of low concentrations of lithium in a matrix containing approximately 140 mmol/L sodium, which is commonly recognized as a problem.

Normally lithium is not present in blood plasma, but it is used as a drug to treat bipolar mood disorder. It is estimated that worldwide up to one million people take lithium on a daily basis [4]. A disadvantage of the use of lithium is the very low therapeutic index, i.e. the ratio between the toxic concentration and the therapeutic concentration. Most patients respond well to a blood plasma concentration of 0.4 to 1.0 mmol/L lithium while side effects can already occur at a lithium concentration of 1.3 mmol/L [5]. A prolonged high blood lithium level can even result in permanent damage to the nervous system. Monitoring of the lithium concentration during treatment is therefore essential, with regular checks every couple of months to adjust the lithium dosage.

To avoid extensive operator handling ion-selective electrodes (ISEs) are routinely used for measurements of blood parameters in an automated fashion [4,6]. These ion-selective electrodes are fast and offer a large dynamic range, however, their response is logarithmic and the required high selectivity for lithium can be a problem. Additionally, in case of lithium intoxication a fast procedure for blood analysis is required. Currently, a venous blood sample must be withdrawn from the patient by specially trained personal, transported to the central laboratory and the blood cells need to be removed before measurement can take place. This procedure can take up to 45 minutes [7]. To minimize sample throughput time miniaturized devices employing ion-sensitive field-effect transistors are available to determine potassium and sodium in whole blood [8] even as a handheld analyzer [9], but not for lithium.

Another approach for point-of-care lithium testing has been recently developed based on changes in the absorbance of light after complexation with a porphyrin compound [10]. To take a reading with this new approach a patient or an operator needs to perform, next to a finger stick, additional handling. First a 50 µl sample is placed onto a clean-up strip, of which the effluent is collected in a pipette. Subsequently, the pipette is discharged manually into a reagent micro-cuvette for complexation followed by the absorbance

measurement. Although this instant test has proven reliable and fast by extensive testing (269 human subjects) it is very specific and does not allow the quantitation of other blood electrolyte parameters simultaneously.

A more generic solution to this request is the application of capillary electrophoresis. This concept was demonstrated for the determination of lithium in diluted serum using a conventional CE system with conductivity detection [11]. Among others, who addressed the potential of microchip CE for alkali metal ions [12-15], we introduced a rapid method for the determination of lithium directly from a whole blood sample placed on the chip with integrated conductivity detection [16]. However, the quantitative analysis of whole blood or even of plasma and serum directly on a CE chip still remains a challenge.

Band broadening in CE is a general problem for samples containing a high concentration of ionic constituents leading to poor resolution [17]. In order to avoid degeneration of the separating performance due to an ionic strength mismatch between sample and the background electrolyte (BGE) different approaches are possible. One approach is to increase the concentration of the BGE. For instance a BGE containing 5 mol/L sodium chloride was used to analyse anions in samples containing inorganic matrix components in concentrations of up to 0.5 mol/L [18]. However, BGEs with a very high concentration are not routinely used because of their vulnerability to Joule heating. In microchip systems however, they can become feasible through better heat dissipation [19]. Another approach is offered by the intrinsic concentration adjusting properties of isotachophoresis (ITP) to separate analytes from the matrix component while keeping the analyte zones confined to small volumes. Under conditions of sample self-stacking, the matrix ion from the sample can be used as either the leading or terminating ion in order to establish ITP conditions. With the BGE co-ion serving as its counterpart, analytes with electrophoretic mobilities in between these two species can be separated from the matrix [20-22]. During the separation run there will be a natural transition from the ITP conditions to capillary zone electrophoresis (CZE), but a certain minimum channel length is required so that both separation modes can fully develop. Alternatively a column-coupling configuration of ITP and CZE can be used to physically separate the two processes providing more control over both stages of the separation [23]. If the analyte is present in a relatively high concentration such that the detection limit is not an issue, a simpler method is the dilution of the sample. For point-of-care testing all the sample treatment steps need to be performed automatically on the chip. The integration of programmable dilution on a microchip format has been demonstrated using the electroosmotic flow (EOF) to pump and mix sample with a diluent [24]. This device relies on a constant pumping speed to reproducibly dilute the samples. Any variations in the EOF due to changes in the surface condition of the channels or variation in the electric field strength will affect the performance.

Since the approaches described above are either complex, sensitive to experimental conditions or the exact mechanisms were not yet completely understood for the quantitation of blood electrolytes we carried out a thorough investigation of on-chip sample pre-treatment based on our earlier studies [16]. There, the sample first formed moving boundaries and subsequently a sample fraction with a time dependent composition was injected into the separation column. The remaining part of this paper describes the operational procedure as a combination of moving boundary electrophoresis [25] and the so-called heart-cutting technique [26]. The method is assessed by fluorescence measurements on model samples. Quantified blood electrolyte analysis with sodium as an internal standard is experimentally compared to a theoretical model for

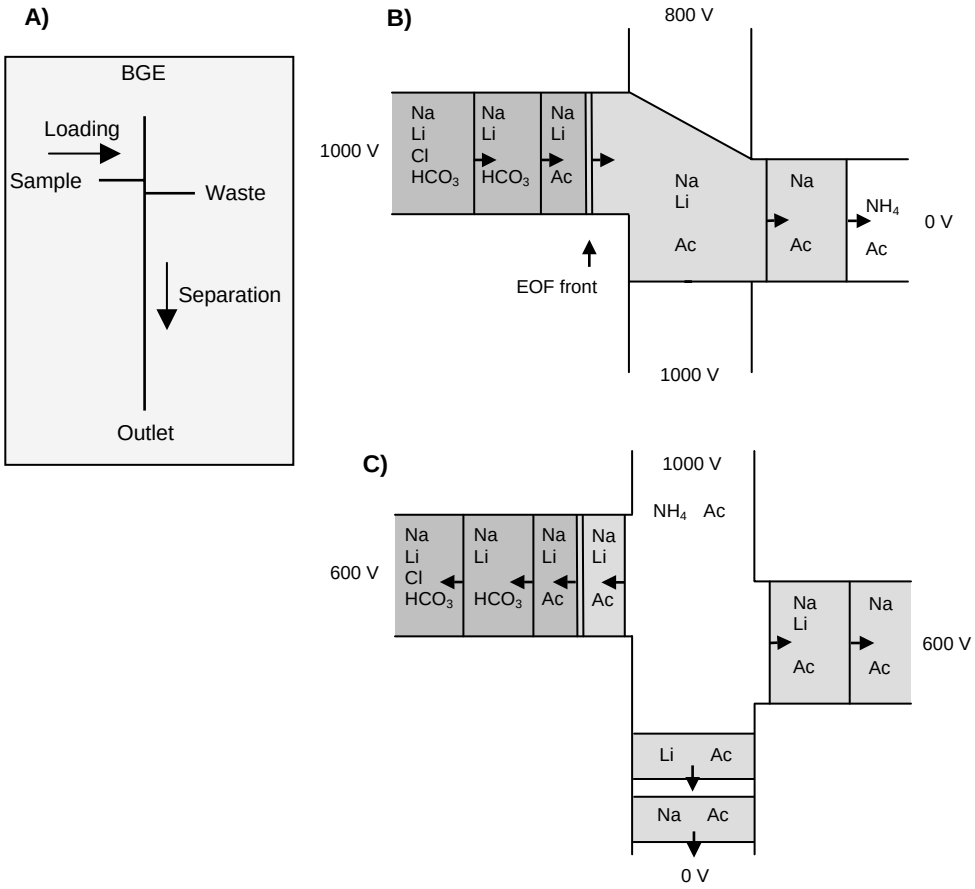

Figure 5.1: *Schematic representation of A) the channel layout of the CE chip with double-T injection geometry, B) the formation of moving boundaries during the sample loading step and C) heart-cutting a particular zone for subsequent separation in CZE mode. The numbers correspond with the voltages applied to the four fluid compartments.*

idealized conditions. Subsequently, this method is verified by quantitation of the lithium concentration in blood plasma from a patient.

5.2 Analytical principle

5.2.1 Moving boundary electrophoresis

In microchip CE the typical channel layout is a heart-cutting configuration of two connecting channels (Fig. 5.1A). The function of the first channel, leading from the sample compartment to the waste (referred to as sample loading channel) is to transport the sample to the channel intersection where a small sample plug is defined by electrokinetic sample pinching [27]. The sample plug is subsequently dispensed into the second channel leading from the background electrolyte compartment to the outlet (referred to as separation channel) for the CZE separation. The electrokinetic transport of sample towards the intersection is a combination of electrophoretic migration of analytes superimposed on the EOF. Since there is a continuous supply of ions migrating into the loading channel from the sample compartment, zones are formed according to the electrophoretic mobility of the ions. An analyte species with a high electrophoretic mobility fills a greater length of the loading channel in a given time period than a species with a lower mobility (see also the simulations in section 3.2). An example of this moving boundary electrophoresis (MBE) is shown in Fig. 5.1B. An artificial blood sample containing sodium chloride, lithium chloride and sodium bicarbonate is used to demonstrate the formation of zones in an ammonium acetate BGE. In a given time period the high mobility of sodium produces a zone with only sodium as cationic species. This zone is followed by a zone with both the fastest and second fastest cationic species, i.e. sodium and lithium. The initial boundary between sample and BGE denoted by a double line in Fig. 5.1B is considered to be stationary because unlike the other boundaries it does not migrate in the electric field. Only the EOF can drive the stationary boundary, also called the concentration boundary, through the channel. On the left of this boundary, the anionic sample components in Fig. 5.1B produce additional zones that migrate towards the sample compartment. Ultimately, for a system consisting of a total of n distinct species in the sample and BGE, a maximum number of $n-1$ boundaries will form. The boundaries between subsequent zones formed by MBE are either self-sharpening resulting in a very steep concentration gradient across the boundaries or they are diffuse. The condition required for sharp boundaries is a BGE co-ion, which will form the leading zone, with a mobility higher than that of the cations in the sample [25]. Similar for zones with sharp transitions on the left of the stationary boundary, the BGE counter-ion mobility has to be slower than any of the anions in the sample. If these conditions are not fulfilled the boundaries between the zones will be diffuse and as a result the behaviour of the system is much more difficult to predict [28]. In this chapter we will therefore only use conditions that produce sharp transitions.

When microchips made of glass are used, the pumping effect of the EOF causes the moving boundary zones to be swept quickly through the channel intersection. Eventually a steady-state is reached where the entire sample loading channel is filled with a homogeneous solution. The exact composition depends on the velocity of the moving boundaries produced by the anionic species and the EOF. If the EOF is faster than any of the anionic boundaries the channel will be filled with the sample solution as present in the compartment. When the EOF is slower, the BGE counter-ion displaces the anionic species from the sample resulting in a channel filled with a solution containing all cationic species from the sample but with the counter-ion of the BGE. When using the EOF for sample loading the composition of cationic species in the sample plug is therefore considered similar to the bulk of the sample. For a reduced or completely absent EOF the MBE and the accompanying concentration adapting effects become the most important mechanism for sample loading. In the zones generated by MBE the concentration of species differs from zone to zone. In particular across the stationary boundary a significant concentration adjustment takes place, which can be used to dilute the sample. The separation of a MBE diluted zone with CZE instead of an undiluted zone trailing the stationary boundary can solve the problem associated with electromigration dispersion caused by samples with an ionic strength higher than the BGE. Using the heart-cutting technique a specific zone can be selected from any of the zones generated by the MBE for further separation in the separation channel (Fig. 5.1C). In order to determine how the concentration adjustment affects the quantitative analysis a more detailed analysis of MBE sample loading is required, which is discussed in the following sections.

5.2.2 Concentration adjustment across the stationary boundary

The entire procedure for diluting high ionic strength samples during the sample loading is based on the processes occurring at the boundary between the sample solution and the BGE. The presence of a stationary boundary or interface between sample and BGE affect the concentration of the ions during electromigration, which is represented by the Kohlrausch regulating function (KRF) [29] that has been redefined as given in Eq. 5.1 [30]:

$$\omega(x) = \sum_{i=1}^{n} \frac{c_i(x) z_i}{\mu_i} \tag{5.1}$$

where c, z and μ are the ionic concentration, valence and electrophoretic mobility respectively and x is the position in the channel. Electrophoretic mobilities and analyte concentrations are signed quantities in the above and all subsequent equations. While Eq. 5.1 is valid for strong electrolytes with constant electrophoretic mobility, Dismukes and Alberty derived a similar Kohlrausch regulating function for monovalent weak electrolytes [31]:

$$\overline{\omega}(x) = \sum_{i=1}^{n} \frac{\bar{c}_i(x)}{r_i} \tag{5.2}$$

where $\bar{c}$ is the combined concentration of neutral and charged forms of a species and r is the relative mobility normalized to the fastest species. For both Eq. 5.1 and 5.2 the values $\omega(x)$ and $\overline{\omega}(x)$ are invariant in time even when a current passes through the system causing ions from the sample to displace the co-ions in the BGE. Initially, all channels in the chip are filled with BGE, which defines one value for the KRF everywhere throughout the entire separation. As analytes migrate from the sample compartment into the sample loading channel the BGE co-ions are displaced. Yet, the concentration of ions from the sample has to adapt so that the local value of the KRF, which was defined by the BGE composition remains unchanged. For samples with a lower ionic strength than the BGE this will result in the so-called stacking effect, while samples with a higher ionic strength are destacked and thus diluted. In fact the sample concentration inside the channels is mainly determined by the composition of the BGE and not by the concentration of ions in the bulk of the sample. One important property of the stationary boundary is that the concentrations ratio between species is the same on both sides. The stationary boundary can therefore be used for diluting samples without changing the relative ratios of analyte concentrations.

5.2.3 Concentration profile in moving boundary zones

In contrast to the stationary boundary, the moving boundaries do induce changes in the concentration ratio of species between zones. In order to establish how the concentrations in the different zones are affected by the sample and BGE composition a more detailed

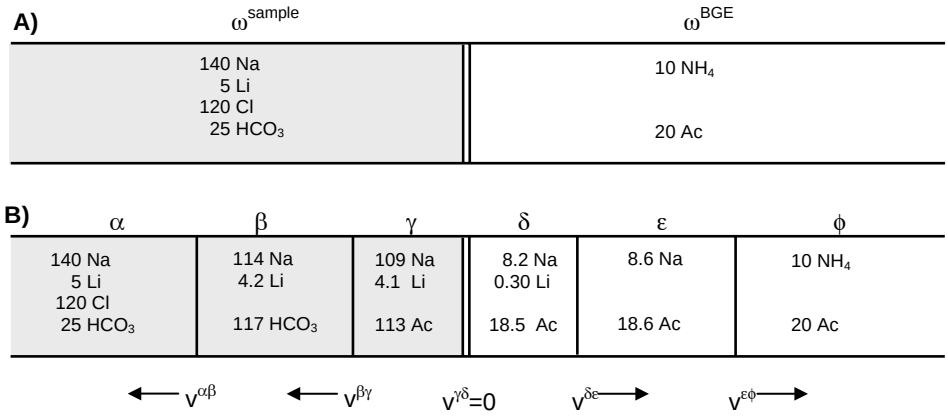

Figure 5.2: *Diagram of the moving boundary electrophoresis using a blood model. A) the starting situation and B) after applying a current. The numbers correspond to the concentrations in mmol/L. Areas with the same shading denote zones with identical value of $\omega(x)$. The Greek symbols denote zones with different composition.*

analysis of the MBE processes is needed. For strong electrolytes, Dole developed a theory that allows the concentration of all species to be calculated in every zone [32]. Consider the situation in Fig. 5.2A showing one half of a channel filled with the artificial blood sample and the other half with the BGE. Figure 5.2B shows the situation after the MBE zones have developed. The concentration of a species *i* in zone β is determined by the ion influx and outflow per unit time. The influx $I^{\alpha\beta}$ across the $\alpha\beta$ boundary that moves with a velocity $V^{\alpha\beta}$ is given by:

$$I_i^{\alpha\beta} = \mu_i E^{\alpha} c_i^{\alpha} - V^{\alpha\beta} c_i^{\alpha} \tag{5.3}$$

where *E* is the electrical field strength. Similarly for the outflow across the boundary between β and γ:

$$I_i^{\beta\gamma} = \mu_i E^{\beta} c_i^{\beta} - V^{\beta\gamma} c_i^{\beta} \tag{5.4}$$

The concentration in zone β is obtained from the net increase of the species divided by the increasing length of the zone:

$$c_i^{\beta} = \frac{I_i^{\alpha\beta} - I_i^{\beta\gamma}}{V^{\beta\gamma} - V^{\alpha\beta}} = c_i^{\alpha} \frac{\mu_i E^{\alpha} - V^{\alpha\beta}}{\mu_i E^{\beta} - V^{\alpha\beta}} \tag{5.5}$$

The general moving boundary equation for strong electrolytes as given by Dole (Eq. 5.6) relates relative electrophoretic mobilities *r*, concentration *c*, relative conductivities σ (calculated using the relative mobilities) and boundary velocity $V^{\alpha\beta}$ between two subsequent zones denoted α and β:

$$c_i^{\beta} = c_i^{\alpha} \frac{V^{\alpha\beta}\sigma^{\beta}\left(V^{\alpha\beta}\sigma^{\alpha} - r_i\right)}{V^{\alpha\beta}\sigma^{\alpha}\left(V^{\alpha\beta}\sigma^{\beta} - r_i\right)} \tag{5.6}$$

For each species and all boundaries an equation of this form can be formulated. Therefore, if the concentration of a species *i* is known in one zone, the concentration in the adjacent zone can be calculated. The set of $V^{\alpha\beta}\sigma^{\beta}$, $V^{\beta\gamma}\sigma^{\gamma}$, etc, products required for the calculations are the solutions of the polynomial equation 5.7, which is graphically shown in Fig. 5.3A [32]:

$$\frac{r_1 - r_n}{r_1 - x} c_1^{\alpha} + \frac{r_2 - r_n}{r_2 - x} c_2^{\alpha} + \ldots + \frac{r_{n-1} - r_n}{r_{n-1} - x} c_{n-1}^{\alpha} = 0 \tag{5.7}$$

where $V^{\alpha\beta}\sigma^{\beta}$ is the most negative value of *x* for which Eq. 5.7 is zero, $V^{\beta\gamma}\sigma^{\gamma}$ the second most negative value, etc. A complementary set of $V^{\alpha\beta}\sigma^{\alpha}$, $V^{\beta\gamma}\sigma^{\beta}$, etc products is obtained

after substituting c_i^{α} by c_i^{β} in Eq. 5.7 (shown graphically in Fig. 5.3B). A special case is a boundary across which two ions disappear. Under these conditions the two $V\sigma$'s are equal to the relative mobilities r of the disappearing ions. For a boundary across which one ion disappears one $V\sigma$ is given by the mobility of the disappearing ion while the other is obtained from Eq. 5.7.

For the case of monovalent weak electrolytes the moving boundary equation transforms to Eq. 5.8 [31]:

$$\frac{c_i^{\alpha} r_i}{V^{\alpha\beta}\sigma^{\alpha}} - \frac{c_i^{\beta} r_i}{V^{\alpha\beta}\sigma^{\beta}} = \bar{c}_i^{\alpha} - \bar{c}_i^{\beta} \tag{5.8}$$

For strong electrolytes, c_i is equal to $\bar{c}_i$ and Eq. 5.8 is equivalent to Eq. 5.6. The values of the concentration profile presented in Fig. 5.2B have been obtained, applying Eq. 5.6.

Equations 5.6 and 5.8 show that the concentration of a species in a zone is a function of its mobility. Therefore the concentration ratio between two species with different mobility will be different in the zones separated by a moving boundary. Only across the stationary boundary the ions experience dilution or concentration with a constant ratio, i.e. when the boundary velocity V is zero both Eq. 5.6 and 5.8 reduce to the form given by Eq. 5.9 where the last term involves the KRF ratio according to Dole [32].

$$\frac{c_i^{\alpha}}{c_i^{\beta}} = \frac{\sigma^{\alpha}}{\sigma^{\beta}} = \frac{\omega^{\alpha}}{\omega^{\beta}} \tag{5.9}$$

Generally, Eq. 5.1 which is required to calculate the dilution, is not applicable to systems of weak electrolytes. For the case discussed in this chapter however, a special situation arises, where there is only one weak analyte present and all other species are strong

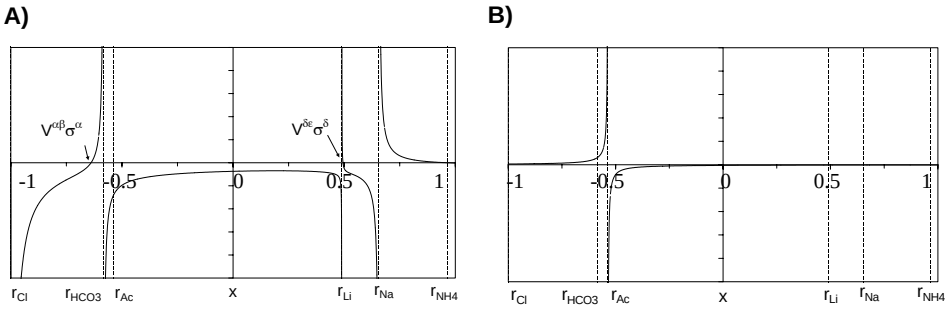

Figure 5.3: *Graphical representation of A) Eq. 5.7 and B) the complementary set with c^{α} substituted by c^{β} in Eq. 5.7. Concentrations used for the calculation as shown in Fig. 5.2A.*

electrolytes. Equation 5.2 can therefore be rewritten as:

$$\overline{\omega}(x) = \sum_{i=1}^{n} \frac{c_i(x)}{r_i} + \frac{c^0_{HAc}(x)}{r_{Ac}} = \omega(x) + \frac{c^0_{HAc}(x)}{r_{Ac}} \tag{5.10}$$

Where c^0_{HAc} is the concentration of the weak analyte that is in the neutral form. From Jovin [33] an additional expression of the KRF for weak electrolytes in zones separated by a moving boundary is given:

$$\omega_0(x) = \sum_{i=1}^{n} c_i^0(x) \tag{5.11}$$

Based on Eq. 5.11, the last term in Eq. 5.10 is constant and we can conclude that Eq. 5.1 is valid for the experimental conditions described.

It is important to consider the change in concentration between species relative to one another if accurate quantitation of the sample is required. During the experiments the zone that leads the stationary boundary is injected into the separation channel (e.g. zone δ in Fig. 5.2B). If no moving boundaries form before the stationary boundary (i.e. the zones β and γ will be absent), the ratio of cationic species in the zone leading the stationary boundary is the same as in the bulk of the sample. Although the actual dilution of sample is generally unknown, an internal standard can be employed for the quantitation since the concentration ratio between the analyte and standard will not change. For samples that do produce additional boundaries due to the presence of multiple anionic species in the sample or BGE the relative amounts of cations in zone δ will shift. For the example shown in Fig. 5.2B the resulting sodium-lithium ratio is 27.3. This ratio is affected by the composition of the sample and a certain error in quantitation has to be expected, even when working with an internal standard. Being aware of these characteristics the experimental section will describe and discuss the formation of moving boundaries and their concentration profile for the specific case of determining lithium in blood.

5.3 Materials and methods

5.3.1 Reagents and sample

Sodium and lithium standards were prepared by dissolving the respective chloride salts (Merck, Darmstadt, Germany) in deionized water (Millipore). To model clinically relevant salt concentrations aqueous solutions were prepared with 0 to 2 mmol/L lithium in the presence of 140 mmol/L sodium chloride. For experiments based on fluorescence detection the cationic rhodamine 123 (Fluka, Buchs, Switzerland) was used. The CE experiments were performed using a background electrolyte consisting of 10 mmol/L ammonium acetate (Sigma, Steinheim Germany) and 10 mmol/L acetic acid (Merck) with 0.01% (hydroxypropyl)methyl cellulose (HPMC, Sigma) as EOF modifier. Only when a chip with a permanent polyacrylamide coating was used no EOF modifier was added to the BGE because this coating suppresses the EOF sufficiently. Heparinized blood plasma (sodium heparin) from a venipuncture on a patient treated with lithium was donated by the hospital (Medisch Spectrum Twente, Enschede). The lithium concentration (0.62 mmol/L) was determined in the hospital with an ion-selective electrode (Cobas Integra 800, Roche, Basel, Switzerland) in a serum sample from the same patient.

5.3.2 Microfabricated CE chips

Borofloat^{TM} glass chips with a double-T injector of 200 µm length (Fig. 5.4) were

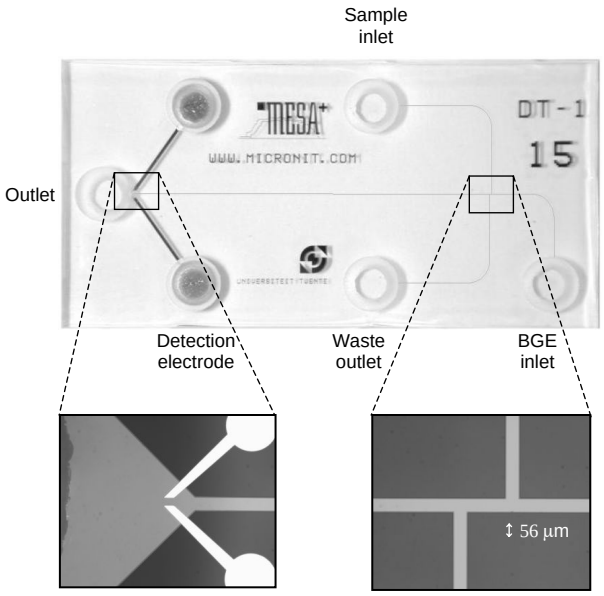

Figure 5.4: *Photograph of the CE microchip with dimensions of 30 × 15 mm. The insets show the position of the electrodes used for the conductivity detection and the channel intersection defining the sample volume.*

obtained from Micronit Microfluidics BV (Enschede, The Netherlands). All channels were isotropically etched to a depth of 8 μm and a top width of 56 μm using hydrofluoric acid. The effective length of the separation channel (from the T-injector to the detection electrodes) is 2 cm. The electrodes for conductivity detection consist of thin platinum films in direct contact with the electrolyte inside of the channel. The chips were placed in a holder made from Delrin™ consisting of a bottom support plate with an opening below the chip. A cover plate with platinum wires inserted into the fluidic compartments was placed on top of the chip to provide electrical connections to the high-voltage supply. The holder containing the chip was placed on an inverted microscope stage (Leica DM/IRM, Wetzlar, Germany). For the experiments using blood plasma samples the chip was coated with linear polyacrylamide using a procedure described elsewhere in order to prevent changes in surface conditions due to the adsorption of proteins [16]. A second type of CE chip for optical studies of MBE was manufactured in-house from Pyrex™ with only a single 6 cm long channel. Both Borofloat™ and Pyrex™ are borosilicate glasses with a very similar composition and material properties so that the behavior should be almost identical.

5.3.3 Capillary electrophoresis on the microfabricated chip

A computer controlled high voltage power supply with four independently controllable voltage outputs (CU 411, IBIS Technologies BV, Hengelo, The Netherlands) was used for the CE experiments together with a custom-made conductivity detector (Sprenkels Consultancy, Lelystad, The Netherlands). The detector signal was recorded with a data acquisition card (DAQCard 6036E, National Instruments, Austin, TX, USA). An in-house written software package combined the control of the power supply, acquisition of data from the detector and the data analysis. A pinched sample loading was used with full plug shaping [34]. The moving boundary separation and subsequent zone electrophoresis was performed using a two-step voltage sequence as given in Fig. 5.1B,C applying voltages of 600, 800 and 1000 V to the individual compartments. Both the sample loading and separation were performed for 60 seconds.

5.3.4 Dilution studies of MBE destacking

Moving boundary electrophoresis experiments were performed on a chip with a single channel only. The channel and outlet compartment were filled with the ammonium acetate BGE with HPMC. The sample compartment was filled with 1 mmol/L rhodamine 123 in a matrix of 150 mmol/L sodium chloride and 5 mmol/L lithium chloride. A continuous potential of 1000 V was applied to perform the MBE. The fluorescence intensity of rhodamine was detected halfway down the separation channel with a photosensor module (H7422-02, Hamamatsu, Japan) connected to the microscope. For excitation a 100 W mercury lamp was used in combination with an I3 filter cube (Leica).

5.4 Results and discussion

5.4.1 Study of the MBE dilution on-chip

The MBE taking place during the sample loading is studied on a chip with a single channel only representing the sample loading channel on the CZE chip. To verify the concept of dilution as described in section 5.2, fluorescence detection is used instead of conductivity detection because the fluorescence intensity is directly proportional to the concentration of the dye. This is not the case for conductivity detection where the signal is also affected by all the other ions at the detection point. In order to measure the dilution across the stationary boundary a moving boundary separation is performed on the chip using 1 mmol/L rhodamine in a matrix of 150 mmol/L sodium chloride as sample. The BGE consist of a mixture of 10 mmol/L ammonium acetate / acetic acid with HPMC as EOF modifier. The fluorescence intensity measured at a fixed point along the separation channel is initially zero for the BGE (zone I, Fig. 5.5). A step in the signal marks the moment that the diluted rhodamine (zone II, Fig. 5.5) reaches the detection position. Another increase in intensity is observed when the stationary boundary moving with the EOF reaches the detection point carrying the undiluted sample (zone III, Fig. 5.5). Since all species in the sample experience the same amount of dilution across the stationary boundary, the change in fluorescence intensity provides a direct measure of the concentration adjustment of all species in the diluted zone. For the sample a dilution with a factor of 12 is measured while calculations using Eq. 5.9 from section 5.2 results in a factor of 13.6. From this result we can verify that the analytical principle can be used for the dilution on chip. The HPMC added to the BGE successfully reduces the EOF. Instead of a diluted zone that passes the detection point in 18 seconds under normal EOF conditions it now takes up to 100 seconds before the diluted zone II is followed by the undiluted sample zone III (Fig. 5.5). If the EOF would be fully suppressed the zone would

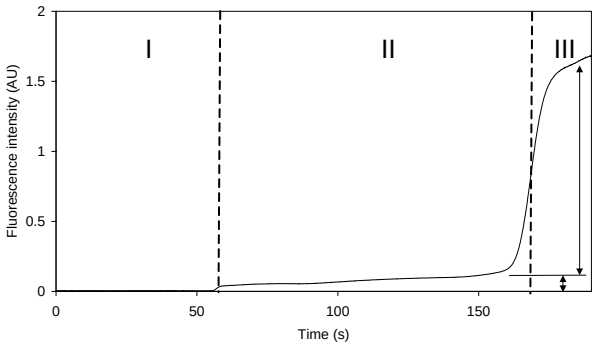

Figure 5.5: *Moving boundary separation of 1 mmol/L rhodamine 123, in a matrix of 150 mmol/L sodium chloride and 5 mmol/L lithium chloride. BGE 10 mmol/L ammonium acetate / acetic acid with EOF modifier. The arrows indicate the steps in the fluorescence signal when the dilute and undiluted rhodamine reaches the detection point.*

be infinitely long since the stationary boundary would stay fixed at the edge between sample compartment and CE channel. Although the dilution is clearly evident, the fluorescence does not reach a plateau value in either the diluted (zone II) or the undiluted zone (zone III), but gradually increases with time. This indicates that the system is more intricate than depicted by the simple MBE model. For example dispersion due to a pressure driven flow caused by local variations in EOF is not included in the model.

These results show that indeed a concentration adjustment occurs across the stationary boundary causing dilution of the sample. Using a chip with the layout shown in Fig. 5.4, the moving boundary separation can be performed in the sample loading channel and with a heart-cutting method the diluted zone can subsequently be dispensed into the separation channel.

5.4.2 Heart-cutting of diluted zones for on-line CZE

The duration of the MBE separation before switching to the zone electrophoresis is important in order to dispense the correct zone. In the early stages of the MBE the ions with a low electrophoretic mobility have not reached the double-T whereas the EOF determines the velocity at which the undiluted sample is pumped to the double-T. In order to determine the robustness of the system the duration of the MBE loading step is varied from 5 to 300 seconds before separating the content of the double-T. Using 150 mmol/L sodium and 5 mmol/L lithium as sample the two components are baseline separated for short loading times (Fig. 5.6A,B). In the electropherograms there is a sudden transition from the conditions under which sodium and lithium are well resolved to a situation in which lithium is not separated from the sodium peak (Fig. 5.6C). Due to the residual EOF, undiluted sample is dispensed into the separation channel when the sample loading is continued for too long. In this experiment the peak areas of sodium and lithium show the

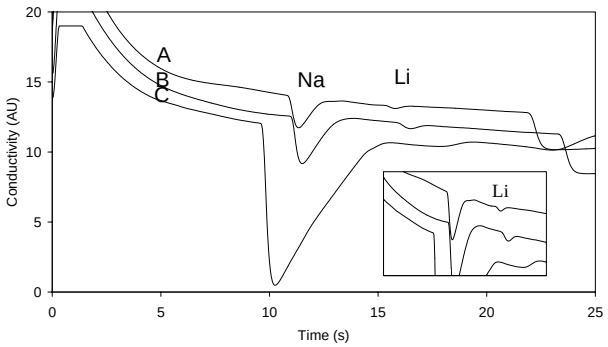

Figure 5.6: *Electropherograms as function of the loading duration. A) 30 seconds sample loading, B) 240 seconds and C) 300 seconds. Sample 150 mmol/L sodium with 5 mmol/L lithium. BGE 10 mmol/L ammonium acetate / acetic acid with EOF modifier. The inset shows an enlargement of the curve around the lithium peak.*

same slight increase over time (Fig. 5.7) as was observed in the previous MBE experiment (Fig. 5.5). After a loading time of approximately 120 seconds the slope (Fig. 5.7) increases even more, possibly because a longer sample plug is dispensed into the separation channel. This can be the case when a substantial part of the sample channel is filled with the undiluted sample, resulting in a weaker electrical field and thus a less effective pullback. This can result in a slight leakage of sample into the separation channel at the start of the CZE separation. Nevertheless, the ratio between the peak area of sodium and lithium remains constant for a loading time between 30 and 240 seconds.

The MBE successfully causes the formation of a diluted sample plug, allowing lithium to be separated from the excess sodium. Since the sodium-lithium ratio stays constant over time and because of the large time window under which diluted sample is injected into the separation channel it can be concluded that the exact moment of switching from the MBE step to the separation is not critical. This in contrast to heart-cutting methods using ITP in the first dimension where narrow zones are formed making switching critical.

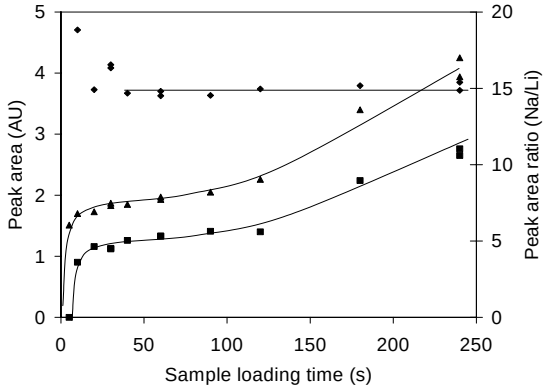

Figure 5.7: *Peak areas as function of the sample loading time for sodium (▲), lithium (■, peak area×10) and the ratio between the peak areas of sodium and lithium (♦). The sample consisted of 150 mmol/L sodium and 5 mmol/L lithium.*

5.4.3 Quantitation of lithium in a sodium matrix

As discussed in section 2.3, the dilution factor of ions across the stationary boundary is determined by both the concentration of species in the sample matrix and by the BGE concentration. With an increasing concentration of sodium in the sample, the amount of dilution on crossing the stationary boundary automatically increases. This means that the peak area of lithium is a function of the sodium concentration. Since the dilution factor will generally be unknown the use of an internal standard is required for quantitation. For the intended application of determination of blood composition, sodium is used as the internal standard. Sodium is readily available and is well regulated in the human body between 135 and 145 mmol/L. Within these limits the sodium concentration can be assumed constant at a concentration of 140 mmol/L, making an error of less than 4% for the lithium quantitation. The calibration curve measured for lithium standards between 0 and 2 mmol/L in a 140 mmol/L sodium chloride matrix is linear (Fig. 5.8). This demonstrates that for these aqueous samples the ratio between the peak areas of lithium and sodium is representative for the lithium concentration in the sample when using the MBE heart-cutting method. Based on the variance of the calibration samples around the fitted curve, the detection limit for lithium in a 140 mmol/L sodium matrix is estimated at 0.1 mmol/L.

When there are multiple anions present in the sample additional moving boundaries are created. In order to investigate the possible shift between the concentration ratio of lithium and sodium we consider the system in Fig. 5.2. This represents a model for blood with the most abundant matrix components sodium, chloride and bicarbonate. Lithium will serve as analyte and ammonium acetate as BGE. Since it is the ratio between the sodium and lithium peaks that is determined in the experiments for quantitation of lithium, the ratio will be considered in this discussion too. When passing an electrical current through this

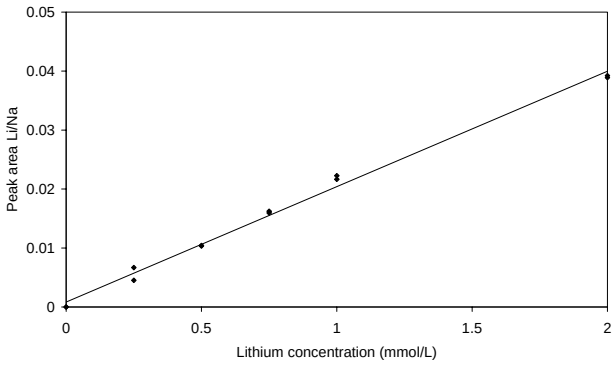

Figure 5.8: *Calibration curve for lithium in aqueous standards containing 140 mmol/L sodium. Separation on a chip coated with polyacrylamide and using a 30 mmol/L ammonium acetate / acetic acid BGE.*

system, two zones separated by moving boundaries will appear in front of the stationary boundary (δ and ε in Fig. 5.2) and two more are behind (β, γ). In order to express the Na-Li ratio directly in front of the stationary boundary in zone γ, which is equal to the ratio in zone δ (see Eq. 5.9), the condition of complete dissociation holds for all electrolytes and Eq. 5.6 is applied respectively to the zones α, β and γ resulting in the moving boundary equations that combine into Eq. 5.12:

$$\frac{c_{Na}^{\gamma}}{c_{Li}^{\gamma}} = \frac{c_{Na}^{\alpha}}{c_{Li}^{\alpha}} \frac{r_{Cl} - r_{Na}}{r_{Cl} - r_{Li}} \frac{V^{\alpha\beta}\sigma^{\beta} - r_{Li}}{V^{\alpha\beta}\sigma^{\beta} - r_{Na}} \frac{r_{HCO_3} - r_{Na}}{r_{HCO_3} - r_{Li}} \frac{r_{Ac} - r_{Li}}{r_{Ac} - r_{Na}} \tag{5.12}$$

The product $v^{\alpha\beta}\sigma^{\beta}$ will have a value somewhere in between the relative mobilities r_{Cl} and r_{HCO3} and needs to be calculated from Eq. 5.7 (Fig. 5.3A,B). Two limiting cases can thus be discerned:

$$\frac{c_{Na}^{\gamma}}{c_{Li}^{\gamma}} = \frac{c_{Na}^{\alpha}}{c_{Li}^{\alpha}} \frac{r_{HCO_3} - r_{Na}}{r_{HCO_3} - r_{Li}} \frac{r_{Ac} - r_{Li}}{r_{Ac} - r_{Na}} \qquad (V^{\alpha\beta}\sigma^{\beta} = r_{Cl}) \tag{5.13}$$

and

$$\frac{c_{Na}^{\gamma}}{c_{Li}^{\gamma}} = \frac{c_{Na}^{\alpha}}{c_{Li}^{\alpha}} \frac{r_{Cl} - r_{Na}}{r_{Cl} - r_{Li}} \frac{r_{Ac} - r_{Li}}{r_{Ac} - r_{Na}} \qquad (V^{\alpha\beta}\sigma^{\beta} = r_{HCO_3}) \tag{5.14}$$

In both cases the sodium-lithium ratio is independent of the concentration of any other species in the sample or the BGE. For this particular example the sodium-lithium ratio, which starts at 28 in the sample, will be 28.1 in the γ-zone (and thus also in the δ zone) in the situation of $V^{\alpha\beta}\sigma^{\beta}=r_{Cl}$ and 26.8 for $V^{\alpha\beta}\sigma^{\beta}=r_{HCO3}$. In vivo both the blood chloride and bicarbonate concentrations are well regulated, yet the question remains whether the calibration solutions should be matched in matrix composition to the blood samples for accurate quantitation. It is difficult to appreciate the value of $V^{\alpha\beta}\sigma^{\beta}$ as function of the sample composition directly from Eq. 5.7. However, since both chloride and bicarbonate are the most abundant anionic species in blood only the terms containing these two species have to be considered in order to yield a good approximation for $V^{\alpha\beta}\sigma^{\beta}$:

$$V^{\alpha\beta}\sigma^{\beta} \approx \frac{r_{HCO_3}a + r_{Cl}}{1 + a} \tag{5.15}$$

where

$$a = \frac{c_{Cl}^{\alpha}}{c_{HCO_3}^{\alpha}} \frac{r_{Cl} - r_{NH\,4}}{r_{HCO_3} - r_{NH\,4}} \tag{5.16}$$

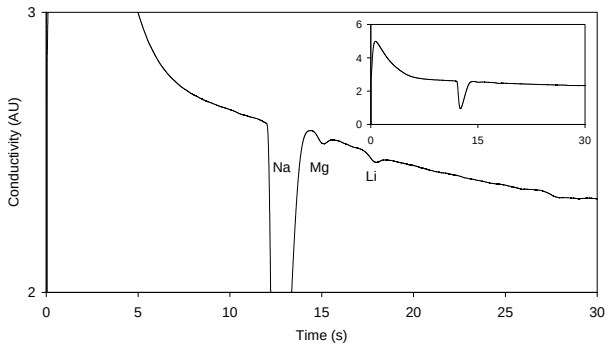

Figure 5.9: *Electropherogram of blood plasma of a patient on lithium therapy using the MBE for dilution. Separation conditions as in Fig.* 5.8.*The inset shows the full-scale electropherogram.*

Blood typically contains 115 mmol/L chloride and 25 mmol/L bicarbonate. Here, $V^{\alpha\beta}\sigma^{\beta}$ is -0.59 and approximates the relative mobility of bicarbonate which is -0.52. Equation 5.14 representing the sodium-lithium concentration ratio for sample without bicarbonate therefore provides a good approximation and calibration can thus be performed with standards containing only the chloride salts. Under these conditions an error of less than one percent is made in the determination of the sodium-lithium ratio. If the calibration solutions are also matched to the bicarbonate concentration in blood, the error even approaches zero since minor concentrations of other anionic species besides chloride and bicarbonate have a negligible influence on the sodium-lithium ratio.

To confirm these findings the sodium-lithium peak area ratio was measured for three samples containing 3 mmol/L lithium combined with 150 mmol/L of different sodium salt matrices. These standards contained either the acetate as counter-ion, which is also present in the BGE, only chloride or a mixture of 115 mmol/L chloride and 25 mmol/L bicarbonate similar to blood. As predicted, the separation of both samples containing chloride as the main species resulted in almost identical peak area ratios (30.6±2.5 in the chloride matrix and 30.7±1.1 in the chloride/bicarbonate matrix, n=3). With acetate as counter ion a slightly different sodium-lithium ratio was obtained (29.6±1.5, n=3). The variation is still within in the measurement error though. Based on these results it can be concluded that for the determination of lithium in blood the calibration can be performed using standards containing only chloride salts without further matching to the blood matrix. The formation of additional boundaries on the anode side of the stationary boundary have only a minor influence on the sodium-lithium concentration ratio.

5.4.4 Determination of lithium in blood plasma

In order to measure the lithium concentration in a blood plasma sample no pretreatment steps are required. The proteins in the sample may have an additional effect on the residual EOF despite the addition of HPMC as a dynamic coating to the BGE. However,

further suppression of the EOF would only have a minor effect on the start of the time window in which the diluted sample zone can be injected into the separation channel. But in order to start with stable conditions, instead of the HPMC coating a permanent polyacrylamide coating was used on the CE chip. The resulting electropherogram shows in addition to sodium and lithium the separation of magnesium (typically around 0.9 mmol/L) in between the two peaks (Fig. 5.9). Potassium, which is also present in plasma in a concentration of around 3.5 to 5 mmol/L cannot be detected because it has the same ionic conductivity as the BGE co-ion ammonium. Using sodium as internal standard a lithium concentration of 0.7±0.1 mmol/L (n=3) was calculated in the plasma sample. This is in agreement with the 0.62 mmol/L specified in the serum sample by the hospital on a dedicated lithium analyzer. It shows that lithium can be quantified in blood plasma at clinically relevant concentrations without any off-chip sample treatment.

5.5 Conclusions

The concentration boundary between sample and BGE can be used to dilute samples with a high matrix concentration on a typical CE microchip. During the moving boundary separation, which is inevitable for electrokinetic sample loading, a sequence of zones is formed in which the concentration of ionic species changes from zone to zone. But in the zones separated by a moving boundary also the ratio of concentrations between species shifts. This means that care has to be taken that the zone that is dispensed into the separation channel is representative for the ion concentration in the bulk of the sample. For blood samples with an excess of sodium chloride, it is not necessary to perfectly match the matrix of the calibration solutions to the blood sample as the shift in concentration is dominated by the most abundant counter ion in the sample. Hence the calibration for the determination of blood composition can be performed using standards containing chloride salt only. With the MBE dilution mechanism it is possible to separate and determine lithium directly in blood plasma with a detection limit of 0.1 mmol/L on the present system. The results prove the potential of microchip CE systems for point-of-care diagnostics. Further tests are planned in cooperation with the hospital to increase the number of blood samples to obtain more detailed statistical data on precision and accuracy of the method.

The effects observed here will also determine the behaviour of sample loading for other types of CE applications where the sample plug is formed by electromigration rather than the EOF. For any microchip CE application where the EOF is suppressed or reversed the presence of a moving boundary separation and the associated concentration altering processes need to be appreciated for accurate quantitation.

5.6 References

1. V Dolník, S Liu and S Jovanovich "*Capillary electrophoresis on microchip"*, Electrophoresis 2000, **21**, 41-54.
2. NA Lacher, KE Garrison, RS Martin and SM Lunte " *Microchip capillary electrophoresis-electrochemistry"*, Electrophoresis 2001, **22**, 2526-2536.
3. E Verpoorte "*Microfluidic chips for clinical and forensic analysis"*, Electrophoresis 2002, **23**, 677-712.
4. NJ Birch "*Inorganic Pharmacology of Lithium"*, Chem. Rev. 1999, **99**, 2659-2682.
5. A Amdisen "*Monitoring of lithium treatment through determination of lithium concentration"*, Danish medical bulletin 1975, **22**, 277-291.
6. GD Christian "*Analytical strategies for the measurement of lithium in biological samples"*, J. Pharm. Biomed. Anal. 1996, **14**, 899-908.
7. Personal communication, Medisch Spectrum Twente Hospital Group, Enschede, The Netherlands
8. A Oki, M Takai, H Ogawa, Y Takamura, T Fukasawa, J Kikuchi, Y Ito, T Ichiki and Y Horiike "*Healthcare Chip for Checking Health Condition from Analysis of Trace Blood Collected by Painless Needle"*, Jpn. J. Appl. Phys. 2003, **42**, 3722-2727.
9. KA Erickson and P Wilding "*Evaluation of a Novel Point-of-Care System, the i-STAT Portable Clinical Analyzer"*, Clin. Chem. 1993, **39**, 283-287.
10. WM Glazer, JG Sonnenberg, MJ Reinstein and RF Akers "*A novel, point-of-care test for lithium levels: description and reliability"*, J. Clin. Psychiatry 2004, **65**, 652-655.
11. X Huang, MJ Gordon and RN Zare "*Quantitation of Li^+ in serum by capillary zone electrophoresis with an on-column conductivity detector"*, J. Chromatogr. 1988, **425**, 385-390.
12. A Berthold, F Laugere, H Schellevis, CR De Boer, M Laros, RM Guijt, PM Sarro and MJ Vellekoop "*Fabrication of a glass-implemented microcapillary electrophoresis device with integrated contactless conductivity detection"*, Electrophoresis 2002, **23**, 3511-3519.
13. J Lichtenberg, NF De Rooij and E Verpoorte "*A microchip electrophoresis system with integrated in-plane electrodes for contactless conductivity detection"*, Electrophoresis 2002, **23**, 3769-3780.
14. M Pumera, J Wang, F Opekar, I Helínek, J Feldman, H Löwe and S Hardt "*Contactless Conductivity Detector for Microchip Capillary Electrophoresis"*, Anal. Chem. 2002, **74**, 1968-1971.
15. J Tanyanyiwa, EM Abad-Villar, MT Fernández-Abedul, A Costa-Garcìa, W Hoffmann, AE Guber, D Herrmann, A Gerlach, N Gottschlich and PC Hauser "*High-voltage contactless conductivity-detection for lab-on-chip devices using external electrodes on the holder"*, Analyst 2003, **128**, 1019-1022.
16. EX Vrouwe, R Luttge and A van den Berg "*Direct measurement of lithium in whole blood using microchip capillary electrophoresis with integrated conductivity detection"*, Electrophoresis 2004, **25**, 1660-1667.

17. J Boden and K Bächmann "*Investigation of matrix effects in capillary zone electrophoresis"*, J. Chromatogr. A 1996, **734**, 319-330.
18. W Ding, MJ Thornton and JS Fritz "*Capillary electrophoresis of anions at high salt concentrations"*, Electrophoresis 1998, **19**, 2133-2139.
19. NJ Petersen, RPH Nikolajsen, KB Mogensen and JP Kutter "*Effect of Joule heating on efficiency and performance for microchip-based and capillary-based electrophoretic separation systems: A closer look"*, Electrophoresis 2004, **25**, 253-269.
20. J Boden and K Bächmann "*Investigation of matrix effects in capillary zone electrophoresis"*, J. Chromatogr. A 1996, **734**, 319-330.
21. JL Beckers and FM Everaerts "*Isotachophoresis with two leading ions and migration behaviour in capillary zone electrophoresis; II. Migration behaviour in capillary zone electrophoresis"*, J. Chromatogr. 1990, **508**, 19-26.
22. P Gebauer, W Thormann and P Boček "*Sample self-stacking in zone electrophoresis Theoretical description of the zone electrophoretic separation of minor compounds in the presence of bulk amounts of a sample component with high mobility and like charge"*, J. Chromatogr. 1992, **608**, 47-57.
23. D Kaniansky, M Masár, J Bielciková, F Iványi, F Eissenbeiss, B Stanislawski, B Grass, A Neyer and M Jöhnck "*Capillary Electrophoresis Separations on a Planar Chip with the Column-Coupling Configuration of the Separation Channels"*, Anal. Chem. 2000, **72**, 3596-3604.
24. SC Jacobson, TE McKnight and JM Ramsey "*Microfluidic Devices for Electrokinetically Driven Parallel and Serial Mixing"*, Anal. Chem. 1999, **71**, 4455-4459.
25. LG Longsworth "*Moving boundary studies on salt mixtures"*, J. Am. Chem. Soc. 1945, **67**, 1109-1119.
26. MR Schure "*Limit of Detection, Dilution Factors, and Technique Compatibility in Multidimensional Separations Utilizing Chromatography, Capillary Electrophoresis, and Field-Flow Fractionation"*, Anal. Chem. 1999, **71**, 1645-1657.
27. LL Shultz-Lockyear, CL Colyer, ZH Fan, KI Roy and DJ Harrison "*Effects of injector geometry and sample matrix on injection and sample loading in integrated capillary electrophoresis devices"*, Electrophoresis 1999, **20**, 529-538.
28. JL Beckers and P Boček "*Sample stacking in capillary zone electrophoresis; Principles, advantages and limitations"*, Electrophoresis 2000, **21**, 2747-2767.
29. F Kohlrausch "*Ueber Concentrations-Verschiebungen durch Electrolyse im Inneren von Lösungen und Lösungsgemischen"*, Ann. Phys. Chem. 1897, **62**, 209-239.
30. H Weber. "*Die partiellen Differential-Gleichungen de mathematischen Physik"*, 6th edition, 1919, Braunschweig, Vieweg and Sohn
31. EB Dismukes and RA Alberty "*Weak Electrolyte Moving Boundary Systems Analogous to the Electrophoresis of a Single Protein"*, J. Am. Chem. Soc. 1954, **76**, 191-197.

32. VP Dole "*A Theory of Moving Boundary Systems Formed by Strong Electrolytes"*, J. Am. Chem. Soc. 1945, **67**, 1119-1126.
33. TM Jovin "*Multiphasic Zone Electrophoresis. I. Steady-State Moving-Boundary Systems Formed by Different Electrolyte Combinations"*, Biochemistry 1973, **12**, 871-879.
34. SC Jacobson, R Hergenröder, LB Koutny, RJ Warmack and JM Ramsey "*Effects of Injection Schemes and Column Geometry on the Performance of Microchip Electrophoresis Devices"*, Anal. Chem. 1994, **66**, 1107-1113.

Chapter 6

Point-of-care sampling for microchip capillary electrophoresis *

Microfluidic technology provides exciting new ways to optimize sample handling procedures. Smaller volumes, fewer manual handling steps and the use of minimal invasive painless samplers, e.g. microneedles are present advantages of miniaturized systems compared to conventional systems at the point of care. Microchip capillary electrophoresis subsequently offers a fast method for determining blood electrolytes. Here novel disposable sample cups are presented that requires sample volumes of less than 10 µl. An integrated filter prevents injection of blood cells into the microchip. The separation of blood is performed on glass microchip CE devices with conductivity detection optimized for the analysis of lithium. Potassium, sodium, lithium, magnesium and calcium are separated in serum in under 20 seconds. Clinical concentrations of these metals are detected without any off-chip sample treatment. The low-cost sample cups facilitate efficient microchip method development. The filter removes the blood cells allowing direct analysis of finger stick samples while multiple measurements can be carried out on the same device.

* This chapter is based on a paper in the proceedings of the MicroTAS 2004 conference (p. 503-505). A full paper is currently in preparation for publication.

6.1 Introduction

The developments in microchip capillary electrophoresis (CE) show exiting potential for point-of-care applications [1]. The concept of microchip CE as a tool for clinical diagnostics has been demonstrated for example for the analysis of proteins [2], cortisol [3] and valproate [4] in serum and lithium in whole blood [5]. In many of these reports the microchip separations are performed in a minute or less. Yet, for point-of-care analysis not only analysis speed but also the user friendliness and robustness are important. In this chapter we study not only the analysis of serum, but also novel disposable sample cups are presented for direct measurement of whole blood from a finger stick.

Lithium still is one of the most important mood stabilizers for treating bipolar mood disorders [6,7]. A disadvantage of lithium is the narrow therapeutic range (0.4-1.2 mmol/L [8]). In the initial phase of the treatment the blood lithium level is measured once or twice a week to prevent exceeding the safe concentration limit. After the concentration has stabilized the testing interval can be reduced to once every couple of months, but monitoring is required regularly.

The standard practice of lithium monitoring has some limitations. Typically the blood sample is obtained from a venipuncture, which can be unpleasant for the patient. The whole procedure of obtaining a blood sample from the patient, transport to the laboratory, sample pretreatment and the actual analysis can take up to 45 minutes before the results are reported back to the clinician. Furthermore, fluctuations in the lithium level remain undetected because of the low frequency of testing. In countries where there are few medical facilities, the lack of equipment or trained personnel may limit the prescription of lithium [9]. A point-of-care test for lithium can solve all of these issues offering enhanced treatment of patients.

Nowadays the plasma or serum lithium level is often determined with ion-selective electrodes (ISEs) [10]. This method is also used in point-of-care tests to determine a range of parameters in approximately 65 µl of whole blood, including potassium and sodium [11]. However, a test for lithium using ISEs is not commercially available. Recently a point-of-care test has been developed specifically for lithium [12]. This test measures the change in light absorbance by a porphyrin compound when it forms a complex with lithium. To perform the test a blood sample is applied onto a cell separator strip and the resulting plasma is subsequently transferred to a cuvette filled with the reagent. These manual handling steps can make a test vulnerable to errors. Also a considerable volume of 50 µl is required for the test. In a comparison of 40 finger stick samples analyzed with the optical test and venous blood analyzed with atomic absorption spectrometry an average lithium concentration of 0.61 mmol/L and 0.70 mmol/L was determined respectively. The deviation was attributed to an actual difference in the concentration of lithium in capillary and venous blood.

Compared to the above methods a separation method such as CE to analyze blood has the advantage that it is not limited to a single analyte. Conventional CE is used for a wide range of substances including lithium [13], organic acids [14], proteins [15] amphetamines [16] and β-agonists [17]. Miniaturization of conventional systems in the form of microchip CE offers the possibility of developing point-of-care tests for the aforementioned and other compounds. Microchip CE provides increased speed compared to conventional CE systems because of the shorter separation column. Another important aspect of point-of-care testing is the opportunity of integrating on-chip sample preparation [18-20].

Microchip CE of inorganic ions, including lithium, in aqueous samples is relatively well established [21-24]. However, none of these papers focus on handling and transfer of small sample volumes onto the chip. While the prospect of analyzing finger stick samples is a great improvement over venous blood samples, even more interesting is the development off painless microneedles that pierce the skin without inflicting pain [25]. These needles can be used for example to sample interstitial fluid from the skin for glucose measurement [26]. In principal these needles can be integrated relatively easily with microfabricated devices such as microchip CE. The microchip needs to be optimized though to work with the extremely small volumes in the order of a few nanoliter sampled by microneedle arrays. The first results are promising, but so far only qualitative analysis of blood samples was demonstrated [27]. Reverse iontophoresis offers an alternative method for painless sampling and was used to extract lithium from the skin [28]. The analysis of extract still has to be performed in the laboratory and it can take up to one and a half hour to collect enough lithium for an accurate analysis. When immediate results are not required reverse iontophoresis can be an interesting alternative to finger stick measurement as is demonstrated by a commercially available glucose meter [29].

In this work venous blood and finger stick samples are used to proof the principle of microchip analysis of lithium for point-of-care use. The aim is to couple microneedles to the microchip at a later stage. Since microneedles are not ready for testing on patients, disposable sample cups are introduced to transfer sample volumes of less than 10 µl to the chip. The cups are equipped with a filter, which prevents the blood cells from entering the CE chip. The cups do not contain any chemicals and can be sterilized so that contact with the wound is safe. The CE separation conditions of the chip are optimized enabling direct analysis of blood electrolytes. By using on-chip conductivity detection the surrounding instrument and electronics stays relatively simple so that a handheld instrument is a real possibility.

6.2 Materials and Methods

6.2.1 Reagents

The CE separations are performed in a background electrolyte consisting of 30 mmol/L ammonium acetate (Sigma, Steinheim Germany) and 30 mmol/L acetic acid (Merck, Darmstadt, Germany) in deionised water (Millipore). In experiments requiring detection of potassium, 5 mmol/L 18-Crown-6 (Merck) is added to the background electrolyte. Similarly, for separating calcium, 4 mmol/L tartaric acid (Baker, Deventer, The Netherlands) is added to the background electrolyte. Calibration solutions are prepared by dissolving lithium chloride (Merck) in a concentration range of 0 to 2 mmol/L in a matrix of 140 mmol/L sodium chloride (Merck). For visualizing the sample plug the fluorescent rhodamine 123 (Fluka, Buchs, Switzerland) is added to the sample when required.

6.2.2 Blood samples

Blood serum (venipuncture) from five patients on lithium therapy was donated by the hospital (Hospital Group, Medisch Spectrum Twente, Enschede). The lithium concentrations were determined in the hospital with an ion selective electrode (Cobas Integra 800, Roche, Basel, Switzerland). The lithium level in the samples was in the range of 0.49 to 0.90 mmol/L. The samples were analyzed with microchip CE on the same day. Whole blood was obtained performing a finger stick on healthy volunteers using

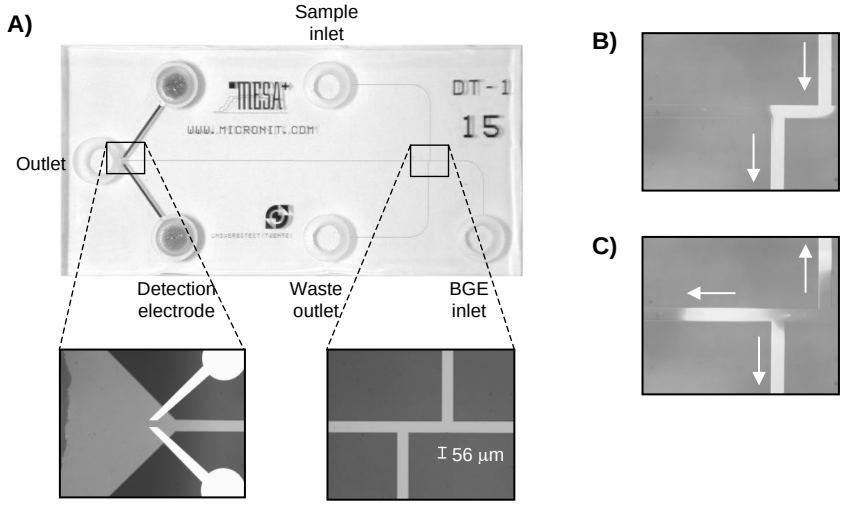

Figure 6.1: *A) Photograph of the CE microchip with dimensions of 30 × 15 mm. The insets show the position of the electrodes used for the conductivity detection and the channel intersection defining the sample volume. B) sample plug formation in the double-T and C) subsequent injection into the separation channel. Blood sample with 1 mmol/L rhodamine 123. The arrows indicate the direction of migration.*

disposable 21 gauge lancets with a puncture depth of 1.8 mm (Haemolance, HaeMedic AB, Munka Ljungby, Sweden). In order to replicate the point-of-care situation as realistically as possible, the CE experiments were performed without the addition of anticoagulant to the blood samples.

6.2.3 microfabricated electrophoresis chips

The CE chips (Fig. 6.1A) made from Borofloat glass were obtained from Micronit Microfluidics BV (Enschede, The Netherlands). The channels are etched to a depth of 8 μm and have a width of 56 μm at the top. The effective length of the separation channel from the 200 μm long double-T injector to the detection electrodes is 2 cm. The detection electrodes for measuring the conductivity consist of thin platinum films in direct contact with the electrolyte solution inside the channel.

The chips are coated with polyacrylamide according to the procedure of Hjertén for fused silica capillaries to reduce the electroosmotic flow and prevent protein adsorption onto the glass channel surface [30]. In brief, the chip is filled with a solution made of 40 μl 3-(trimethoxysilyl)propyl methacrylate (Aldrich, Milwaukee, USA) in 10 ml water adjusted with acetic acid (Merck) to pH 3.5. After one hour the channels are washed with water and filled with a mixture of 3% (w/v) acrylamide (Aldrich), 0.1% (v/v) N,N,N',N'-tetramethylethylenediamine (Sigma) and 0.1% (w/v) potassium persulfate (Aldrich) in water. During the polymerization reaction the microchip compartments are covered with a microscope cover slip to prevent inhibition by oxygen from the air. After 30 minutes the solution is flushed out and the channels are washed with water.

6.2.4 Sample cups

Disposable sample cups are CNC milled from solid Plexiglas™. A capillary is drilled in the centre with 1.0 mm diameter and a length of 7.0 mm defining a volume of 5.5 μl. Such a small volume can be drawn easily from a single finger stick. A filter membrane (Millipore, mixed cellulose esters, 0.22 μm pore size) is heat bonded onto the bottom of the cups using a hotplate at 120ºC. Each sample cup is used only once to prevent sample carry-over. The microchip does not come into direct contact with the blood samples and can therefore be used repeatedly.

6.2.5 Instrumentation

For the CE experiments a computer controlled high voltage power supply with four independently adjustable outputs is used (CU 411, IBIS Technologies BV, Hengelo, The Netherlands). The detector is a custom-made conductivity detector (Sprenkels Consultancy, Lelystad, The Netherlands). The detector signal is recorded with a data acquisition card (DAQCard 6036E, National Instruments, Austin, TX, USA). An in-house written software package is used to control the power supply as well as acquiring and processing the data.

6.2.6 Measuring protocol for blood samples

The chip is placed in a home built holder consisting of a Delrin™ bottom support plate and a Plexiglas™ cover block with fluid compartments (Fig. 6.2). Platinum wires inserted into the compartments provide electrical connections to the high-voltage supply.

The procedure for analyzing blood samples starts with filling the chip with the background electrolyte (BGE) solution. The channels automatically fill by capillary action after dispensing 50 µl BGE in the outlet compartment (see Fig. 6.1A). With an inverted microscope (Leica DM/IRM, Wetzlar, Germany) the channels are inspected to verify that there are no air pockets trapped inside. Subsequently the three remaining compartments are filled with BGE. A blank separation run is performed to ensure that the baseline is stable. The experiment starts with a sample loading step applying 1000 V to the sample compartment (6.1A), 0 V to the waste compartment and 1000 V and 800 V to the outlet and BGE inlet respectively. Using this pinched injection procedure [31] sample is transported from the sample compartment into the channels. A sample plug is defined in the double-T channel intersection using pinching fields from the sides to prevent leakage of sample. Figure 6.1B shows the plug formation in the double-T with a fluorescent dye.

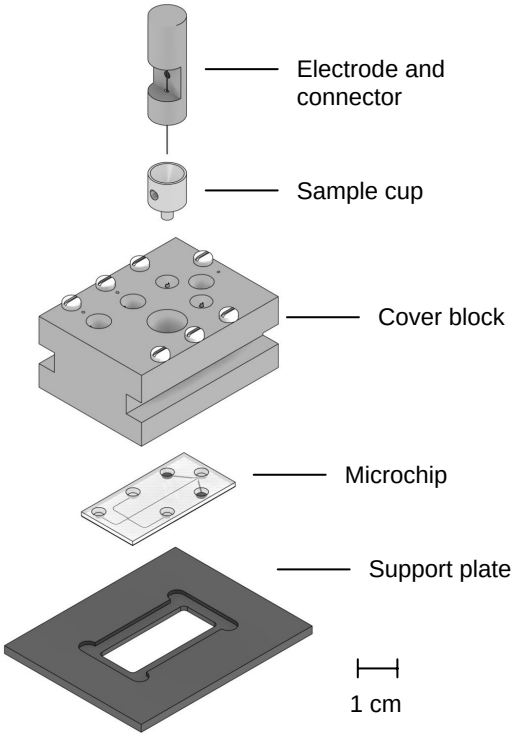

Figure 6.2: *Diagram showing the different components of the microchip CE system.*

After 60 seconds the separation is started by changing the voltages to 600 V on the sample and waste compartments, 1000 V on the BGE inlet and 0 V on the outlet. The sample plug is injected into the separation channel (Fig. 6.1C) where it is separated. During the separation step, which lasts 60 seconds, the conductivity signal is recorded. If the measured electrical current through the four channels is within established limits and a stable baseline signal is obtained on the detector, the chip is ready for analyzing the sample.

A calibration sample with 1 mmol/L lithium and 140 mmol/L sodium is run first. The BGE is removed from the sample compartment, which is cleaned and filled with 7 µl water. A sample cup is filled with the calibration solution before it is inserted into the chip holder. The membrane at the underside of the sample cup has to make contact with the water in the compartment. A platinum wire electrode is inserted into the sample cup (Fig. 6.2) and the analysis is started using the aforementioned voltage sequence. After finishing the separation run two more separation runs are performed without refreshing the system. The peak areas of the three electropherograms are used to obtain statistical information on the precision. In order to prepare the chip for the blood sample the sample compartment is cleaned with water first. The channels are flushed with BGE by pressurizing the BGE inlet manually with a syringe for 10 seconds to ensure that the separation conditions for each sample are always the same. To verify that the chip is clean a blank run is performed with BGE. If there are no peaks in the electroperogram the sample compartment is filled with 7 µl water and a sample cup filled with the blood sample is inserted into the holder. Three sperations are performed based on the above procedure. Using this protocol with washing steps inbetween samples, multiple runs can be performed on a single CE chip.

6.2.7 Operating principle

Most microchips presented in the literature have a dedicated compartment in which the sample is placed. From there the sample is driven into the channels to form a sample plug using either electromigration or electroosmotic flow. The sample cups are a new addition to the microchip CE system, which create an additional interface between the sample and the microchip. The critical factor is the formation of a sample plug in the double-T that is representative for the blood sample in the sample cup. The electrical contact between the blood sample and the separation electrolyte is made with a small volume of water. This water plug forms an integral part of the sample loading procedure. By applying an electrical potential difference between the sample and the waste outlet compartment the cations in the sample migrate through the filter membrane and enter the water plug (Fig. 6.3). From there the ions continue to migrate into the channel filled with BGE leading to the waste compartment. In this electrofiltration step the blood cells cannot pass the filter membrane and remain in the sample cup. The difficulty is that only a certain amount of the blood sample enters the water plug in the sample compartment during the injection by electromigration. The concentration of ions from the sample is therefore much lower in the water plug than in the sample itself. The most important property of the system is that

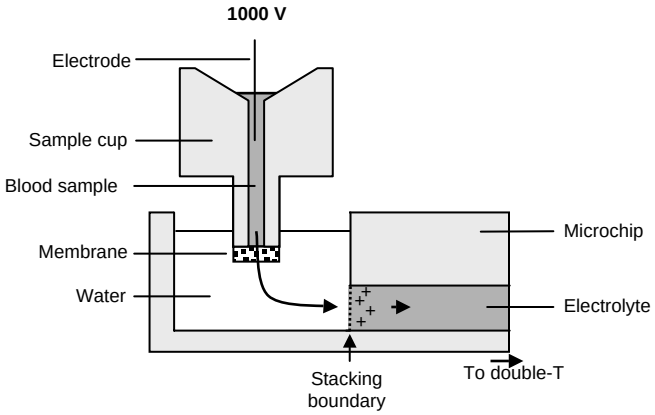

Figure 6.3: *Schematic representation of the injection and stacking of sample. Note that the figure is not to scale.*

the water plug creates the conditions that enable field amplified stacking [32]. At the moment that the ions migrate from the water into the BGE they experience a stacking or concentrating effect. The stacking efficiency is highly dependent on the conductivity difference of the water plug and the BGE. If for example BGE would be used instead of water no stacking occurs at all. Also the composition of the sample matrix affects the stacking. It is therefore not possible to predict the analyte concentration in the sample plug received after stacking without knowledge of the exact composition of the sample. However, when using an internal standard in the sample it is possible to quantitate other sample components since the standard is also stacked. This also rules out any deviation that would be caused by differences in the volume of the sample or water plug. For the analysis of blood sodium can be used as an internal standard [28]. It has even been suggested that the ratio between the sodium and lithium concentration is a more destinctive parameter to monitor lithium treatment than the absolute lithium concentration [33]. The sodium concentration in blood plasma is stable between 135 and 145 mmol/L, which makes it ideal as an internal standard.

For improved sample cleanup it is also possible to use sample cups with a dialysis membrane instead of a filter membrane. In this way an on-line electrodialysis is performed, removing high molecular weight biomolecules. But for the analysis of lithium the removal of only the blood cells is sufficient.

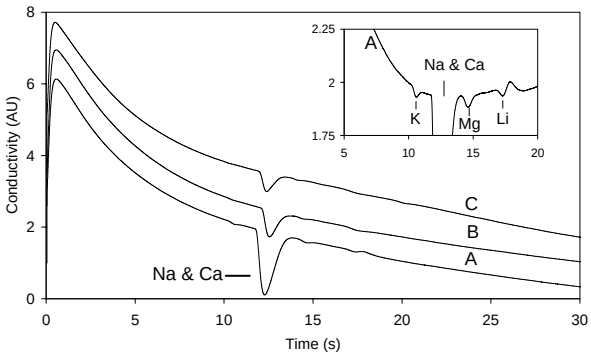

Figure 6.4: *Electropherogram of A) undiluted sample, B) 220 fold diluted sample and C) 2,200 fold diluted sample. The initial sample prior to dilution consists of 140 mmol/L Na, 4 mmol/L K, 2.5 mmol/L Ca, 1 mmol/L Mg and 1 mmol/L Li in water. BGE 30 mmol/L ammonium acetate / acetic acid with 5 mmol/L 18-crown-6. The inset shows a magnified portion of curve A after baseline correction.*

6.3 Results and discussion

First the on-chip stacking of diluted calibration samples is studied to assess the method before using the sample cups. An aqueous calibration sample is placed in the sample compartment on the chip without the use of a sample cup. The sample represents an artificial blood sample consisting of 140 mmol/L sodium, 4 mmol/L potassium 2.5 mmol/L calcium and 1 mmol/L magnesium and lithium. Figure 6.4A shows that the separation is performed in less than 20 seconds. Of the five components only calcium and sodium are not separated from each other. The sample is subsequently diluted 220 fold with water and analyzed again. Compared to the undiluted sample the peak sizes decrease with only a factor of three (Fig. 6.4B). This demonstrates that the concentration of analytes in the sample plug is very similar to the previous separation using undiluted sample, owing to an efficient sample stacking. Even when the sample is diluted 2,200 fold, so that the sodium concentration is only 64 μmol/L, the peak areas only decrease with a factor of four compared to the undiluted sample (Fig. 6.4C). This also proofs that in principal it is possible to analyze the small amount of liquid sampled by microneedle arrays [27,34]. Considering an array of four by four needles with an internal volume of 1 to 2 nl each, a total sample volume of only 16 to 32 nl is obtained. When this is completely dispensed into the volume of the sample compartment on the microchip, which holds approximately 4 μl, a dilution with a factor of 125 to 250 occurs. To analyze sample drawn into a needle array, the concept shown in Fig. 6.5 can be used. Here a water plug is used again to stack analytes from the array placed on top of the microchip. The high-voltage electrode needs to make contact to the sample via an electrically conductive coating on the surface of the array, or the surface needs to be wetted with sample or water. A polymer microneedle array [35] was filled by pipetting manually a calibration solution

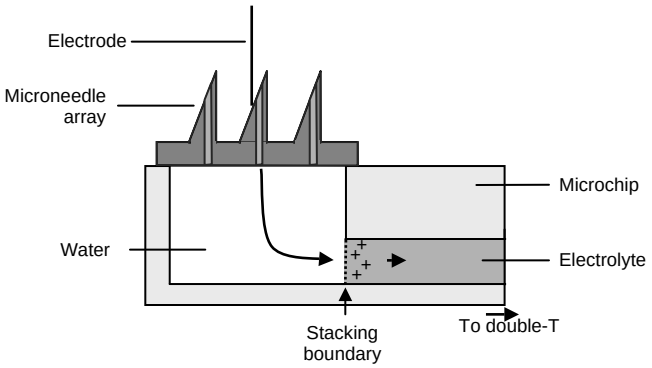

Figure 6.5: *Diagram showing the coupling of a microneedle array to the CE microchip.*

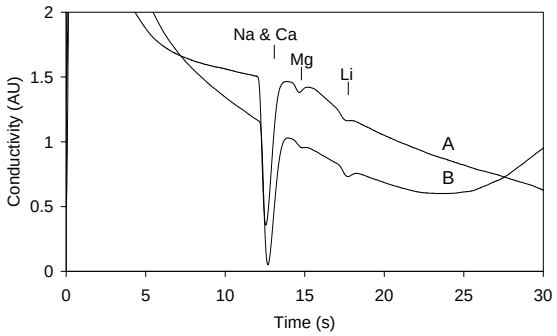

Figure 6.6: *Electropherograms of sample loading via a microneedle array.A) aqueous calibration sample with 150 mmol/L Na and 2 mmol/L Ca, Mg and Li. B) whole blood spiked with 2 mmol/L lithium.*

on the needles. The electropherograms shown in Fig. 6.6 demonstrate that this concept for coupling the needle array to the microchip works for calibration solutions and whole blood. The needle arrays have not been tested yet to actually sample liquid from the skin and require further development. The remaining experiments are therefore performed using the sample cups.

To determine the effect of sample stacking on the quantitation of lithium a calibration curve is recorded for solutions placed directly in the chip. Since the peak areas are affected by the stacking efficiency, as shown in chapter 5, they are not necessarily proportional to the concentration in the sample. Using sodium as internal standard a linear response is obtained for up to 2 mmol/L lithium (Fig. 6.7). This confirms the validity of the method for quantitation of lithium in a high ionic strength sodium chloride matrix.

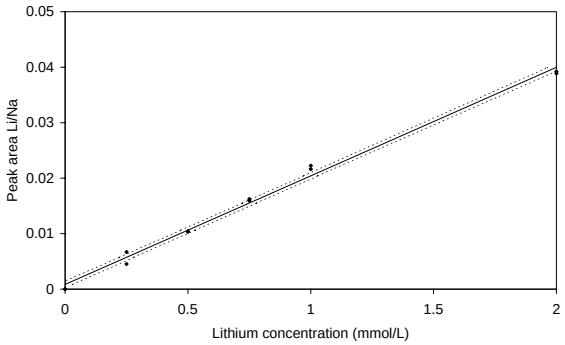

Figure 6.7: *Calibration curve for aqueous lithium standards in a matrix of 140 mmol/L sodium chloride with 95% confidence interval indicated by the dotted line. BGE 30 mmol/L ammonium acetate / acetic acid BGE. Slope: 0.0196, Y-intercept: -0.000843, r^2: 0.994.*

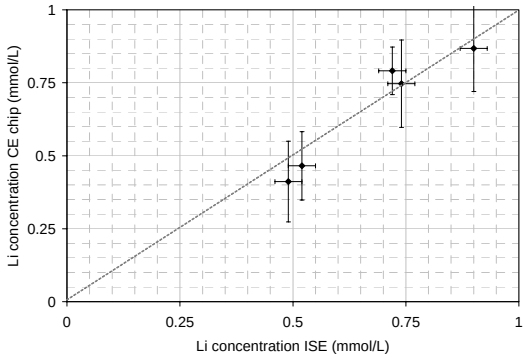

Figure 6.8: *Correlation plot of the lithium determined in five serum samples with microchip CE and an ion selective electrode. The error bars indicate twice the standard deviation. Slope: 1.17, Y-intercept: -0.131, r^2: 0.937.*

In order to test the method using the sample cups five patient serum samples are analyzed on a single CE chip. Serum samples are more stable than whole blood samples and allow a direct comparison with the routine analysis of lithium in the hospital. The chip is calibrated by running a standard with 1.09 mmol/L lithium (determined with ISE) and 140 mmol/L sodium, also using a sample cup. The correlation plot shown in Fig. 6.8 shows that for this limited number of samples both methods correlate well with each other. The relative standard deviation for repeated measurements on the same microchip is on average 10% (n=6) for the microchip, while it is 2.3% for the ISE. Based on a calibration sample, the detection limit defined by a signal height of three times the noise level is 0.15 mmol/L, which is beneath the lower limit of the therapeutic window. In the current system

configuration the relatively poor signal-to-noise ratio restricts the accurate calculation of the peak area for the lithium peak. Optimization of the sensitivity is possible by raising the BGE concentration, which increases the sample stacking efficiency. Also the microchip design itself, in particular the conductivity detection cell, is not fully optimized. The discussion in section 2.4.3 showed the effect of electrode geometry on the cell constant and sensitivity.

The sample cup was also tested for analyzing whole blood using a finger stick sample from a healthy volunteer. A drop of blood applied on the top of the cup flows down the center hole in a matter of seconds. Meanwhile the air escapes through the pores in the filter membrane. Microscope observations of the chip during the CE analysis show that the cells do not go through the filter. The chip therefore stays clean and can be used for multiple samples.

The microchip system can be used also for other blood electrolytes besides lithium. Potassium and magnesium for example are also detected (Fig. 6.4). In order to determine potassium, a crown ether is added to the BGE that selectively forms a complex with potassium. This decreases the conductivity of the potassium zone so that it gives a signal different from the background conductivity. By adding other complexing agents to the BGE such as tartaric acid it is possible to separate sodium and calcium (Fig. 6.9). Tartaric acid decreases the effective electrophoretic mobility of calcium and if a sufficient amount is added to the BGE the calcium peak even appears after the lithium peak [36]. In chapter 7 the use of tartaric acid and its effect on analyte mobilities is investigated in more detail for the application of microchip CE to water monitoring.

For multiple use of the microchip in this configuration it is important to thoroughly replenish the loading channel with BGE and the chip compartment, in which the sample cup is placed, with water. During the analysis the water is contaminated with ions from

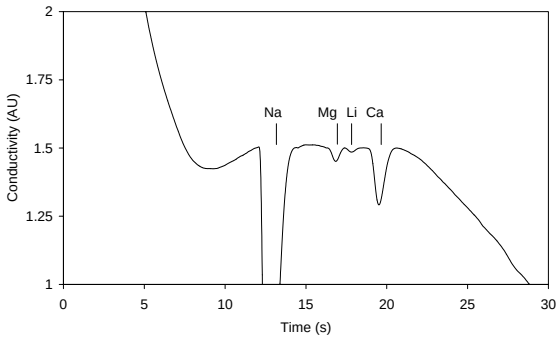

Figure 6.9: *Electropherogram of a serum sample with 144 mmol/L Na, 0.74 mmol/L Li and 2.59 mmol/L Ca, using a sample cup. BGE 30 mmol/L ammonium acetate / acetic acid with 4 mmol/L tartaric acid. Figure after baseline correction.*

the sample, which can result in carry-over effects. In order to turn the system into a product for point-of-care testing, the chip will have to be disposable using cheaper fabrication technologies, for example by using replication processes in plastics [37]. The excellent results obtained with the polymer-coated glass chips compared to the restricted performance of the bare glass chips discussed in chapter 3, indicate that polymers also provide better separating performance. Another important aspect is the surrounding instrumentation, which needs to be reduced in size. Figure 6.10 shows handheld versions of a three channel high-voltage supply and conductivity detector. Both operate for more than eight hours on standard 9 volt batteries. Preliminary results for metal ion separations were achieved with the battery-driven handheld system. All the components to produce a point-of-care test for blood electrolytes i.e. electronics, software and microfluidic chip are therefore presently available. Integration of these components into a user-friendly product should be the next step to enable patient trials on a larger scale.

6.4 Conclusions

Microchip CE is a versatile method for analyzing blood samples. Separations of potassium, sodium, magnesium, calcium and lithium are performed in less than 20 seconds without manual sample pretreatment. The disposable sample cups presented here offer a convenient method for transferring a finger stick blood sample to the chip while also serving to filter out the potentially interfering blood cells. The chip itself does not come into direct contact with the sample and can be used repeatedly. The sample stacking using a water plug works reliable when sodium is used as internal standard. Clinically relevant lithium levels are determined in serum samples and are consistent with ion selective electrode measurements. The detection limit of 0.15 mmol/L is below the lower limit of the therapeutic lithium window. The restricted precision is an issue requiring further optimization for improved quantitation. Further testing should be performed,

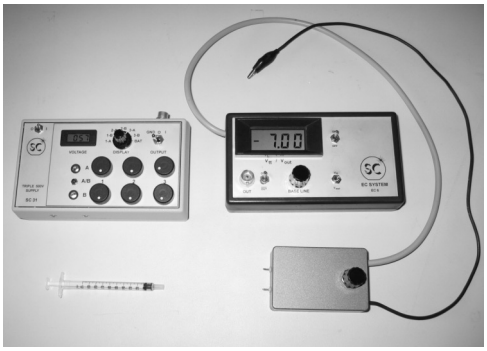

Figure 6.10: *Battery operated conductivity detector with separate preamplifier and high voltage power supply.*

including whole blood from patients to prove the method for its actual use at the point of care.

The option of analyzing small sample volumes using a sample stacking procedure demonstrates the potential for integration of microneedle arrays onto the microchip. Combined with a portable instrument a rapid and painless analysis of blood electrolytes can become a reality.

6.5 References

1. LJ Kricka "*Miniaturization of analytical systems"*, Clin. Chem. 1998, **44**, 2008-2014.
2. CL Colyer, SD Mangru and DJ Harrison "*Microchip-based capillary electrophoresis of human serum proteins"*, J. Chromatogr. A 1997, **781**, 271-276.
3. LB Koutny, D Schmalzing, TA Taylor and M Fuchs "*Microchip Electrophoretic Immunoassay for Serum Cortisol"*, Anal. Chem. 1996, **68**, 18-22.
4. E Ölvecká, M Koníková, N Grobuschek, D Kaniansky and B Stanislawski "*Direct determination of valproate in serum by zone electrophoresis–isotachophoresis on a column-coupling chip"*, J. Sep. Sci. 2003, **26**, 693-700.
5. EX Vrouwe, R Luttge and A van den Berg "*Direct measurement of lithium in whole blood using microchip capillary electrophoresis with integrated conductivity detection"*, Electrophoresis 2004, **25**, 1660-1667.
6. NJ Birch "*Inorganic Pharmacology of Lithium"*, Chem. Rev. 1999, **99**, 2659-2682.
7. B Müller-Oerlinghausen, A Berghöfer and M Bauer "*Bipolar disorder"*, The Lancet 2002, **359**, 241-247.
8. A Amdisen "*Monitoring of lithium treatment through determination of lithium concentration"*, Danish medical bulletin 1975, **22**, 277-291.
9. Personal communication, P Kölling, Medisch Spectrum Twente Hospital Group, Enschede, The Netherlands
10. S Linko "*Automated ion-selective measurement of lithium in serum. A practical approach to result-level verification in a two-way method validation"*, Accred. Qual. Assur. 2001, **6**, 31-36.
11. KA Erickson and P Wilding "*Evaluation of a Novel Point-of-Care System, the i-STAT Portable Clinical Analyzer"*, Clin. Chem. 1993, **39**, 283-287.
12. WM Glazer, JG Sonnenberg, MJ Reinstein and RF Akers "*A novel, point-of-care test for lithium levels: description and reliability"*, J. Clin. Psychiatry 2004, **65**, 652-655.
13. X Huang, MJ Gordon and RN Zare "*Quantitation of Li^+ in serum by capillary zone electrophoresis with an on-column conductivity detector"*, J. Chromatogr. 1988, **425**, 385-390.
14. V Dolník and J Dolníková "*Capillary zone electrophoresis of organic acids in serum of critically ill children"*, J. Chromatogr. A 1995, **716**, 269-277.

15. V Dolník "*Capillary zone electrophoresis of serum proteins; study of separation variables"*, J. Chromatogr. A 1995, **709**, 99-110.
16. G Boatto, MV Faedda, A Pau, B Asproni, S Menconi and R Cerri "*Determination of amphetamines in human whole blood by capillary electrophoresis with photodiode array detection"*, J. Pharm. Biomed. Anal. 2002, **29**, 1073-1080.
17. T Zhou, Q Hu, H Yu and Y Fang "*Separation and determination of β-agonists in serum by capillary zone electrophoresis with amperometric detection"*, Anal. Chim. Acta 2001, **441**, 23-28.
18. J Cheng, LJ Kricka, EL Sheldon and P Wilding "*Sample Preparation In Microstructured Devices"*, Topics in Current Chemistry 1998, **194**, 215-231.
19. AJ Tüdõs, GAJ Besselink and RBM Schasfoort "*Trends in miniaturized total analysis systems for point-of-care testing in clinical chemistry"*, Lab on a Chip 2001, **1**, 83-85.
20. DD Cunningham "*Fluidics and sample handling in clinical chemical analysis"*, Anal. Chim. Acta 2001, **429**, 1-18.
21. J Lichtenberg, NF De Rooij and E Verpoorte "*A microchip electrophoresis system with integrated in-plane electrodes for contactless conductivity detection"*, Electrophoresis 2002, **23**, 3769-3780.
22. M Pumera, J Wang, F Opekar, I Helínek, J Feldman, H Löwe and S Hardt "*Contactless Conductivity Detector for Microchip Capillary Electrophoresis"*, Anal. Chem. 2002, **74**, 1968-1971.
23. A Berthold, F Laugere, H Schellevis, CR De Boer, M Laros, RM Guijt, PM Sarro and MJ Vellekoop "*Fabrication of a glass-implemented microcapillary electrophoresis device with integrated contactless conductivity detection"*, Electrophoresis 2002, **23**, 3511-3519.
24. J Tanyanyiwa, EM Abad-Villar, MT Fernández-Abedul, A Costa-Garcìa, W Hoffmann, AE Guber, D Herrmann, A Gerlach, N Gottschlich and PC Hauser "*High-voltage contactless conductivity-detection for lab-on-chip devices using external electrodes on the holder"*, Analyst 2003, **128**, 1019-1022.
25. ML Reed and W-K Lye "*Microsystems for Drug and Gene Delivery"*, Proceedings of the IEEE 2004, **92**, 56-75.
26. E Mukerjee, SD Collins, RR Isseroff and RL Smith "*Microneedle array for transdermal biological fluid extraction and in situ analysis"*, Sens. Actuators A 2004, **114**, 267-275.
27. R Luttge, HJGE Gardeniers, EX Vrouwe, and A van den Berg "Microneedle array interface to CE on chip". In: MA Northrup, KF Jensen, and DJ Harrison, eds. Proceedings of micro total analysis systems 2003. San Diego: Transducers Research Foundation, vol. 1, 511-514
28. B Leboulanger, J-M Aubry, G Bondolfi, RH Guy and MB Delgado-Charro "*Lithium monitoring by reverse iontophoresis in vivo"*, Clin. Chem. 2004, **50**, 2091-2100.
29. MJ Tierney, JA Tamada, RO Potts, L Jovanovic, S Garg and Cygnus Research Team "*Clinical evaluation of the GlucoWatch® biographer a continual, non-invasive*

glucose monitor for patients with diabetes", Biosensors & Bioelectronics 2001, **16**, 621-629.

30. S Hjertén "*High-performance electrophoresis; Elimination of electroendosmosis and solute adsorption"*, J. Chromatogr. 1985, **347**, 191-198.
31. LL Shultz-Lockyear, CL Colyer, ZH Fan, KI Roy and DJ Harrison "*Effects of injector geometry and sample matrix on injection and sample loading in integrated capillary electrophoresis devices"*, Electrophoresis 1999, **20**, 529-538.
32. C-X Zhang and W Thormann "*Head-Column Field-Amplified Sample Stacking in Binary System Capillary Electrophoresis; A Robust Approach Providing over 1000-Fold Sensitivity Enhancement"*, Anal. Chem. 1996, **68**, 2523-2532.
33. E Metzger, R Dohner, W Simon, DJ Vonderschmitt and K Gautschi "*Lithium/Sodium Ion Concentration Ratio Measurements in Blood Serum with Lithium and Sodium Ion Selective Liquid Membrane Electrodes"* , Anal. Chem. 1987, **59**, 1600-1603.
34. EX Vrouwe, R Luttge, and A van den Berg "Sampling for point-of-care analysis of whole blood with microchip CE". In: T Laurell, J Nilson, K Jensen, DJ Harrison, and JP Kutter, eds. Proceedings of micro total analysis systems 2004. Cambridge: The Royal Society of Chemistry, vol. 1, 503-505
35. Personal communication. R Luttge, University of Twente, Enschede, The Netherlands
36. K Ito and T Hirokawa "*Separation of alkali and alkaline-earth metal and ammonium cations by capillary electrophoresis using poly(ethylene glycol) and tartaric acid"*, J. Chromatogr. A 1996, **742**, 281-288.
37. H Becker and LE Locascio "*Polymer microfluidic devices"*, Talanta 2002, **56**, 267-287.

Chapter 7

Rapid quantitative determination of inorganic anions and cations in drinking water*

Microchip capillary electrophoresis (CE) was used to separate inorganic ions in less than 15 seconds enabling online monitoring of drinking water quality. This application requires accurate quantitation, which at present is still a challenge for microchip CE. In this paper we therefore discuss the requirements for quantitative microchip CE of drinking water using glass chips with conductivity detection. The separation can be affected by interaction of metal ions from the sample with the glass surface of the chip causing severe peak deformation and variation in electroosmotic flow (EOF). Using optimized separation conditions these two effects can be minimized. A small amount of potassium in the background electrolyte (BGE) reduces surface interaction while the addition of tartaric acid as a complexing agent improves the resolution for the cationic species K, Na, Ca and Mg. The anionic species Cl, SO_4 and HCO_3 are separated in a BGE containing CTAB (cetyltrimethylammonium bromide) using reversed EOF co-migration. The detection limits are 20 μmol/L for the monovalent cationic and anionic species and 10 μmol/L for the divalent species. These values are low enough for many applications such as process control of water softening installations.

* This chapter has been submitted for publication in Journal of Chromatography A.

7.1 Introduction

Microchip capillary electrophoresis (CE) has been introduced as a tool for fast quantitative analysis in a small instrument. Instead of bringing samples to the laboratory it is possible to perform the analysis on-site. The microchip CE systems that are commercially available have been developed primarily for use in the field of life sciences where high throughput is the main benefit and quantitation is of lower importance than identification. In this chapter we focus on the determination of abundant inorganic anions and cations in drinking water using microchip CE. The aim of this work is to establish the requirements for accurate quantitation and to evaluate microchip CE performance in the field of drinking water analysis

Ion chromatography is an established technique for quantitative analysis of inorganic ions, but capillary electrophoresis has been demonstrated as a viable alternative for the analysis of drinking water [1-7]. The advantages of conventional CE compared to ion chromatography are faster separations in combination with higher resolution [8]. Examples of high-resolution separations are the determination of 27 metal species in 6 minutes [9] and that of a mixture of 30 organic and inorganic anions in just 3 minutes [10]. One of the inherent characteristics of CE is that the separation time can be reduced with a minimal effect on separation resolution purely by shortening the length of the capillary [11]. When also high electric field strengths are used it is possible to perform separations in just a few microseconds [12]. In contrast, for a chromatographic separation a reduction of the length of the separation column inevitably leads to a loss of resolution. Rapid analysis can make microchip CE superior to chromatography for applications requiring (semi) continuous monitoring.

Microchip CE systems are not only faster than traditional CE instruments, but they can also be made more compact. Portable CE instruments have been developed based on conventional systems, but are limited in their application by a considerable weight of approximately 7.5 kg [13]. One of the limitations for making a conventional CE system more portable is formed by the size and weight of the high-voltage power supply and the batteries. In a chip relatively low separation voltages in the order of a few hundred volts are sufficient to generate electrical field strengths that are comparable to what is used for conventional CE systems. The lower demands on the power supply for a microchip system provides a significant size and weight reduction. It is even possible to use standard household batteries to operate a CE chip [14-16]. When also a detection principle with moderate power requirements is used, for example an electrochemical method, a truly handheld system is feasible.

Inorganic ions can be determined with high sensitivity using conductivity detection. Mixtures containing alkali metal salts are frequently used for testing the performance of microchip CE devices in combination with conductivity detection methods [17-20]. There

are however only few publications that give details about quantitation [18,21-23]. This indicates that quantitation with microchip CE is not trivial. Still, the potential benefits of a microchip CE system appeals to the industry. An example of an application for which microchip CE would be particularly suitable is in the analysis of drinking water [24]. Since clean drinking water is vital to human health, maintaining a constant high quality is of foremost importance for the water companies. Strict regulations on the maximum allowed concentration of many potential contaminants guarantee that tap water is safe for consumption. The United States Environmental Protection Agency for example has listed over 80 species in the National Primary Drinking Water Regulations [25]. Similar lists have been compiled by the European Union and the World Health Organization [26,27]. Besides the harmful substances on these lists, which need to be determined at very low concentration levels, the exact concentrations of constituents present in higher concentrations are also of interest. These include potassium, sodium, calcium, magnesium, chloride, sulfate and bicarbonate. Not only do high concentrations of these species affect the taste of drinking water, but too low amounts of sodium or calcium are considered unhealthy while the calcium and bicarbonate concentrations affect how corrosive tap water is to the plumbing system [28]. Of special interest is the water hardness, which is determined by the calcium and magnesium concentration. Domestic and industrial use of hard water can cause problems due to formation of scale deposits on water heating elements and the inside of pipes. Also the formation of precipitates with soap is an unwanted side effect. In regions with naturally high concentrations of calcium or magnesium water companies therefore often reduce the hardness. On a small scale this can be done via ion exchange, though for large volumes there is a more economical alternative by adding sodium hydroxide or calcium hydroxide to the water in a reactor. This causes calcium and magnesium carbonate to precipitate, which is subsequently removed. Feedback to the dosing system of such a reactor is provided by determining hardness in an indirect way via the electrical conductivity and pH of the treated water [29]. Direct determination of calcium, magnesium and carbonate is also possible with the use of ion selective electrodes. However, microchip CE can be a valuable addition to determine water quality since it can be used to determine many water constituents simultaneously whereas ion selective electrodes are available only for a limited number of species. The use of a CE chip to control the water softening provides exact data on the concentrations of calcium, magnesium and bicarbonate, which will give better control of the process compared to the existing system measuring only pH and conductivity.

In addition to the large-scale production of drinking water there are other fields where water quality monitoring is of interest. Examples are water management installations in greenhouses to enable correct dosing of nutrients and fertilizers into the water fed to the plants, or for quality control of recycled drinking water used in the environment of space [30].

To obtain a good indication of the quality of drinking water it is necessary that both cationic and anionic species are determined. Capillary electrophoresis can be used to separate many like-charged components in a single separation run. Cationic species are separated with a co-migrating electroosmotic flow (EOF). For separating anionic species the EOF is typically reversed first with, for example, CTAB [31]. When an application requires that both cations and anions need to be analyzed in a single sample a choice has to be made whether to determine them in separate CE runs, or to analyze them simultaneously. Untreated glass and fused silica capillaries exhibit a natural EOF in the direction of the cathode. This means that anions that have an electrophoretic mobility lower than the EOF are transported to the detector end of the capillary, even though their electrophoretic migration is in the opposite direction. Conversely, cations have been separated under anodic conditions after reversing the direction of the EOF [32]. It is possible to use a complexing agent like EDTA (ethylene diamine tetra acetic acid) to form negatively charged complexes with some of the cations for separating them in the anodic mode [33]. For inorganic ions, which typically have electrophoretic mobilities exceeding the opposing EOF it is not possible to use an EOF counter migration approach. Still a simultaneous analysis can be performed by injecting sample into both ends of the separation capillary. The cations and anions migrate to opposite ends and are detected in the middle of the capillary [1-3,7]. This method has also been used on a microchip system [34]. Alternatively, a chip can be designed with a channel layout that allows the sample plug to be introduced in the middle of the separation capillary, with subsequent detection at both ends [35]. A disadvantage of these methods for simultaneous analysis is that only half the electrical field is used for the separation for either species, which reduces the resolution. Furthermore, separation conditions need to be found that are suitable for resolving all species of interest sufficiently. For conventional CE systems a simultaneous analysis can be of advantage as it can save time. The chip technology makes it possible to fabricate CE chips with multiple parallel separation channels on a single device that can be used at the same time. The separations of anionic and cationic species can therefore be performed separately without decreasing the throughput.

In this chapter optimized conditions are established for separating anionic and cationic species. The separation of calcium and magnesium from sodium in the cationic mode is optimized using a complexing agent to modify the electrophoretic mobilities of the ions. The separation of anionic species is performed with EOF co-migration using CTAB to reverse the direction of the EOF.

7.2 Experimental

7.2.1 Chemicals

Calibration solutions for the cationic species were prepared by dissolving the chloride salts of sodium, potassium, calcium (Merck, Darmstadt, Germany) and magnesium

(Baker, Deventer, The Netherlands) in deionized water (Millipore). Mixtures of the four species were prepared in a range of concentrations from 0.1 to 2 mmol/L. For the anions calibration standards were prepared from sodium acetate (Aldrich, Milwaukee, USA), sodium bicarbonate (Merck) and sodium chloride. Separation buffers were prepared from 2-(N-morpholino)ethanesulfonic acid (MES, Sigma, Steinheim Germany), histidine (His, Fluka, Buchs, Switzerland), 4-(2-hydroxyethyl)-1-piperazineethane sulfonic acid (HEPES, Merck) and HEPES sodium salt (Aldrich). Tartaric acid (Baker) is added to the background electrolyte (BGE) as complexing agent. Cetyltrimethylammonium bromide (CTAB) was used in various concentrations to change the direction of the EOF. The water sample is domestic tap water from the city of Enschede (Vitens water company, Velp, The Netherlands)

7.2.2 Microchip CE system

Borofloat glass chips (Fig. 7.1) with a double-T injector of 200 μm length were obtained from Micronit Microfluidics BV (Enschede, The Netherlands). All channels were etched to a depth of 8 μm and a width at the top of the channel of 56 μm using hydrofluoric acid. The effective length of the separation channel (from the double-T injector to the detection electrodes) is 2 cm. The electrodes for conductivity detection consist of thin platinum films in direct contact with the electrolyte inside of the channel. Before the chips are used for the first time they are heated in an oven for one hour at 600ºC, which improves the

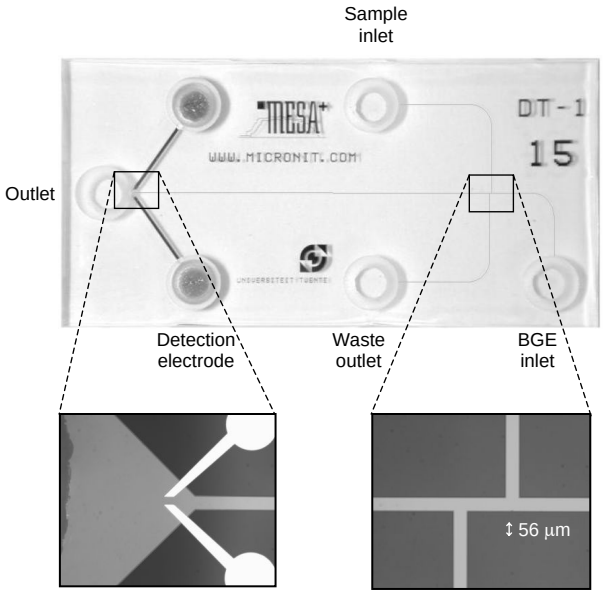

Figure 7.1: *Photograph of the CE microchip with dimensions of 30 × 15 mm. The insets show the position of the electrodes used for the conductivity detection and the channel intersection defining the sample volume.*

separation resolution of the cations under consideration. The chips were placed in a holder made from Delrin™ consisting of a bottom support plate and a cover with fluid compartments. Platinum wires inserted into the fluidic compartments provided electrical contact to a computer controlled high-voltage power supply (CU 411, IBIS Technologies BV, Hengelo, The Netherlands) with four independently controllable positive voltage outputs. A custom-made conductivity detector (Sprenkels Consultancy, Lelystad, The Netherlands) was used and the signal was recorded with a data acquisition card (DAQCard 6036E, National Instruments, Austin, TX, USA). An in-house written software package combined the control of the power supply, acquisition of data from the detector and the subsequent data processing.

7.2.3 Separation of cationic species

For separating the cationic species a BGE was used consisting of 30 mmol/L MES/His, 4 mmol/L tartaric acid and 0.5 mmol/L KCl. The chip is filled manually with BGE and sample solution. A pinched sample plug is formed using full plug shaping [36]. A complete CE run consists of two steps. Sample is pumped through the double-T by applying 1000 V to the sample inlet and 0 V to the waste outlet (see Fig. 7.1). Simultaneously, pinching is performed by applying 800 V to the BGE inlet and 1000 V to the outlet. After 60 seconds the content of the double-T is injected into the separation channel and separated by applying 1000 V to the BGE inlet and 0 V to the outlet. To the sample inlet and waste outlet 600 V is applied to pull the sample away from the cross in order to prevent leakage of sample into the main channel. The separation step is continued for 60 seconds.

7.2.4 Separation of anionic species

The anionic species are separated in a BGE containing 10 mmol/L HEPES, 10 mmol/L sodium HEPES and 0.05 mmol/L CTAB. The addition of CTAB to the BGE causes a reversal of the EOF enabling the separation of anions in the EOF co-migration mode. The same sequence of voltages used for separating cations is also used for the anions (section 2.3).

7.2.5 Determination of the electroosmotic flow velocity

For anionic separations the EOF has to be optimized by the concentration of a suitable EOF modifier, here CTAB. To determine the EOF for various CTAB concentrations a solution with 1 mmol/L rhodamine B (Sigma) is dissolved in the BGE and used as neutral fluorescent marker. The rhodamine solution is placed in the BGE inlet compartment (Fig. 7.1) while the rest of the chip is filled with BGE without the marker. A constant potential of 1000 V applied between the BGE inlet compartment and outlet compartment is used to drive the rhodamine solution through the chip with the EOF. The two remaining chip compartments are not connected to the voltage supply. A fluorescence microscope (Leica DM/IRM, Wetzlar, Germany) with a 100 W mercury lamp filtered through an I3 filter cube (Leica) is used for excitation of the rhodamine. The fluorescence intensity is

measured at the end of the separation channel with a photosensor module (H7422-02, Hamamatsu, Japan) attached to the microscope.

7.3 Results and discussion

7.3.1 Formation of a representative sample plug

For accurate quantitative analysis the formation of a sample plug that is representative for the sample irrespective of the composition of the sample (i.e. matrix effects) is crucial. Although it is known for conventional CE systems that electrokinetic injection causes a mobility induced bias [37], it is routinely used for sample introduction on CE chips. Commonly the EOF is used to drive sample from the sample compartment via the channel intersection to the waste outlet (Fig. 7.1). A sample plug is defined by the volume of the intersection together with the amount of pinching from the sides using the voltage scheme described in section 7.2.3. The plug is subsequently dispensed into the separation channel for the actual CE separation. However, the concentration profile of ions in the sample plug is not necessarily the same as in the sample [23]. Consider the situation shown in Fig. 7.2A where a section of the channel leading from the sample compartment to the channel intersection is depicted. Part of the channel is filled with sample while the remainder is filled with the BGE. At the moment the electric field is applied the EOF drives the sample further into the channel which is shown in Fig. 7.2B by an advance of the boundary denoted by a double line. Superimposed on the bulk flow is the migration of ionic species in the sample and BGE. This causes zones to form having different compositions, which are denoted by Greek symbols. Here α and ε stand for zones with a composition identical

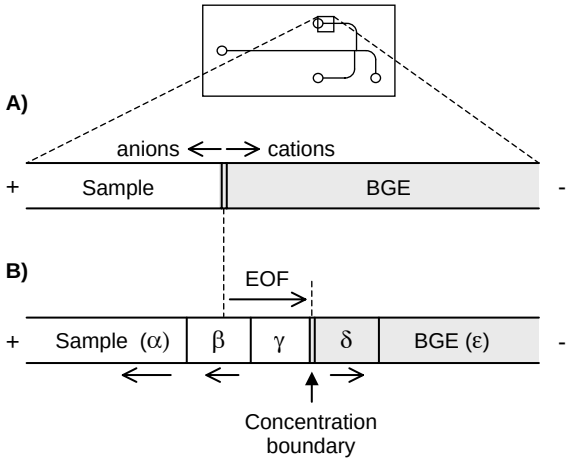

Figure 7.2: *Schematic representation of the different zones created at the interface between sample and background electrolyte during the electrokinetic transport of sample to the double-T. A) Starting situation, B) the situation after applying voltage. See the text for a description of the symbols.*

to the sample and BGE, respectively. Zone β represents a zone that has been depleted of the fastest anionic sample species. Similarly, zone γ represents a zone depleted from not only all the fast anionic species in the sample, but also the slow anionic species. In fact, the counter-ions from the BGE have completely replaced the anions from the sample. In these zones α, β and γ all cationic species from the sample are present. Further to the right, zone δ denotes a zone consisting of cationic sample species that have displaced the cations in the BGE. In this situation, zone α is the only zone that contains all sample components including the fastest anionic species. Yet, this zone moves faster to the anode than the EOF drives it towards the channel intersection. Only zones δ, γ and β can reach the intersection when they are allowed sufficient time. For a simultaneous reliable analysis of cations and slow anions the sample loading therefore has to be performed long enough for zone β to reach the intersection. For the determination of cations both zones β and γ can be used. Zone δ is a special case because the boundary between the sample and BGE (the so called concentration boundary) causes field amplified stacking [38]. The stacking efficiency and concentration of sample components in zone δ strongly depends on the composition of the sample [39]. Consequently, peak sizes in the electropherogram obtained from zone δ cannot be related directly to a concentration without the use of an internal standard in the sample to account for the amount of stacking. In order to obtain meaningful results without the use of an internal standardization method, it is of importance to inject a zone that is driven to the channel intersection by the EOF.

In order to form a sample plug containing the fastest anionic species, the electric field used for the injection can be reversed. In this counter EOF mode only the anions with an electrophoretic mobility faster than the EOF can reach the channel intersection. However, these ions will cross the concentration boundary and are consequently stacked. For quantitative analysis of fast anionic species therefore an internal standard has to be used as shown in chapter 5. Alternatively, the direction of the EOF can be reversed so that the separation is performed in the co-migrating EOF mode and no stacking occurs.

7.3.2 Separation of inorganic cations

The most abundant cationic species in drinking water are the alkali and alkaline earth metals. Potassium, sodium, calcium and magnesium are present in the range of 0.1 to 1.5 mmol/L (Table 7.1). The first step for the determination of these species is selection and subsequent optimization of the BGE with respect to resolution and detection sensitivity of the system. When conductivity detection is used the choice of the BGE has a large influence on the signal sensitivity, as discussed in section 2.4.2. To achieve a high signal-to-noise ratio, the ionic conductivity of the BGE co-ion, which is directly related to the electrophoretic mobility, should differ from that of the analytes as much as possible [40]. A BGE formulation that is frequently used in combination with conductivity detection, also for conventional CE, is a mixture of equimolar amounts of histidine and MES. Both compounds have relatively low mobilities, which make them an ideal choice for the analysis of inorganic ions with a high mobility. Furthermore, their pKa values are almost identical which translates in good pH buffering performance. However, for the separation of calcium, sodium and magnesium this BGE is not sufficient because the electrophoretic mobilities of these compounds are too close together. Various reports can be found in the literature concerning organic acids as complexing agents for improving the resolution in CE separations. These include oxalic acid, lactic acid, tartaric acid and HIBA (hydroxyisobutyric acid) [6,41,42], but also neutral substances like poly(ethylene glycol) [43]. For this study tartaric acid was selected, which has been used with success for separating similar samples on conventional systems [43]. For background electrolytes with different concentrations of tartaric acid, the electrophoretic mobilities and separation resolution were determined using a calibration solution with 1 mmol/L potassium, sodium, calcium and magnesium (Fig. 7.3A and B). The most significant change in mobility is observed for calcium, while magnesium is slightly affected. Baseline separation (resolution higher than 1.5) is achieved with a tartaric acid concentration of 3 mmol/L. For the remaining separations 4 mmol/L is used, which makes the system more

Table 7.1: *Typical concentration of selected inorganic ions in tap water.*

	Specified in tap water mg/L, (mmol/L)[1]	Maximum allowed concentration mg/L, (mmol/L)[2]
K^+	4.6 (0.12)	n.a.
Na^+	25 (1.1)	150 (6.52)
Ca^{2+}	48 (1.2)	(1 - 2.5)[3]
Mg^{2+}	5.7 (0.23)	(1 - 2.5)[3]
Cl^-	44 (1.2)	150 (4.23)
SO_4^{2-}	46 (0.48)	150 (1.56)
HCO_3^-	112 (1.84)	minimum 60 (0.98)

[1]Annual average concentrations over 2003 in Enschede, The Netherlands.

[2]Values according to Dutch legislation.

[3]Combined concentration of Ca and Mg should be within these limits.

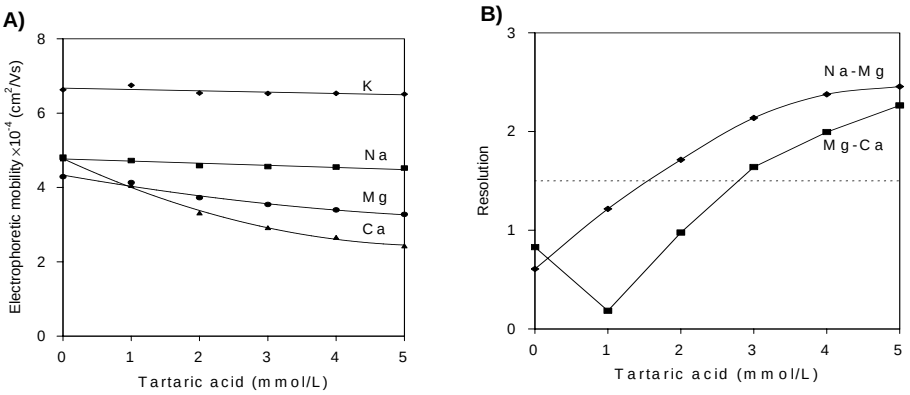

Figure 7.3: *Effect of the concentration of tartaric acid on A) the electrophoretic mobility and B) the resolution between sodium and magnesium, and between magnesium and calcium respectively. Sample consisted of a 1 mmol/L mixture of the four cationic species. BGE 30 mmol/L MES/His with 0.5 mmol/L KCl.*

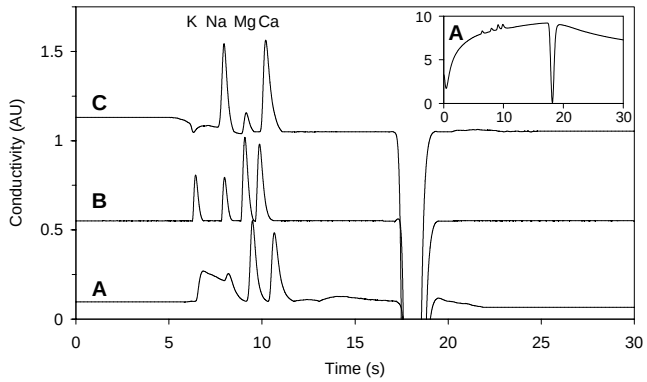

Figure 7.4: *Electropherogram of A) a calibration solution consisting of 1 mmol/L K, Na, Mg and Ca using a BGE with 30 mmol/L MES/His and 4 mmol/L tartaric acid, B) the same calibration solution using a BGE composition as in A but with 0.5 mmol/L KCl added to the BGE, C) a tap water sample using the same BGE as in B. The electropherograms are corrected for baseline drift. The inset shows the actual electropherogram for the calibration solution without baseline correction.*

robust for small variations in the effective electrophoretic mobility.

The electropherogram in Fig. 7.4A shows that calcium and magnesium are well separated, but the resolution between potassium and sodium is insufficient. Typical for conductivity detection is the presence of a negative water peak resulting from a discontinuity in the local concentration of BGE produced by injecting a sample plug with a dissimilar composition. In particular the peak formed by potassium is characterized by extensive

tailing, increasing the spatial peak variance significantly. Such strong tailing behavior is an indication that there is interaction of analytes with the glass channel surface. It is known that silica surfaces can act as ion exchanger for inorganic cations allowing even chromatographic separation [44]. A significant improvement of peak shapes was observed after adding a small amount of potassium (approximately 0.5 mmol/L KCl) to the BGE (Fig. 7.4B). It is assumed that the performance increase is achieved due to a saturation of the active sites on the glass surface, preventing further interaction of analytes with the surface. However, the BGE system now has two co-ionic species instead of one, which can result in the occurrence of system peaks as discussed in section 3.3.4 [45]. For example a vacancy peak (i.e. a dip in the signal) can be expected near the position of potassium when there is only little potassium present in the sample (Fig. 7.4C). The detection sensitivity does not suffer from the small amount of potassium in the BGE as both the potassium and sodium peaks in the standards become sharper and higher.

Concluding from these experiments the optimized BGE consists of 30 mmol/L MES/His, 0.5 mmol/L potassium chloride and 4 mmol/L tartaric acid. It provides baseline separation of potassium, sodium, calcium and magnesium in less than 15 seconds. Analysis of a tap water sample shows that the sensitivity of the system is sufficient to detect sodium, calcium and magnesium (Fig. 7.4C). However, due to the presence of potassium in the BGE a system peak appears which makes determination of small amounts of potassium in the sample difficult.

7.3.3 Separation of inorganic anions

Anionic species are separated on the same type of chip as used for the cations. However, the buffering electrolyte and EOF conditions have to be modified. A HEPES BGE with a pH of 7.5 is used to maintain a pH above the pKa of 6.4 for bicarbonate. Again the buffer system is selected with the requirement of a low co-ionic mobility for sensitive

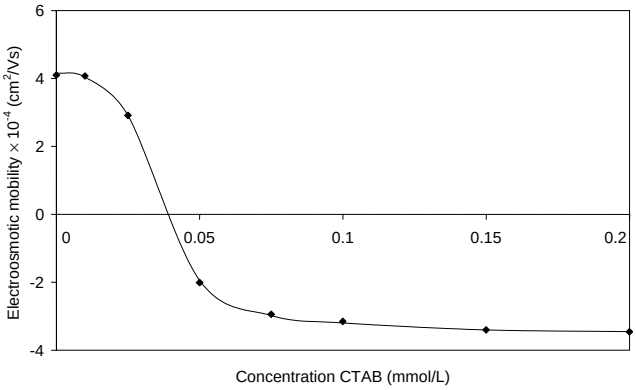

Figure 7.5: *Effect of the CTAB concentration in the BGE on the EOF. BGE 20 mmol/L HEPES, pH 7.5.*

conductivity detection. In order to use the EOF to form a sample plug the direction of the EOF needs to be reversed. Therefore a small amount of the cationic surfactant CTAB is added to the BGE [31]. Adsorption of CTAB micelles onto the capillary surface results in the formation of a layer with positive charge causing a reduction or even a complete reversal of the EOF [46,47]. Figure 7.5 shows the EOF mobility versus the CTAB concentration, which was experimentally determined on the chip. A reversal of the EOF takes place at a CTAB concentration in the BGE of between 25 and 50 μmol/L (Fig. 7.5). Further increasing the CTAB concentration to 0.1 mmol/L causes the electroosmotic mobility to stabilize at a value of approximately -3.5×10^{-4} cm^2/Vs. This is almost as high as the electroosmotic mobility of $+4.2\times10^{-4}$ cm^2/Vs generated by the bare glass surface, but with an opposite sign. For the separation of bicarbonate from chloride and sulfate it was established that a moderate EOF at a concentration of 50 μmol/L CTAB offered better resolution than separation conditions using a faster EOF. However, operating in the sloped region of the EOF velocity curve can result in a less predictable EOF velocity and hence a less reproducible net migration time. For example, the water peak (i.e. the negative peak in the electropherogram indicating the velocity of the EOF) can shift its position as shown in the electropherogram for a calibration sample and tap water (Fig. 7.6A, B). But with the easily identifiable water peak as reference it is possible to correct the migration time for any variation in EOF velocity.

Over the course of more than 20 separation runs the conditions suddenly changed resulting in a decrease in the magnitude of the water peak. As a second effect, and more importantly, peak areas started to deviate from the linear dependency on the analyte concentration. Visual inspection of the chip indicated that the entrance of the channel in the sample compartment were blocked with a deposit. This problem appears to be related to the use of this particular BGE system as for the cationic separations no problems of

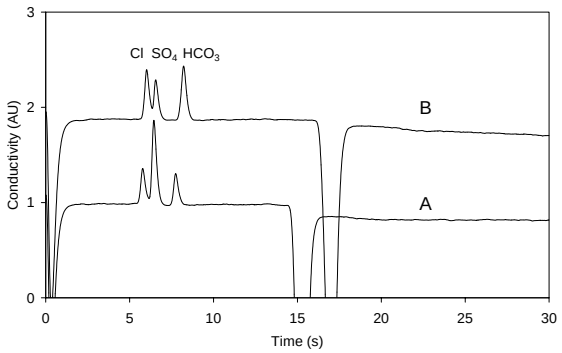

Figure 7.6: *Separation of anionic species. A) calibration solution comprised of 1 mmol/L Cl, SO_4 and HCO_3 and B) a tap water sample. BGE 20 mmol/L HEPES with 0.05 mmol/L CTAB.*

clogging were observed for more than 100 consecutive runs. Nevertheless, a series of calibration standards and samples can be run without any apparent performance shift before the chip must be cleaned. The sensitivity of the system is sufficiently high for detection of chloride, sulfate and bicarbonate in tap water (Fig. 7.6B).

7.3.4 Quantitation of inorganic ions in tap water with microchip capillary electrophoresis

After establishing the optimized conditions suitable for separating water samples on the chip, the quantitative aspects can be examined. Calibration curves were recorded for both cationic and anionic species of interest (Figs. 7.7 and 7.8). For the curves obtained of the cations a second order polynomial provides a good fit. There are several possible causes that can lead to the non-linear behavior for the cationic species. First, the detector signal

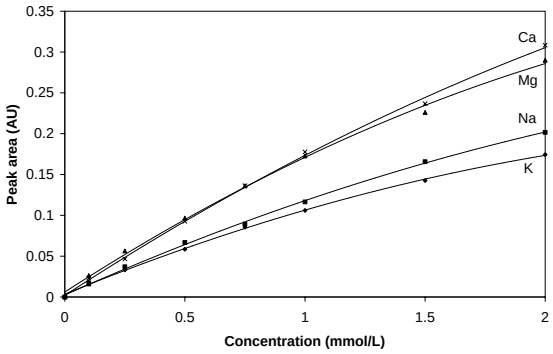

Figure 7.7: *Calibration curves for potassium, sodium, calcium and magnesium. BGE 30 mmol/L MES/His with 4 mmol/L tartaric acid and 0.5 mmol/L KCl.*

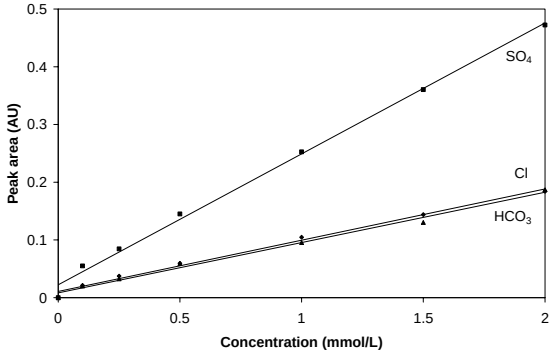

Figure 7.8: *Calibration curves for bicarbonate, chloride and sulphate. BGE 20 mmol/L HEPES with 0.05 mmol/L CTAB.*

itself can be non-linear with the concentration. Yet, a calibration curve measured for sodium in the absence of the other components is linear to at least 5 mmol/L and also the calibration curves for the anions are linear. From this we can conclude that it is not a problem caused by the detection. Second, the absolute amount of the cationic analytes in the separated zones is not linearly proportional with the concentration in the bulk of the sample. The most direct cause of this is a variation of the sample plug size being injected into the separation channel. When considering the length of the sample plug, it is mainly determined by the size of the double-T channel intersection. But also the amount of pinching or plug shaping during filling will affect the volume of the sample plug and additional sample can leak out of the side channels into the separation channel during the separation due to insufficient sample pull-back. Of all these factors, the pinching of the sample plug is influenced by the combination of electric field strengths in all four channels. And as the sample matrix varies in conductivity, also some variation in the field strengths will occur. Still, this does not explain adequately why the same curving does not occur in the calibration curve of the anions. It is more likely that the EOF in the sample channel itself is altered by the sample composition. Alkaline earth metals in particular interact with the glass surface and can have a marked effect on the EOF. Even small amounts in the order of 5 mmol/L can cause a drop to half the original value [48]. The effect of metal species on the EOF follows the trend of affinity for cation exchange materials in the order of Ca>Mg>>K>Na. In section 7.3.2 we already observed wall interaction resulting in the tailing of the potassium peak. Combined with those observations it is likely that the EOF is influenced by the sample composition. When the EOF drops in the channel containing the sample, the pinching effect becomes stronger since EOF in the remaining channels stays constant. This leads to a smaller volume of the sample plug in the double-T when the concentration of Ca and Mg in the sample increases. Under the conditions for separating the anions there is no such effect as only sodium salts are used for making the calibration standards and sodium does not interact with the surface as strong as the alkaline earth metals. Consequently the EOF remains stable during anionic separations on the microchip regardless of the concentration of the calibration standard. Concluding, the EOF needs to be stable for samples that differ in compositions. It turns out that small variations in EOF are inherent for the glass chips used in this study, especially in the cationic separation mode. A surface treatment minimizing the interaction with the sample or a weaker pinching of the sample plug might reduce this matrix effect.

Table 7.2: *Analysis results of a tap water sample and detection limits of the microchip CE system.*

	Determined in tap water (mg/L ± 2 s.d.)	Detection limit mg/L, (mmol/L)
K^+	n.d.[1]	0.78 (0.02)
Na^+	34.0 ± 1.3	0.46 (0.02)
Ca^{2+}	59.2 ± 3.0	0.40 (0.01)
Mg^{2+}	4.33 ± 0.32	0.24 (0.01)
Cl^-	50.8 ± 2.1	0.71 (0.02)
SO_4^{2-}	45.7 ± 2.9	0.96 (0.01)
HCO_3^-	119 ± 4.0	1.2 (0.02)

[1]Not determined due to overlap with the system peak.

Although the shape of the calibration curves of the cations depicted in Fig. 7.7 is not linear, quantitation is still possible. For the tap water sample shown in Figs. 7.4C and 7.6B the concentration of the seven species was determined (Table 7.2). With the exception of potassium the determined values are in agreement with the average water composition shown in Table 7.1. The relative standard deviations of the determined peak areas for replicate separation runs (n=3) are around 3%. Determination of potassium, which should be present at a concentration of approximately 0.1 mmol/L, is hindered by the dominating effect of the negative system peak produced by the presence of 0.5 mmol/L potassium in the BGE.

The detection limits are calculated based on three times the noise level on the baseline in the electropherograms obtained from a 100 μmol/L calibration standard (Table 2). For the alkaline earth metals calcium and magnesium a detection limit of 10 μmol/L is reached and for the alkali metals sodium and potassium 20 μmol/L. Similarly, the detection limit is 10 μmol/L for chloride and bicarbonate and 20 μmol/L for sulfate. Also the stability of the system was examined during an entire day by separating a sample every 30 minutes (Fig. 7.9). The chip was filled with BGE only once, before the start of the first experiment to model real-world operating conditions. The figure shows that during the 51 separation runs the area of the sodium peak increases with 7%. The relative standard deviation of the peak area is only 5%. Depending on the required accuracy a single calibration per day can suffice.

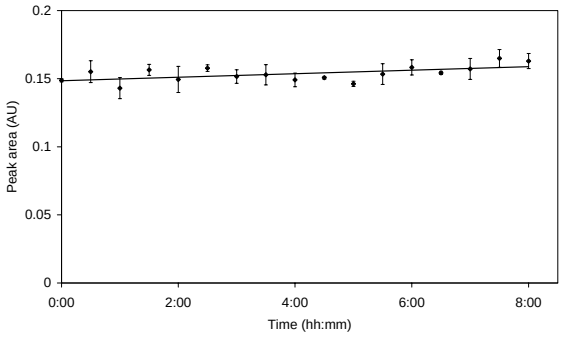

Figure 7.9: *Stability test of the microchip showing the peak area for sodium over a time period of 8 hours. Three separation runs are performed every 30 minutes without refreshing the BGE. Separation conditions as in Fig. 7.4B.*

7.4 Conclusions

Microchip CE is a generic tool for fast ion analysis allowing separations in less than 15 seconds. A single chip design can be used for anion and cation separations after changing the BGE composition, the direction of the EOF and the polarity of the voltages. Together with the use of on-chip integrated conductivity detection a compact CE instrument is feasible. The system presented in this paper offers sufficient separating performance and sensitivity for determining the concentration of abundant ions in tap water. Detection limits are 20 µmol/L for monovalent ions and 10 µmol/L for divalent ions. At the moment the microchip system requires manual filling with BGE and sample. Since there is no defined cleaning or conditioning step before the start of each measurement there is a risk that the separating conditions change due to fouling. Especially in the anionic mode the results becomes irreproducible after 20 runs, while in the cationic mode the chip continues to operate stable.

An issue is the interaction of cationic species with the glass surface, causing extreme peak tailing and problems with EOF stability. The poor resolution between potassium and sodium can be resolved by adding a small amount of potassium to the BGE, but at the expense of producing an additional system peak. It is therefore recommended to use a surface coating for glass chips or a BGE modifier that reduces surface interaction and provides better EOF stability. When carrying out the optimization issues, we believe that microchip CE systems are a valuable addition to the established ion analysis techniques for water process control and related analytical fields of work.

7.5 References

1. P Kuban and B Karlberg "*Simultaneous Determination of Small Cations and Anions by Capillary Electrophoresis"*, Anal. Chem. 1998, **70**, 360-365.
2. A Padarauskas, V Olšauskaite and V Paliulionyte "*Simultaneous determination of inorganic anions and cations in waters by capillary electrophoresis"*, J. Chromatogr. A 1998, **829**, 359-365.
3. V Unterholzner, M Macka, PR Haddad and A Zemann "*Simultaneous separation of inorganic anions and cations using capillary electrophoresis with a movable contactless conductivity detector"*, Analyst 2002, **127**, 715-718.
4. B Saad, FW Pok, ANA Sujari and MI Saleh "*Analysis of anions and cations in drinking water samples by Capillary Ion Analysis"*, Food Chem. 1998, **61**, 249-254.
5. JA Jurado-González, MD Galindo-Riaño and M García-Vargas "*Factorial designs applied to the development of a capillary electrophoresis method for the analysis of zinc, sodium, calcium and magnesium in water samples"*, Talanta 2003, **59**, 775-783.
6. P Kubán, P Kubán and V Kubán "*Simultaneous determination of inorganic and organic anions, alkali, alkaline earth and transition metal cations by capillary electrophoresis with contactless conductometric detection"*, Electrophoresis 2002, **23**, 3725-3734.
7. I Haumann, J Boden, A Mainka and U Jegle "*Simultaneous determination of inorganic anions and cations by capillary electrophoresis with indirect UV detection"*, J. Chromatogr. A 2000, **895**, 269-277.
8. J Havel, P Janoš and P Jandik "*Capillary electrophoretic estimation of sulfate stability constants of metal ions and determination of alkali and alkaline earth metals in waters"*, J. Chromatogr. A 1996, **745**, 127-134.
9. Y Shi and J Fritz "*Separation of metal ions by capillary electrophoresis with a complexing electrolyte"*, J. Chromatogr. A 1993, **640**, 473-479.
10. WR Jones and P Jandik "*Controlled changes of selectivity in the separation of ions by capillary electrophoresis"*, J. Chromatogr. 1991, **546**, 445-458.
11. JW Jorgenson and KD Lukacs "*Zone Electrophoresis in Open-Tubular Glass Capillaries"*, Anal. Chem. 1981, **53**, 1298-1302.
12. ML Plenert and JB Shear "*Microsecond electrophoresis"*, Proc. Natl. Acad. Sci. USA 2002, **100**, 3853-3857.
13. T Kappes, B Galliker, MA Schwarz and PC Hauser "*Portable capillary electrophoresis instrument with amperometric, potentiometric and conductometric detection"*, Trends Anal. Chem. 2001, **20**, 133-139.
14. DJ Jackson, JF Naber, TJ Roussel Jr, MM Crain, KM Walsh, RS Keynton and RP Baldwin "*Portable High-Voltage Power Supply and Electrochemical Detection Circuits for Microchip Capillary Electrophoresis"*, Anal. Chem. 2003, **75**, 3643-3649.
15. D Erickson, D Sinton and D Li "*A miniaturized high-voltage integrated power supply for portable microfluidic applications"*, Lab on a Chip 2004, **4**, 87-90.

16. CD García, Y Liu, P Anderson and CS Henry "*Versatile 3-channel high-voltage power supply for microchip capillary electrophoresis"*, Lab on a Chip 2003, **3**, 324-328.
17. J Lichtenberg, NF De Rooij and E Verpoorte "*A microchip electrophoresis system with integrated in-plane electrodes for contactless conductivity detection"*, Electrophoresis 2002, **23**, 3769-3780.
18. M Pumera, J Wang, F Opekar, I Helínek, J Feldman, H Löwe and S Hardt "*Contactless Conductivity Detector for Microchip Capillary Electrophoresis"*, Anal. Chem. 2002, **74**, 1968-1971.
19. A Berthold, F Laugere, H Schellevis, CR De Boer, M Laros, RM Guijt, PM Sarro and MJ Vellekoop "*Fabrication of a glass-implemented microcapillary electrophoresis device with integrated contactless conductivity detection"*, Electrophoresis 2002, **23**, 3511-3519.
20. J Tanyanyiwa, EM Abad-Villar, MT Fernández-Abedul, A Costa-Garcìa, W Hoffmann, AE Guber, D Herrmann, A Gerlach, N Gottschlich and PC Hauser "*High-voltage contactless conductivity-detection for lab-on-chip devices using external electrodes on the holder"*, Analyst 2003, **128**, 1019-1022.
21. B-F Liu, H Hisamoto and S Terabe "*Subsecond separation of cellular flavin coenzymes by microchip capillary electrophoresis with laser-induced fluorescence detection"*, J. Chromatogr. A 2003, **1021**, 201-207.
22. E Ölvecká, M Koníková, N Grobuschek, D Kaniansky and B Stanislawski "*Direct determination of valproate in serum by zone electrophoresis–isotachophoresis on a column-coupling chip"*, J. Sep. Sci. 2003, **26**, 693-700.
23. EX Vrouwe, R Luttge and A Van den Berg "*Direct measurement of lithium in whole blood using microchip capillary electrophoresis with integrated conductivity detection"*, Electrophoresis 2004, **25**, 1660-1667.
24. Applicability of microsystems for drinking water analysis. Kiwa Water Research, Nieuwegein, The Netherlands, Publication number BTO 2003.067.
25. National Primary Drinking Water Standards, U.S. Environmental Protection Agency, publication number 816F03016, June 2003.
26. European Union Drinking Water Directive, Council Directive 98/83/EC on the quality of water intended for human consumption, adopted by the Council on 3 November 1998.
27. World Health Organization, Guidelines for Drinking-water Quality. Vol. 1, third edition, Geneva, 2004.
28. A Sander, B Berghult, A Elfström Broo, E Lind Johansson and T Hedberg, Corrosion Science 1996, **38**, 443-455.
29. Personal communication, J van den Broeke, KIWA Water Research, Nieuwegein, The Netherlands
30. D Orta, PD Mudgett, L Ding, M Drybread, JR Schultz and RL Sauer "*Analysis of water from the Space Shuttle and Mir Space Station by ion chromatography and capillary electrophoresis"*, J. Chromatogr. A 1998, **804**, 295-304.

31. MFM Tavares, R Colombara and S Massaro "*Modified electroosmotic flow by cationic surfactant additives in capillary electrophoresis; Evaluation of electrolyte systems for anion analysis"*, J. Chromatogr. A 1997, **772**, 171-178.
32. C Johns, W Yang, M Macka and PR Haddad "*Simultaneous separation of anions and cations by capillary electrophoresis with high magnitude, reversed electroosmotic flow"*, J. Chromatogr. A 2004, **1050**, 217-222.
33. P Kubán, P Kubán and V Kubán "*Simultaneous capillary electrophoretic separation of small anions and cations after complexation with ethylenediaminetetraacetic acid"*, J. Chromatogr. A 1999, **836**, 75-80.
34. J Wang, G Chen, A Muck Jr and GE Collins "*Electrophoretic microchip with dual-opposite injection for simultaneous measurements of anions and cations"*, Electrophoresis 2003, **24**, 3728-3734.
35. JE Prest, SJ Baldock, PR Fielden, NJ Goddard and BJ Treves Brown "*Bidirectional isotachophoresis on a planar chip with integrated conductivity detection"*, Analyst 2002, **127**, 1413-1419.
36. LL Shultz-Lockyear, CL Colyer, ZH Fan, KI Roy and DJ Harrison "*Effects of injector geometry and sample matrix on injection and sample loading in integrated capillary electrophoresis devices"*, Electrophoresis 1999, **20**, 529-538.
37. X Huang, MJ Gordon and RN Zare "*Bias in Quantitative Capillary Zone Electrophoresis Caused by Electrokinetic Sample Injection"*, Anal. Chem. 1988, **60**, 377-380.
38. JP Quirino and S Terabe "*Sample stacking of cationic and anionic analytes in capillary electrophoresis"*, J. Chromatogr. A 2000, **902**, 119-135.
39. DS Burgi and R-L Chien "*Optimization in Sample Stacking for High-Performance Capillary Electrophoresis"*, Anal. Chem. 1991, **63**, 2042-2047.
40. MU Katzmayr, CW Klampfl and W Buchberger "*Optimization of conductivity detection of low-molecular-mass anions in capillary zone electrophoresis"*, J. Chromatogr. A 1999, **850**, 355-362.
41. T-I Lin, Y-H Lee and Y-C Chen "*Capillary electrophoretic analysis of inorganic cations. Role of complexing agent and buffer pH"*, J. Chromatogr. A 1993, **654**, 167-176.
42. AR Timerbaev "*Strategies for selectivity control in capillary electrophoresis of metal species"*, J. Chromatogr. A 1997, **792**, 495-518.
43. K Ito and T Hirokawa "*Separation of alkali and alkaline-earth metal and ammonium cations by capillary electrophoresis using poly(ethylene glycol) and tartaric acid"*, J. Chromatogr. A 1996, **742**, 281-288.
44. RL Smith and DJ Pietrzyk "*Liquid Chromatographic Separation of Metal Ions on a Silica Column"*, Anal. Chem. 1984, **56**, 610-614.
45. JL Beckers, P Gebauer and P Bocek "*System zones in capillary zone electrophoresis"*, Electrophoresis 2001, **22**, 3648-3658.

46. J-F Liu and WA Ducker "*Surface-Induced Phase Behavior of Alkyltrimethylammonium Bromide Surfactants Adsorbed to Mica, Silica, and Graphite"*, J. Phys. Chem. B 1999, **103**, 8558-8567.
47. RBM Schasfoort, S Schlautmann, J Hendrikse and A Van den Berg "*Field-Effect Flow Control for Microfabricated Fluidic Networks"*, Science 1999, **286**, 942-945.
48. DJ Pietrzyk, S Chen and B Chanthawat "*Enhanced capillary zone electrophoretic separation of dinitrophenyl-amino acid derivatives through control of electroosmotic flow by the buffer cation"*, J. Chromatogr. A 1997, **775**, 327-338.

Chapter 8

Summary and outlook

The work in this thesis adds valuable fundamental expertise for quantitative ion analysis using microchip capillary electrophoresis. The major shortcoming of microchip CE is the sample loading by electromigration, inducing changes in the composition of the formed sample plug. To deal with this problem the fundamental aspects of the sample loading have been studied. Based on this knowledge quantified analysis of blood and drinking water has become possible. In this chapter the findings from the previous chapters are summarized. In addition to listing the achievements, suggestions are made for further development of the microchip system for ion analysis and specifically for point-of-care testing.

8.1 Summary of achievements

The fundamental processes of electromigration and the electrophoretic separations based on them have been studied for more than 100 years. This knowledge, combined with the recent studies on microfluidic devices, make it possible to design optimized microchips for capillary electrophoresis. Computer simulations were performed to assist in the optimization of the microchip design and the experimental separation conditions. Microchips with custom layouts were manufactured, first in-house and later purchased from specialized companies.

Chapters 1 to 3 provide an overview of the various activities in the field of microchip capillary electrophoresis. Chapter 3 also focuses on the design and manufacturing aspects of the microchip for point-of-care use. Here it was shown that glass microchips can be manufactured relatively easily, using standard cleanroom processes. However, the interaction of metal ions with the surface during the separation results in a restricted separation performance compared to the simulations. The manufacture, especially the temperature during the annealing has a large influence on the surface roughness and separation performance. This was characterized by AFM roughness measurements and the effect on the separation of mixtures containing potassium, sodium and lithium. Surface coatings were very successful in suppressing the interaction and also the addition of potassium chloride to the background electrolyte (BGE) greatly improved the separation. However, by adding potassium to the BGE a system peak is produced, which can interfere with the quantitation when it overlaps with the analytes.

In chapter 4 it was demonstrated that whole blood can be analyzed without removing the cellular constituents when a polyacrylamide coating is applied on the surface of the channels. The coating serves three purposes. First it suppresses the adsorption of proteins and cells from the sample so that the conditions are stable during multiple separations. Secondly, it provides the conditions for sample destacking by suppressing the EOF. Finally, by suppressing the EOF the blood cells cannot enter the channel during the sample loading step and remain in the sample compartment. The sample plug formed in the double-T of the microchip is therefore free of cells. This allows the lithium concentration in blood plasma to be determined using whole blood from a finger stick as sample. Reuse of the microchip was enabled when anticoagulant was added to the sample.

For quantitative analysis of the sample it was shown that, the formation of the sample plug during the loading step is as important as the actual separation. Chapter 5 discussed the electrokinetic sample loading as a combination of electromigration of the analytes and the electroosmotic flow (EOF). Under conditions of suppressed EOF, the stacking of dilute samples or destacking of high ionic strength samples affects the concentration of analytes in the sample plug loaded into the separation channel. This enables direct analysis of lithium in blood plasma or serum without an off-chip dilution. For accurate quantitation

an internal standard is required though. In the case of blood, sodium can be used as an internal standard that is readily available in the plasma. During the sample loading also a moving boundary separation takes place. In the zones that form, the ratio of concentrations between ionic species, for example between sodium and lithium, can shift. For blood where chloride and bicarbonate form the major anionic species, the shift can be neglected if the microchip is calibrated with standards consisting of the chloride salts.

For point-of-care testing a convenient method for analyzing small sample volumes is required. In chapter 6 disposable sample cups were presented requiring less than 10 µl of blood. A filter membrane on the bottom of the cups prevents direct contact of the blood sample with the microchip, which can therefore be used repeatedly. Under optimized conditions potassium, sodium, magnesium, calcium and lithium are separated from whole blood in less than 20 seconds without any off-chip sample pretreatment. The use of a water plug in the sample compartment of the microchip provides the sample stacking conditions that are needed when using the sample cups. The lithium levels determined in five serum samples from patients on lithium therapy are in good agreement with ion selective electrode measurements performed in the hospital, thus providing the proof of principle for the analysis of blood electrolytes with microchip CE. The relatively high detection limit for lithium of 0.15 mmol/L and low precision are issues needing further optimization for improved quantitation at the point of care.

Finally, the microchip was also used to measure the composition of tap water, which is described in chapter 7. A particular application is the determination of water hardness. When the chip is used without a coating on the channels there is a direct relation between the concentration of analytes in the sample plug formed during the loading step and in the bulk of the sample. When the EOF is used to form the sample plug instead of the electromigration, an internal standard is not required. Potassium, sodium, magnesium and calcium were separated using the complexing agent tartaric acid in the BGE to improve the resolution. In order to prevent wall interaction, potassium was added to the BGE, which made quantitation of the potassium concentration in tap water difficult due to the formation of a system peak. Chloride, sulfate and bicarbonate were measured after reversing the EOF by adding CTAB to the BGE. Detection limits are 20 µmol/L for monovalent ions and 10 µmol/L for divalent ions. The detection limits are approximately 10 times lower than for the blood measurements because the sample is not destacked during the loading step. Under cationic separating conditions the microchip is very stable allowing more than 100 subsequent separations. The anionic conditions however resulted in fouling of the channel entrance in the sample compartment, allowing only a restricted number of separations.

8.2 Outlook and recommendations

8.2.1 Microchip capillary electrophoresis of inorganic ions

Although separation conditions can be found that are suitable for the analysis of metal ions in blood and drinking water, the interaction with the glass surface is a problem. Polymer chips are an attractive alternative for glass, especially for disposable devices. The selection of the right material could also eliminate the need for a coating to suppress the EOF. Conversely, if an EOF is required it can be necessary to apply a coating in order to obtain a charged surface.

The absence of an automated sample handling system makes cleaning and conditioning of the microchip a tedious process. Especially if the chip is to be used repeatedly, automation will be a valuable addition. This offers consistency which will translate to a more reliable system.

The use of direct contact detection restricts the design of the electrodes, which have to fit inside the separation channel. The conductivity detector used in this thesis, for example only allows the electrodes to be positioned close to the exit of the separation channel due to coupling with the high-voltage supply. The solution to obtain more freedom in the design is to use different detector electronics or to switch to contactless detection. For polymer chips the contactless detection was proven by other researchers to be a good alternative, also from the viewpoint of less complicated fabrication. The channels can be closed with a thin foil to keep the distance between the electrodes and the channel small. Other researchers made glass devices with thin insulating layers deposited on the electrodes, but those layers were vulnerable to electrical breakdown. Taking the layout restrictions into account, a simple contact detection is a reliable choice for glass microchips.

8.2.2 Microchip capillary electrophoresis for point-of-care testing

For point-of-care testing the system has to be simple to use. This means that the chip has to be delivered ready to use, which might include a pre-filled channel system. Also some provision has to be made for the calibration solution so that this is measured automatically before or after the blood sample. The tests with the sample cups showed the potential of microchip CE for blood analysis, but further testing is needed to validate the method for clinical use. Further tests are planned in cooperation with the hospital to obtain more detailed statistical data, which will provide additional information on the prospect of developing the microchip into a commercial product for point-of-care use.

Coupling of painless microneedles to the microchip can offer an even more appealing product. The stacking of small sample volumes should allow measurement of ions in sample volumes down to a few nanoliter.

The use of other detection methods can furthermore expand the application to other blood substances. Amperometry and fluorescence detection can provide the lower detection limits needed for many biological compounds.

8.3 Conclusions

Microchip CE separation conditions were found that provide rapid quantitative analysis of inorganic ions in aqueous solution, e.g. drinking water. No internal standard is required when the EOF is used for the sample loading. Qualitative analysis of undiluted blood plasma or even whole blood was performed relatively easily, provided that sample loading conditions are used that result in a concentration adjustment. For the quantitative analysis an internal standard is needed though, while also a calibration solution has to be analyzed to determine the relative sensitivity of the detector for the internal standard and analyte. In a blood sample sodium can be used as a readily available internal standard, however an error will be introduced due to the fact that its concentration can fluctuate within certain limits. Taking the current achievements into account, already a point-of-care system for lithium can be developed that helps patients to avoid the risk of lithium intoxication. Lithium concentrations of more than 1 mmol/L can be detected easily and quantified with an accuracy of 0.1 mmol/L. Using the instrument as a warning system may lead to market introduction of a new handheld system. Also, given that electrophoresis is universally applicable, it remains an exiting technique also for the analysis of other blood constituents than lithium. The use of other detection methods, such as fluorescence, is interesting to obtain increased sensitivity and reduce the electromigration dispersion. Conversely, the additional optics might hamper system integration and make it less suitable for handheld instruments and should target other applications. The high throughput offered by microchip CE makes it an excellent separation method for use in the fields of high throughput screening, genomics and proteomics.

Appendix A

List of symbols

ε	Dielectric constant [F/m]
ε_r	Relative permittivity of the medium
ε_0	Dielectric constant/ permittivity of vacuum [8.854×10^{-12} F/m]
ζ	Zeta potential [V]
η	Viscosity [Pa·s]
κ	Electrical conductivity [S/m]
λ	Limiting equivalent ionic conductivity [$S\cdot m^2/mol$]
Λ	Specific molar conductivity [$S\cdot m^2/mol$]
μ	Electrophoretic mobility [$m^2/V\cdot s$]
ρ	Density [kg/m^3]
σ	Surface charge density [C/m^2]
σ^2	Variance
ω	Value of the Kohlrausch regulating function
c	Concentration [mol/L]
d	Distance [m]
e_0	Electron charge [1.60×10^{-19} C]
g	Gravitational constant [9.81 m/s^2]
h	Height [m]
j	Imaginary unit
l	Length [m]
k	Boltzman's constant [1.38×10^{-23} J/K]
k^{-1}	Debeye length [1/m]
r	Radius [m]
t	Time [s]
v	Velocity
w	Width [m]
z	Valence
A	Area [m^2]
C	Capacitance [F]
D	Diffusion coefficient [cm^2/s]
E	Electrical field strength [V/m]
E_A	Activation energy [J/mol]
F	Faraday constant [9.65×10^4 C/mol]
G	Electrical conductance [S]
H	Plate height [m]

I	Electrical current [A]
I	Ionic strength [mol/L]
$I^{\alpha\beta}$	Ion flux across a boundary [mol/m^2·s]
K_a	Acid dissociation constant
K_b	Thermal conductivity [W/m·K]
K_{cell}	Cell constant (1/m)
L	Length [m]
N	Plate number
N_A	Advogadro's constant [6.022×10^{23} 1/mol]
R	Electrical resistance [Ω]
R	Molar gas constant [8.314 J/mol·K]
R_s	Resolution
T	Temperature [K]
U	Electrical potential [V]
$V^{\alpha\beta}$	Boundary velocity

Appendix B

Electrophoretic mobilities of selected ions in aqueous solution

	μ (10^{-9} $m^2/V{\cdot}s$)	pK_a
Ca^{2+}	61.7	13.6
H^+	362.5	14
His^+	28.8	6.04
His^{2+}	44.7	2.00
K^+	76.2	13.0
Na^+	51.9	13.7
NH_4^+	76.2	9.25
Li^+	40.1	13.8
Mg^{2+}	55.0	12.2

	μ (10^{-9} $m^2/V{\cdot}s$)	pK_a
NO_3^-	74.1	-1.37
SO_4^{2-}	82.9	1.92
Cl^-	79.1	-2.00
MES^-	28.0	6.10
$HEPES^-$	23.5	7.50
$Tartrate^-$	32.6	3.04
$Tartrate^{2-}$	60.7	4.37
TRIS	29.5	8.08
$Oxalate^-$	42.4	1.27
$Oxalate^{2-}$	77.0	4.27
$Acetate^-$	42.4	4.76
HCO_3^-	46.1	6.35
CO_3^{2-}	71.8	10.33
His^-	28.3	9.33
OH^-	205	

Mobilities taken from the database in Peakmaster [http://www.natur.cuni.cz/~gas/].

Appendix C

Manufacture of glass CE chips with integrated platinum electrodes

The process provided here is used for the manufacture of glass microchips with integrated electrodes. The instrument settings and parameters are provided as guidance only. The experiments in this thesis were performed on chips made by a company, though for a large part in the MESA$^+$ cleanroom using similar protocols.

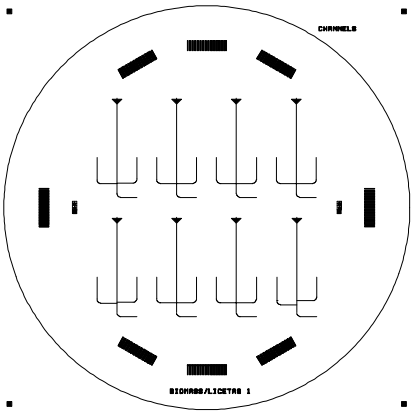

Mask 1: Channels

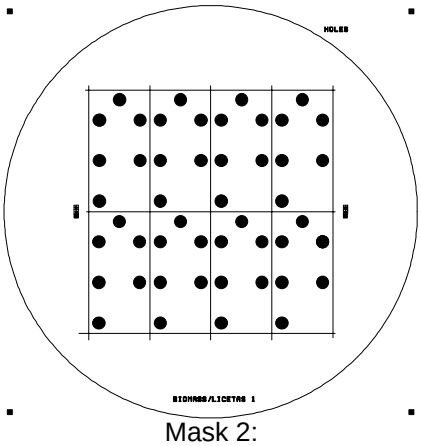

Mask 2: Compartments and dicing lines

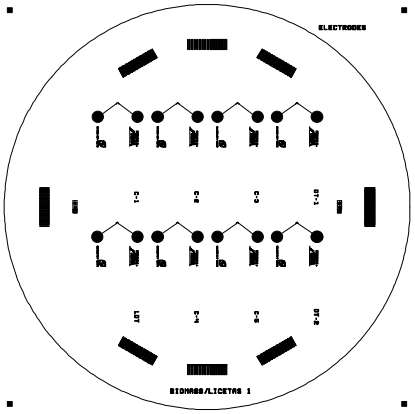

Mask 3: Electrodes

1. Electrode wafer process

Step	Process	Parameters
1	Cleaning fuming HNO_3 (Removal of organic contaminants)	**Wet Bench** -HNO_3 (100%), 15min. -quick dump rinse, DI, <0.1 µS -spin drying
2	Lithography-Olin 908-Ti35 Image reversal resist	**Karl Süss 55** -dehydration bake 120°C, 5 minutes -priming: HMDS, 4000 rpm, 20 s -resist: Olin 908-Ti35, 4000 rpm, 20 s -prebake: 95°C, 120 s -mask: Electrode mask -exposure time 20 s -stabilisation step: >20 minutes at room temperature -reversal bake: 115°C, 2-3 minutes -flood exposure, *60* s -developing: OPD 4262, 9*0* s -quick dump rinse, DI, <0.1 µS -spin drying -visual microscopic inspection -postbake: 120°C, 5 minutes
3	Etching trench with buffered HF	-NH_4F/HF (1:7) Merck -etchrate 20 nm/minute -etch a trench, 200 nm (~10 min) -quick dump rinse, DI, <0.1 µS -spin drying
4	Sputtering of chrome and platinum	**Home built sputtering equipment** -gas flow: Ar/ 45 sccm -base pressure $1.0 \cdot 10^{-6}$ mbar -sputter pressure: $5.0 \cdot 10^{-3}$ mbar -power 200 W -deposition of 10 nm Cr (rate ~10 nm/minute) -deposition of 180 nm Pt (rate ~18 nm/minute)

5	Lift-off of excess metal	-Acetone -ultrasonic bath >15 minutes -IPA spray method, 30 s -spin drying -visual microscopic inspection
6	Cleaning fuming HNO_3	-HNO_3 (100%), 15 minutes -quick dump rinse, DI, <0.1 μS -spin drying

2. Channel wafer process

Step	Process	Parameters
1	Cleaning fuming HNO_3	-HNO_3 (100%), 15 minutes -quick dump rinse, DI, <0.1 µS -spin drying
2	PECVD amorphous silicon	**Elektrotech PF 310/340** -SiH_4 2% + 98% Ar 2000 sccm -pressure 650 mTorr -T = 250 °C -t = 50 minutes -thickness ~ 500 nm
3	Lithography-Olin 908-Ti35 Image reversal resist	**Karl Süss 55** -dehydration bake 120°C, 5 minutes -priming: HMDS, 4000 rpm, 20 s -resist: Olin 908-Ti35, 4000 rpm, 20 s -prebake: 95°C, 120 s -mask: Channel mask -exposure time: 20 s -stabilisation step: >20 minutes at room temperature -reversal bake: 115°C, (2-3 minutes) -flood exposure, 60 s -developing: OPD 4262, 90 s -quick dump rinse, DI, <0.1 µS -spin drying -visual microscopic inspection -postbake: 120°C, 30 minutes
5	Plasma etching of amorphous Silicon isotropic	**Elektrotech PF 310/340** -dirty chamber -styros electrode -electrode temperature 10°C -SF_6 flow 50 sccm -pressure 75 mTorr -power 75 W -~1:20 – 1:45 minutes Glass will act as etch stop

6	Etching channels	-HF 10% (w/v) etch rate: 0.321 μm/minute -rinse in DI -etching 6 μm ~ 20 minutes -quick dump rinse, DI, <0.1 μS -spin drying
7	Stripping of Olin 908 in acetone	-acetone, spray method, 60 s -IPA, spray method, 30 s -spin drying -visual microscopic inspection
8	Etching amorphous Si with KOH	-25% (w/w) KOH, 75°C -quick dump rinse, DI, <0.1 μS -spin drying Glass will act as etch stop
9	Lithography Ordyl BF 410 foil (powderblasting)	-remove thick (75 μm) PET layer from BF410 foil (Foil thickness = 100 μm) -switch on laminator: 130°C,speed 3 -apply BF foil with roller -laminate on substrate -cut the wafer out of the foil -put wafer on hotplate, 95°C, 60 s -remove thin PET film with thin knife -Karl Süss 55 -mask: Holes mask -exposure time 20 s -Developing -0,2% Na_2CO_3, spray development -90 s developing -rotate 4” wafer 180 degrees -90 s developing -rinse in DI -spin drying
10	Add protective foil	-apply dicing foil without heat on backside of wafer for protection
11	Powderblasting Pyrex Low resolution	-particles: 30 μm Alumina -pressure: 4.6 bar -mass flow: 3-12 g/minute -etchrate approximately 59 μm per g/cm^2 -for feature size > 100μm -remove protective foil

12	Cleaning ultrasonic	-acetone, ethanol or IPA, > 10 minutes -demi water, > 10 minutes -quick dump rinse, DI, <0.1 µS -spin drying

3. Wafer bonding

Step	Process	Parameters
1	Cleaning fuming HNO_3	-HNO_3 (100%), 15 minutes -quick dump rinse, DI, <0.1 µS -spin drying
2	Direct bonding and annealing	**Electronic Visions AL-6** -align wafers in EV maskaligner -apply pressure to get a prebond -annealing 600°C, 4 h.
3	Dicing	**Disco DAD-2H/6T** -laminate the wafer pair with dicing foil by standard procedure (contact holes up) -dicing foil thickness 85 µm -sawing blade 12A -machine parameters: dicing length: 11 mm dicing speed: 1 mm/s (preset 3) y increment: 15 mm y increment (after rotation): 30 mm height to foil: 85 µm package height: 1.5 mm rotation: 90°

Summary

This thesis describes the development of a microchip capillary electrophoresis system for measuring inorganic ions in samples at the point of care. The analysis of inorganic ions in whole blood, specifically lithium to monitor the treatment of patients suffering from manic depression is investigated. To realize this goal a microchip and measurement protocol is developed that enables us to quantitate the lithium concentration in a drop of blood obtained from a finger stick. The blood components are separated on the chip by means of capillary electrophoresis and measured using embedded electrodes for conductivity detection. The separation conditions are studied to find a method to extract the inorganic ions from the blood sample. In addition a method was developed to dilute the extracted ions on chip, which is necessary to prevent interference from the high sodium concentration with the separation. Finally, different approaches are presented to transfer the blood from the patient to the chip. These methods include the use of sample cups with a volume of less than 10 µl or the utilization of microneedle arrays. Under optimized separation conditions not only lithium is detected, but also potassium, calcium and magnesium, while sodium is used as internal standard. The complete analysis of a blood sample is performed in less than five minutes. A comparative study of five patient samples analyzed with the microchip and with a commercial lithium analyzer shows good agreement.

In a second application the same microchip layout has been applied to the monitoring of drinking water. Using tartaric acid as a complexing agent to enhance the separation, sodium, calcium and magnesium were quantified in tap water. Anionic species were detected after reversing the electroosmotic flow by adding cetyltrimethylammonium bromide (CTAB) to the background electrolyte. Without any off-chip sample pretreatment, chloride, sulfate and bicarbonate were measured in tap water. The obtained results demonstrate the versatility of the system for on-site measurement of inorganic ions.

Samenvatting

Dit proefschrift beschrijft de ontwikkeling van een capillaire elektroforese system op microchip voor het ter plekke meten van anorganische ionen in monsters. De voornaamste toepassing welke onderzocht is, is het meten van lithium in volbloed voor het monitoren van de behandeling van manisch-depressieve patienten. Voor dit doel een microchip en meetprotocol was ontwikkeld welke het mogelijk maakt om de lithium concentratie gekwantificeerd te meten in een druppel bloed. De verschillende bloedcomponenten worden op de chip gescheiden door middel van capillaire elektroforese en vervolgens met behulp van geintegreerde geleidbaarheidselektroden gemeten. De scheidingscondities zijn bestudeerd om een methode te vinden waarbij de anorganische ionen uit het bloedmonster geextraheerd worden. Daarnaast is een methode ontwikkeld om de ionen op de chip te verdunnen om interferentie met de hoge natrium concentratie te voorkomen. Tenslotte zijn verschillende methoden gepresenteerd om het bloed over te brengen van de patient naar de chip. Daarbij horen het gebruik van monstervaatjes met een volume kleiner dan 10 µl en het gebruik van micronaalden arrays. Onder geoptimaliseerde omstandigheden is niet alleen lithium, maar ook kalium, calcium en magnesium gemeten, waarbij natrium als interne standaard gebruikt is. De volledige analyse van een bloedmonster is mogelijk in minder dan vijf minuten. Een vergelijkende studie van serummonsters van vijf patienten laat een goede overeenstemming zien tussen de microchip en een commercieel verkrijgbare lithium analyzer.

In een tweede toepassing is dezelfde microchip gebruikt voor het monitoren van drinkwater. Met gebruik van wijnsteenzuur als complexvormer om de scheiding te verbeteren werden natrium, calcium and magnesium in leidingwater gekwantificeerd. Anionische stoffen werden gemeten na het omkeren van de elektroosmotische flow door het toevoegen van cetyltrimethylammonium bromide (CTAB) aan het achtergrond elektolyt. Cloride, slufaat en bicarbonaat werden gemeten zonder enige monstervoorbewerking. De verkregen resultaten laten zien dat het systeem breed inzetbaar is voor het ter plekke meten van anorganische ionen.

Acknowledgements

This work would not have been possible without contributions by a number of people. First of all I would like to thank Anne. You showed me a different perspective on life and without the discussion we had I probably would not even have started on a PhD at all. The project started smoothly thanks to the help of Richard who supervised the work in the first couple of months. I would like to thank Albert for pushing me to start writing up the results and publish them, which ultimately led to a more structured approach of the research. Furthermore I would like to acknowledge everyone in the user committee of the LiCETAS project for their interest in the work and their support. The discussions with Pieternel on lithium treatment of manic depression and with prof. Vermes on the clinical analysis of blood were very helpful. With the help of Ron we could make the chip holder for point-of-care testing that was designed by Rob. I also would like to thank Ad for his help with the electronics of the system.

Due to the structure of the former MICS group it always was somewhat unclear where I belonged. Although I officially was part of the Micmec group, I immediately found shelter and a place to work in the Bios group. Later I officially became a member of Bios and I would like to thank everyone here for their collegiality over the four years.

Special gratitude also goes to the people in the group of Electromigration Separation processes at Charles University in Prague which I had the pleasure to visit during three weeks thanks to the connection of prof. Everaerts. Especially Bob I am grateful for making me feel welcome and for the discussions on the theoretical backgrounds. I thank Vlastik for his patients while explaining the excellent simulation program Simul. Michal and Jana I would like to thank for the Czech lunches we had together.

Finally, but most of all I am thankful for all the support and help given by Regina. Without your enthusiasm to manage the project I am sure it would be much less successful. I will not forget the times that we were staying until midnight to do some more experiments just for the fun of it, or to make the finishing touches to a paper. In all, I would not have wanted anyone else as supervisor and coach.